WIRELESS SENSOR FUSION APPROACH FOR MONITORING CHEMICAL MECHANICAL PLANARIZATION (CMP) PROCESS

By

AMIT OHRI

Bachelor of Technology

Lovely Institute of Technology

Punjab Technical University

Punjab, INDIA

2006

Submitted to the Faculty of the
Graduate College of the
Oklahoma State University
in partial fulfillment of
the requirements for
the Degree of
MASTER OF SCIENCE

December, 2010

WIRELESS SENSOR FUSION APPROACH FOR

MONITORING CHEMICAL MECHANICAL

PLANARIZATION (CMP) PROCESS

Thesis Approved:

Dr. Ranga Komanduri

Thesis Advisor

Dr. Satish Bukkapatnam

Committee member

Dr. S.P.Harimkar

Committee member

Dr. Mark E. Payton

Dean of the Graduate College

ACKNOWLEDGMENTS

This thesis would not have been possible without the support of many people and I wish to convey my gratitude to all of them.

First and foremost, I want to express my sincere gratitude to my advisor, Dr. Ranga Komanduri, Regents Professor and A.H Nelson, Jr. Endowed Chair in Engineering. I am thankful to him for giving me the guidance during my work in chemical mechanical planarization.

Secondly, I owe my deepest gratitude to Dr. Satish Bukkapatnam for giving me the opportunity to work on wireless sensor, statistical analysis, nonlinear analysis without which my work would be incomplete. I want to thank Dr Zhenyu Kong for giving me helpful suggestions for my thesis. I want to thank Dr. Harimkar for agreeing to serve in my thesis committee.

I sincerely thank my parents and my elder brother for their patience and affection without whom I will not be here.

I thank Mr. Jakkrit Kuntung and Mr. Akkarapol Sangasoongsong for their help on wireless sensors. I thanks are due to Dr. Rutuparna Narulkar, Mr. Omer Beyca, Mr. Prahlad Rao, Mr. Puneet Jethani, Dr. Milind Malshe, Dr. Hui Yang, Mrs Martha lann, Mrs. Kimberly dyer and Mr. Ravi Chandra. I also want to thank my colleague Mr. Ekansh Gupta for assisting me in conducting the experiments.

I am thankful to Mr. Jerry Dale and Mr. John Gage for helping me with the machining work throughout my thesis work.

This work was supported by grants from the National Science Foundation (NSF) (CMMI 0700680 and CMMI 0830023). This researcher acknowledges the opportunity provided by the Division of Design, Manufacturing, and Industrial innovation (DMI) of the NSF.

Table of Contents

Contents **Page**

Abstract 1

Chapter 1: Introduction 3

Chapter 2: Literature review... 8

2.1 Mechanism of CMP polishing of copper 8

2.2 Slurry 8

2.3 Abrasive.. 14

2.4 Polishing pad 15

2.5 Temperature 22

2.6 Analysis of vibrations in CMP process... 27

2.7 CMP Modeling:.. 27

Chapter 3: Sensors in chemical mechanical planarization (CMP)...................................... 32

Chapter 4: Problem statement 55

Chapter 5: Initial CMP Studies 57

5.1 Submerged Face-up CMP:.. 57

Chapter 6: Experimental Apparatus and Design of Experiments....................................... 71

6.1 CMP polishing apparatus 71

6.1 Wireless Sensor 73

6.2 Design of experiments (DOE): 75

Chapter 7: Feature Extraction and Process Dynamic Visualization 82

7.1 Statistical features: 83

7.2 Time series visualization 83

7.3 Energy features 84

7.4 Time-frequency visualization 85

7.5 Nonlinear features 89

7.5 Nonlinear dynamic visualization: 91

Chapter 8: Sensor Fusion Regression Modeling 96

8.1 Technical approach: 96

8.2 Modeling roughness: 98

8.3 Modeling MRR: 106

8.4 Modeling Preston constant (K_p): 114

Chapter 9: Conclusions and Future Work 124

References 127

List of Figures

Figures 1(a) and (b): Rotary and linear CMP arrangements [2] 4

Figure 2: Input and Output parameters in CMP [2] 9

Figures 3 (a) and (b): Potentiodynamic curve of copper in 5% HNO3 and in 1% NH4OH 10

Figure 4: Dispersion and agglomeration of EDL on the silica particles [9] 11

Figures 5 (a) and (b): Eoc of copper at different pH values with alumina abrasive (a) without glycine (b) with glycine [12] 13

Figure 6: Variation of removal rate for different H2O2 concentrations [16] 13

Figure 7: SEM of surface and cross section of a unpolished pad [31] 15

Figure 8: Cross-section (SEM) of IC1000/suba stacked pad [32] 16

Figure 9: Dynamic shear modulus of Pads [35] 17

Figure 10: DMA and TMA run for hard pad [37] 18

Figure 11: a) Path as mapped by 10 µm and 90 µm stylus. b) Pad surface mapped by WLI [31] 19

Figure 12: SEM of a fixed abrasive pad [42] 21

Figure 13: Polishing mechanism of tungsten CMP using hydrophilic polymer based pad [44] 22

Figure 14: Variation of temperature with relative velocity and pressure [48] 23

Figure 15: Variation of coefficient of friction with temperature [49] 24

Figure 16: Effect of temperature on dishing [49] 26

Figure 17: variation of real contact area with respect to temperature [50] 26

Figure 18: Variation of pH value with temperature [50] 26

Figure 19: Vibration in chemical mechanical polishing 27

Figure 20: Infrared set-up for measuring the temperature at the -pad interface [62] 29

Figure 21: Variation of Von Misses stresses with distance from center [69] 30

Figure 22: Acceleration sensor implementation and procedure [72] 32

Figure 23 (a) and (b): Vibration signal based monitoring system [72] 33

Figures 24 (a) and (b): (a) Horizontal and (b) Vertical components of the vibration spectra of a polishing head [72, 73] 34

Figure 25 (a) and (b): Vibration intensity change detection during (a) copper multilayer polishing and (b) under different defect exposures [74] 35

Figure 26: Vibration sensor monitoring systems in CMP [77-80] 38

Figure 27: Thermal monitoring systems in CMP [81-84] 39

Figure 28: Variation of pad temperature with polishing time [82] 41

Figure 29: Variation of temperature slope with polishing time [83] 41

Figure 30: Variation of temperature with time in multilevel polishing [84] 42

Figure 31: Variation of temperature with pressure for slurry and water in CMP process [85] 43

Figure 32: AE sensor arrangement in the CMP process [88] 44

Figure 33: AE signal during polishing [89] 45

Figure 34: AE signal obtained when micro scratches were formed [89] 45

Figure 35: AE signal without abrasive [88] 46

Figure 36: Cumulative energy for 16 levels for in-control and out-of-control AE signal [91] 46
Figure 37: AE sensor monitoring systems in CMP [97, 100, 102, 103] 50
Figure 38: Acoustic or sound sensor monitoring systems in CMP [104, 105] 52
Figure 39: CMP polishing machine 57
Figure 40: Front and Top views of the face-up CMP apparatus 58
Figure 41: Sensors arrangement in the face-up CMP apparatus 58
Figure 42: Vibration signals at 95 rpm, 500 Hz 59
Figure 43: Acoustic/sound signals at 75 rpm, 500 Hz 60
Figure 44: Face up CMP with wireless sensor 60
Figure 45: Copper cup arrangement for temperature signals in CMP 61
Figure 46: Pad temperature signal 62
Figure 47: Optical image of copper wafer using multistage polishing using a face-up CMP polishing apparatus 63
Figure 48: IC 1000 pad before and after 25 min. of polishing time with colloidal silica slurry (1:2) 64
Figure 49: FBP 1000 pad before and after polishing 65
Figure 50: Vibration signal and Power spectrum at 50 lb load 65
Figure 51: Power spectrum during the polishing process 66
Figure 52: Vibration frequency power spectrum for analysis 68
Figure 53: Vibration signals under dry and wet polishing conditions 69
Figure 54: Power spectrum at different loading conditions under constant spindle speed of 400 rpm 70

Figure 55: Transmitter base i.e. Buehler polishing machine for vibration and temperature signal 72
Figure 56: Receiver base for vibration and temperature signals........ 72
Figure 57: Tmote sky-based wireless platform........ 74
Figure 58: Sartorius weighing balance machine........ 74
Figure 59: MicroXam, Optical laser interference microscope........ 76
Figure 60: MRR repetition for Run R1 (see Table 7 for details)........ 76
Figure 61: Microstructure of copper sample before and after polishing 78
Figures 62 (a) and (b): 3D surface profiles of the sample before and after polishing 79
Figure 63: Comparison of time series of the signals under two different loading conditions of (10 lb and 5 lb) and same platen rotating speed of 500 rpm 80
Figure 64: Power spectrum at 30 sec under Run R2 conditions [see Table 7] 80
Figure 65: Power spectrum at 120 sec under Run R2 condition [see Table 8]........ 81
Figure 66: Temperature profiles with time during CMP polishing (platen rotational speed: 300 rpm, load: 10 lb, and pad: Microcloth) 81
Figure 67: Vibration signal during the polishing process during the (a) Initial and (b) After 2 min of polishing under load 5 lb........ 84
Figure 68: Time-frequency representation of the vibration signal at 300 rpm, 10 lb and slurry ratio 1:5 86
Figure 69: Spectrogram under Run R2 conditions with two repetitions [see Table 7].... 87
Figure 70: Time delay portrait with time delay 3 under Run R2 conditions at the start of polishing (See Table 7) 88

Figure 71: 3D Phase space portrait under Run R2 conditions at the start of polishing (See Table 7) 88

Figure 72: Recurrence plot obtained after the start of polishing: speed of the platen 300 rpm, load 10 lb, and slurry ratio 1:3 93

Figure 73: Recurrence plot: End of polishing: speed of the platen 300 rpm, load 10 lb, and slurry ratio 1:3 94

Figure 74: Sensor fusion methodology 97

Figure 75: Plot of the residual versus the fitted values 97

Figure 76: MRR repetition for Run R2 (see Table 7) 106

LIST OF TABLES

Table 1: Patents on vibration sensors in CMP 47

Table 2: Patent on AE sensors in CMP 48

Table 3: Patent on sound sensors in CMP 51

Table 4: Patent on temperature sensor in CMP 53

Table 5: Multistage polishing process in a colloidal silica slurry 62

Table 6: Process frequency band at various conditions 66

Table 7: Full factorial design of CMP experiments 77

Table 8: High and low level in CMP experimental design 77

Table 9: Machine parameters and slurry temp (°C) 95

Table 10: Statistical features and MRR (mg/sec) 95

Table 11: Energy features, Temperature features (°C), peak to peak and Roughness, nm 95

Table 12: RQA (Nonlinear) features 95

Table 13: Regression model of Ra using process parameters 99

Table 14: Regression model of Ra using statistical features 100

Table 15: Regression model of Ra with statistical and energy features 101

Table 16: Regression model of Ra with statistical, energy, and RQA features 102

Table 17: Regression model of Ra with thermal features only 103

Table 18: Regression model of Ra with statistical, energy, RQA, and temperature features 105

Table 19: Sensor fusion based roughness estimation 106

Table 20: Regression model of MRR model using machine parameters alone............. 108

Table 21: Regression model of MRR using statistical features..................................... 109

Table 22: Regression model of MRR using statistical and energy features 110

Table 23: Regression modeling of MRR using statistical, energy, and RQA features... 111

Table 24: Regression modeling of MRR using thermal features only 112

Table 25: Regression modeling of MRR using statistical, energy, RQA, and Temperature features (R^2= 90.23%, R^2 (adj.) = 84.86%, df_r=20) 113

Table 26: Sensor fusion based MRR estimation... 114

Table 27: Regression model of Kp using statistical features... 116

Table 28: Regression model of Kp model using statistical and energy features........... 117

Table 29: Regression model of Kp using statistical, energy, and RQA features........... 119

Table 30: Regression model of Kp using thermal features only 120

Table 31: Regression model of Kp using statistical, energy, RQA, and temperature features (R2= 86.00% R2 (adj.) = 75.9%, dfr=19) 121

Table 32: Regression model of Kp with sensors features and process parameter.......... 122

Table 33: Summary of the Kp model 123

Table 34: Regression models of surface roughness and MRR 125

Table 35: Regression models of Preston Constant 126

ABSTRACT

Chemical mechanical planarization (CMP) is used in the microelectronics and optical industries for local as well as global planarity and for producing mirror finished surfaces. Roughness (Ra), within- non-uniformity (WIWNU), and material removal rate (MRR) are the major performance variables in polishing. CMP is a complex process involving some 36 input variables. Analysis of the review of the literatures showed that static models that use process parameters are inadequate for estimating and monitoring the performance variables in the CMP process. Pad-level interactions play a major role in polishing. Sensor based monitoring techniques enables monitoring of the CMP process. Additionally, sensor fusion techniques may facilitate in improving the robustness and monitoring the process beyond using one sensor. In this work, wireless vibration (Z-axis) and temperature sensors mounted on a bench top polisher (ECOMET polisher from Buehler) are used to monitor the material removal rate (MRR) and surface finish (Ra). The wireless sensor platform has a sampling rate of 500 Hz for the vibration sensor and 4 Hz for the temperature sensor. Alumina-based alkaline slurry is used in polishing process. The process conditions include two loading conditions (10 lb and 5 lb) and two rotational speeds (500 rpm and 300 rpm). The polishing studies were conducted on a 1.6" copper samples and Microcloth pad (from Buehler).

The overall approach used involves relating the various sensors signal features to MRR and Ra from the CMP process. The vibration features were extracted using statistical, frequency, and RQA (non-linear) analysis techniques. The vibration features were combined with temperature features to build multiple linear regression models. The regression fitting accuracy for the roughness model is ~ 93% using the statistical features, such as maximum and kurtosis, time-frequency features, such as energy, nonlinear features such as LAM and Lmax and thermal features such as net temperature rise and temperature rise rate. The regression fitting accuracy for the MRR model is ~ 91% using the statistical features, such as variance and skewness, time-

frequency features, such as energy and nonlinear features, such as time delay and temperature rise rate as temperature features. The thermal features are able to increase the coefficient of determination of roughness model by 10%.

This wireless sensor fusion based regression models are found to be more efficient compared to a single sensor as it takes care of both the mechanical effects using a vibration sensor and thermal effects using a temperature sensor. It appears that this is the first time that a sensor fusion based technique is attempted for predicting Ra and MRR in the CMP process.

Chapter 1: Introduction

1.1 CMP Process

Chemical mechanical planarization (CMP) process is used in the manufacture of microelectronic devices to produce flat, mirror finished surfaces on field emission displays and semiconductor wafers. It combines chemical and mechanical actions, i.e., chemical action of the slurry weakens the surface layers by chemical reactions and mechanical action by the abrasive that removes this layer. It includes creation of porous unstable oxides by the surface chemical reaction with the chemical slurry. It is one of the safest processes for wafer planarization when compared to reactive dry-etch process because of the absence of hazardous gases.

In the past, aluminum was used for metallization of the semiconductor wafers but this has been replaced by copper because of its lower electrical resistance. Also, chips made of copper run faster with less heat generation due to higher thermal conductivity thereby increasing the efficiency and chip capacity. The ability of the CMP process to planarize multiple materials in the nanometer size range with global planarity has led to its wide application in the semiconductor industry. Zantye *et al*. [1] state that CMP is affected by more than 30 factors. They include types of slurry, abrasive size, pad, wafer, equipment etc. Polishing occurs by the rotation of the wafer ring and the plate. Due to this rotation, centrifugal forces cause the spread of slurry uniformly over the surface. Companies using this technology include Seagate, Intel, Micron, Sony, Intel, IBM, Nikon, Sematach Int., and Motorola.

Previously, lapping machine was used in the process of planarization but the level of planarization was not in accordance with the required specification of the product. Due to continuous size reduction of ICs, there was a need for a process with high level of accuracy thereby maintaining specifications. This expectation of accuracy is maintained by CMP. In a way, it is the advanced version of the lapping process. The CMP is a complex and a dynamic process due to variation in the applied pressure by the wafer and wear of the pad. The main components

of the process are the slurry, pad, wafer, carrier and platen. In order to maintain a continuous advancement for the process performance, there is a need for the optimization of the performance parameters, such as material removal rate (MRR), roughness (Ra), and within--non- uniformity (WIWNU). In this process, there is a rotating unit, on the top is carrier or wafer holder and on the bottom is platen or pad holder. In addition to these, there is a separate unit for the slurry which pours from the unit.

CMP machine tools are mainly of two types: rotary and linear. In the rotary type of arrangement, the platen rotates while the pad has a linear motion in the case of linear polisher. Figures 1(a) and (b) shows the two types of arrangements of CMP. Slurry plays an important role in the CMP process. It constitutes a mixture of chemicals and abrasives which move below the surface of wafer during the rotation of the plate. It enables pre-weakening of the surface of the wafer before the planarization process. Normally it includes an abrasive material, e.g., silica, alumina, suspended in an oxidizing agent and an aqueous medium, such as hydrogen peroxide. Various statistical techniques and dynamic modeling methods are used in the study of the CMP process.

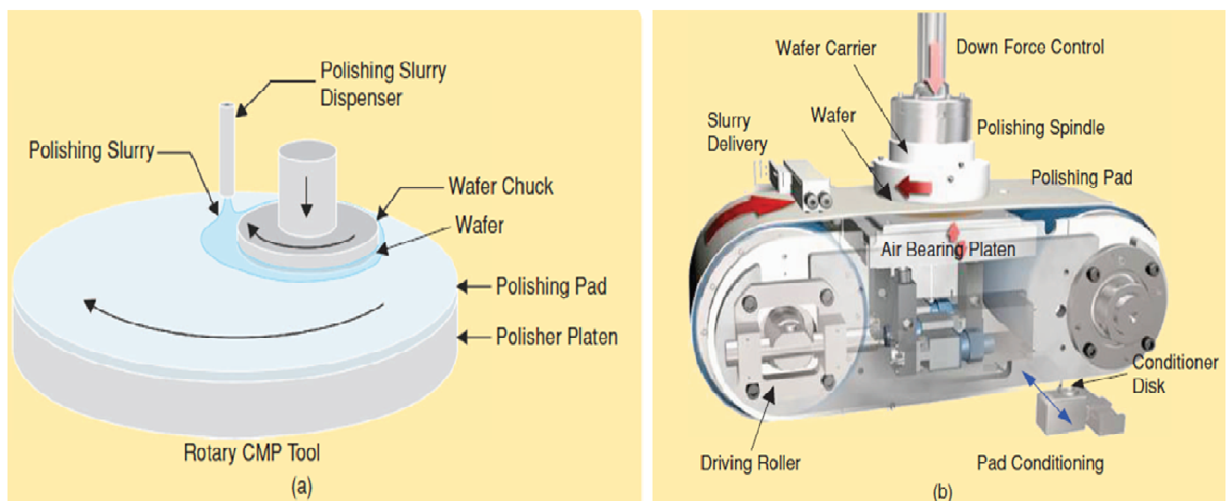

Figures 1(a) and (b): Rotary and linear CMP arrangements [2]

1.2 Objective:

The objective of the present investigation is to relate the surface roughness (Ra) and material removal rate (MRR) of copper sample in the CMP process in real time using features extracted from MEMS vibration sensor and temperature sensor signals (RFID sensor tags) using design of experiments and statistical modeling methods. The approach uses sensor fusion modeling techniques to combine information from vibration and temperature sensors. Additionally, Preston constant is estimated using the above developed sensor fusion modeling technique. Experiments were conducted on a Buehler bench top machine (ECOMET 250) using vibration and temperature sensors, a copper sample, a microcloth pad, and colloidal alumina slurry (50 nm abrasive size). Various statistical features, time-frequency domain energy features, and recurrence quantification features were extracted from the signals.

Sensor fusion based modeling techniques are developed using response surface methodology for monitoring the surface roughness and MRR of the wafer polished. The signals from the sensors were collected by systematically conducting design of experiments. The sensor fusion technique includes the use of vibration and temperature signals. Various features extracted from the vibration signals are statistical, time-frequency, and nonlinear features. This is followed by inclusion of temperature features for improving the estimation of the process outcome. The thermal features are able to increase significantly the performance of the roughness model. The model developed takes cares of individual factors and their interaction in the process dynamics.

This thesis is organized as follows: Chapter 2 presents a review of the literature which includes some relevant prior work in the slurry, pad, and abrasive modeling and experimentation. Also temperature effects in the CMP are discussed in this chapter. Chapter 3 presents a brief review on the application of sensors in monitoring the CMP process including end point detection (EPD). It is based on the review of literature (journals and patents) on vibration sensors, temperature sensors, acoustic or sound sensors, and acoustic emission (AE) sensors. Chapter 4 presents the problem statement of this thesis, which is related to the need for the application by sensor fusion techniques for modeling and monitoring the CMP process. Chapter 5 presents preliminary results from initial experiments in CMP. This includes the design and construction of the CMP apparatus, and implementation of the wireless sensors in the CMP apparatus. Chapter 6 describes the experimental apparatus used as well as the data collection equipment required for the design of experiments. The design of experiments is implemented to collect data from different sensors for sensor fusion modeling of Ra and MRR of the wafer. In this chapter, explanation of the fixture and wireless platform are provided. Chapter 7 describes various feature extraction techniques used in the modeling. They include statistical features such as mean, peak to peak amplitude, variance, time-frequency domain based energy features and recurrence quantification analysis based features such as recurrence, determinism, entropy. In addition, qualitative analysis is done through visualization by spectrogram and recurrence analysis. Chapter 8 consists of modeling Ra, MRR and the Preston constant. This includes modeling using various vibration features, such as statistical, time-frequency, and nonlinear features followed by

thermal features. Chapter 9 summarizes the main research findings from the thesis. It also includes future recommendation for increasing the effectiveness of the models.

Chapter 2: Literature review

2.1 Mechanism of CMP polishing of copper:

According to Saka *et al.* [3], three types of contact regimes exist between the wafer and the pad, namely, direct contact mode, mixed or partial contact and hydroplaning. For effective MRR, the CMP process should be conducted in the contact mode. CMP is a very complex process involving many input parameters namely, slurry, pad, wafer and polishing equipment. Figure 2 shows various input and output parameters in the CMP process. Among the current studies, there are two broad sets of models proposed to explain the mechanism of CMP, namely, Hertzian indentation, and fluid based wear [4]. In the Hertzian indentation model, the abrasive particles are dragged across the surface as cutting tools while in case of fluid based wear, the particles impinges on the surface at some angle and with high velocity. Steigerwald *et al.* [5] proposed the explanation for the mechanisms of the copper removal in two modes i.e., mechanical abrasion in the first mode and chemical dissolution of the removed particles in the second mode. When Benzo-tri-azole (BTA) is added to the slurry, it forms a passivation or non-corrosive layer. This layer is removed after abrasive action and etches the copper surface. In the CMP, it was found that for effective material removal rate (MRR), the slurry should contain hydrogen peroxide, BTA, and organic acid. Improvement in the dispersibility of the slurry results in an increase in the MRR because the abrasive involved in polishing increases as a result [6]. Pietsch *et al*. [7] studied the chemical-mechanical material removal using Fourier-transform infrared spectroscopy. They state the termination of OH^- results in material removal.

2.2 Slurry:

It is a chemical solution containing acidic or alkaline compounds which reacts with the wafer surface thereby preparing a passive layer followed by pre-weakening of the wafer surface during

polishing. It is a medium in which abrasive particles are dispersed. It is generally made up of two chemical compositions which are used for the dissolution of upper layer and abrasive material to remove the dissolving layer physically. It helps in reducing the surface features thereby enabling tighter design fabrication. The slurry usually contains an oxidizing agent, a complexing agent, a corrosion inhibiter, an abrasive, a reagent, and a chelating agent. Reagent is added in the slurry to increase the solubility of the copper in the slurry and to prevent the dissolution of copper in the recessed areas on the surface. Slurry chemistry mainly includes citric acid, hydrogen peroxide, glycine, Benzotriazole (BTA). Where glycine and citric acid are the complexing agents, BTA is the corrosion inhibiter and hydrogen peroxide is oxidizing agent.

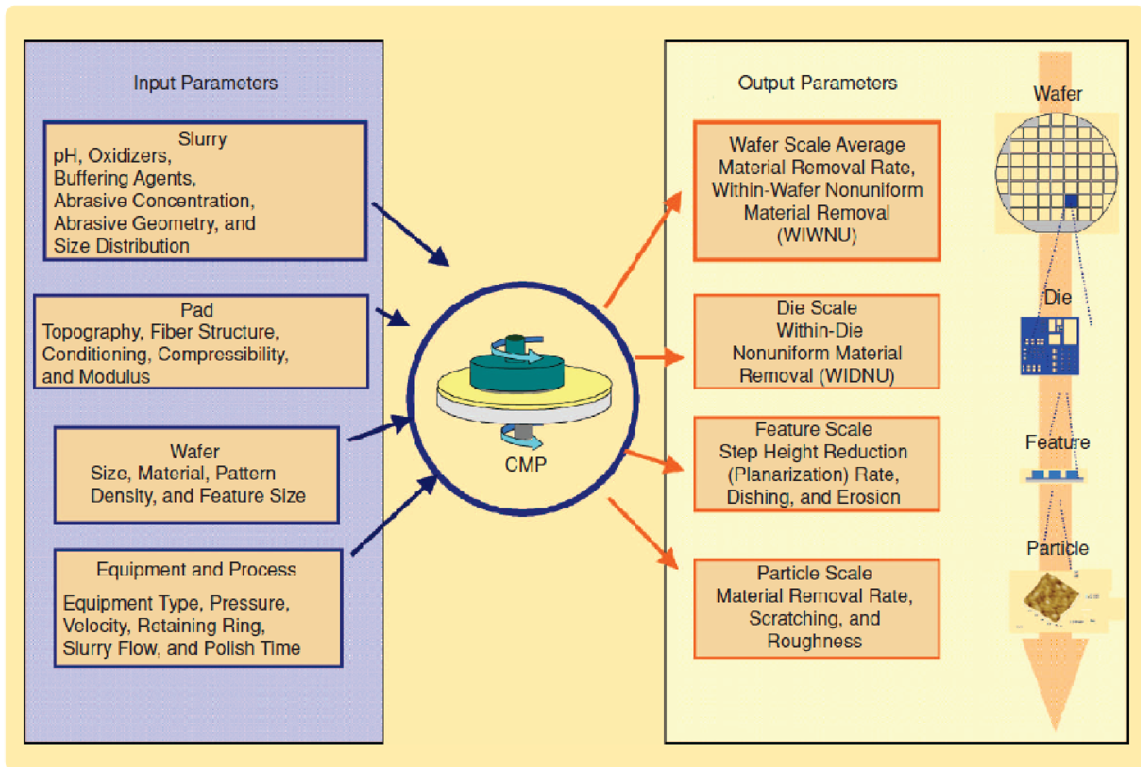

Figure 2: Input and Output parameters in CMP [2]

Carpio *et al.* [8] studied the and based chemistries having silica or alumina abrasive for copper CMP. For a slurry based on , which is a strong copper etchant, potentiodynamic curve shows no passivation behavior stating the copper dissolution, while for

NH_4OH^- based slurry passivation takes place. Figures 3 (a) and (b) shows, the d.c. potentiodynamic curve of (a) abraded and (b) non abraded copper surface in HNO_3 and NH_4OH. In HNO_3, absence of passivation was demonstrated by the steep slope in the anodic range and little difference between the corrosion potentials of the abraded and non abraded copper surface. However, the presence of passivation in NH_4OH was demonstrated by the 300 mV difference between these two corrosion potential.

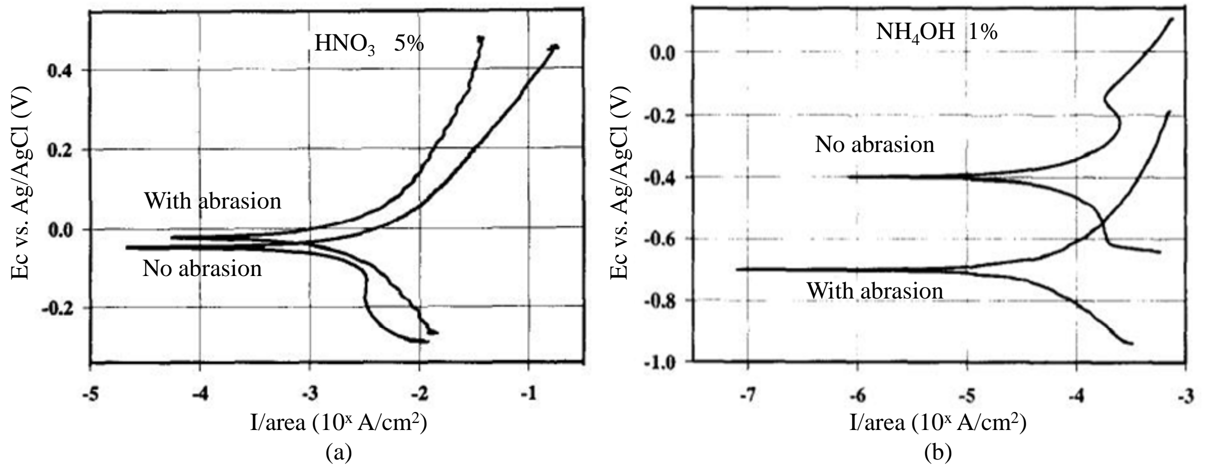

Figures 3 (a) and (b): Potentiodynamic curve of copper in 5% HNO3 and in 1% NH4OH

Ammonium salt-based slurries can mechanically improve the material removal process compared to KOH based slurries. The potential energy between the colloidal particles results due to attractive potential (by van dar Wall forces) and repulsive potential. Agglomeration occurs when the repulsive potential reduces compared to attractive potential. Agglomeration also occurs when reduction of electric double layer width takes place when salt was added in the neutral slurry causing decomposition of the salt in to anions and cations with reduced surface potential [9]. Figure 4 shows the dispersion and agglomeration behavior on silica particle surrounded by positive ions in high pH and neutral pH slurry solution. They found that the polishing selectivity increases in NH_4OH^- based slurry using $NaClO_3$.

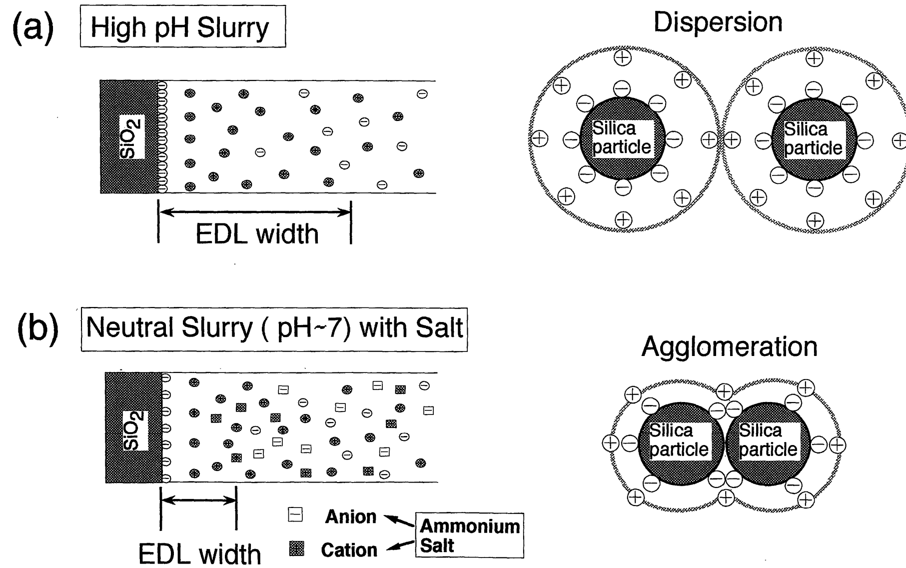

Figure 4: Dispersion and agglomeration of EDL on the silica particles [9]

Luo *et al.* [10] investigated copper CMP using Al_2O_3 abrasive in NH_4OH slurry medium with BTA addition to it. Polarization curves were used for measuring the corrosion current density for explaining the CMP behavior in this slurry. The dissolution rate of the copper decreases, when 0.05 M of BTA was used to control the etching rate of ammonium salt with the oxidizer. Addition of 0.1M of $NaClO_3$ into 3wt% NH_4OH slurry leads to an increase in the removal rate with slight increase in current density i.e. 2 nA/cm^2 indicating the mechanical dominance during polishing. Polarization curves were used for measuring the corrosion current density, which indicates that the process was more mechanical dominant.

Aksu *et al.* [11] showed improvement in the planarization during passivation. Glycine leads to higher chemical dissolution of material from the surface due to abrasion at 10^{-2} M glycine and pH 12 reduces the copper oxide formation thereby increasing the CMP performance [12]. They conducted *in-situ* polarization experiments to understand the electrochemistry of copper-glycine and have investigated open circuit potential (E_{OC}) at a pH of 4, 9 and 12. Figures 5 shows the electrochemical potential study with and without glycine at a rotational speed of 200 rpm and

27.6 kpa. In this case, abrasion will start at 60 sec at stable copper E_{oc} and second abrasion will start at 420 sec and this was observed in the case of pH 9 and 12 which will decrease rapidly due to copper and hydroxide removal [12]. The abrasion with glycine was observed to decrease less compared to without glycine from E_{oc} vs. time curve.

Doyle *et al.* [13] studied the chemical and electrochemical effects of peroxide in the aqueous solution containing glycine by modeling chemical effects on polishing. They found that the dissolution rate in acetate buffer with pH 3 and pH 4 is more as compared to higher pH. They found that an increase in the relative velocity leads to increase in the removal rate and high planarity as the film thickness of the slurry will increase in the case of high relative velocity [14]. Haba *et al.* [15] used fumed silica slurry settlement method to remove large particles (above 1μm) in slurry which leads to mirror like polish on the wafer with less defects.

Seal *et al.* [16] studied the interaction between glycine, hydrogen peroxide, and copper in Cu CMP using polarization curve, X-ray spectroscopy and AFM. They showed that removal rate decreases at higher concentrations of hydrogen peroxide but addition of glycine above 1%, increases the removal rate.

Du *et al.* [17] investigated the copper removal mechanism by combining the effects of hydrogen peroxide as an oxidizer, glycine as a complexing agent and β Tri-amino-triazol as an inhibitor. They found that the removal rate reduces below alkaline pH and dynamic increase in the removal rate occurs as 0.1 M of glycine is added in the hydrogen peroxide solution. The improvement in the planarization was further observed when BTA was added to that solution.

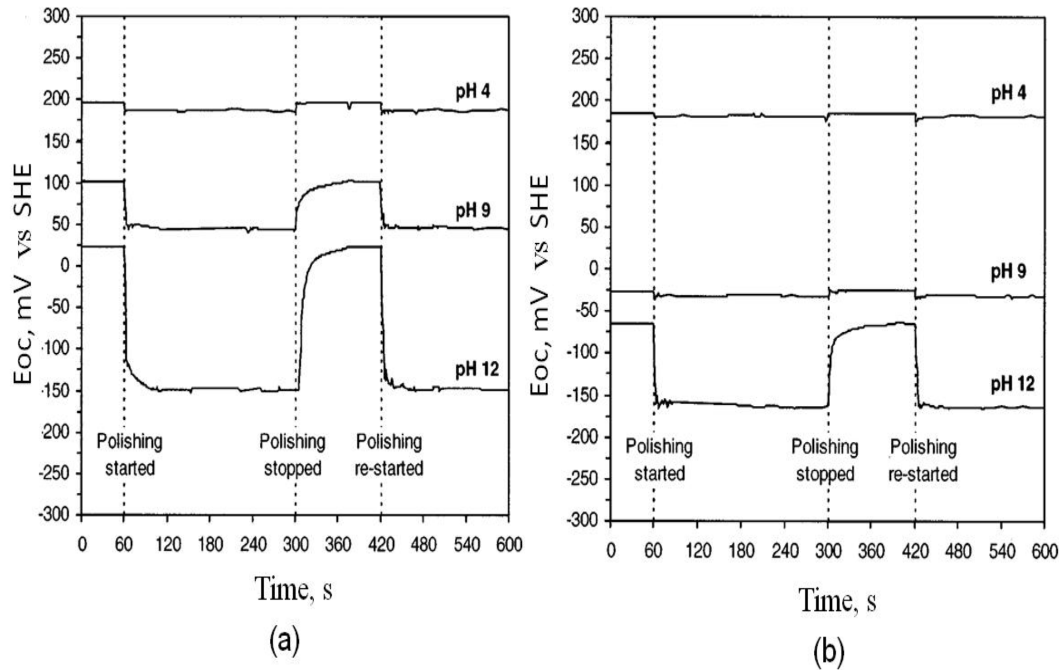

Figures 5 (a) and (b): Eoc of copper at different pH values with alumina abrasive (a) without glycine (b) with glycine [12]

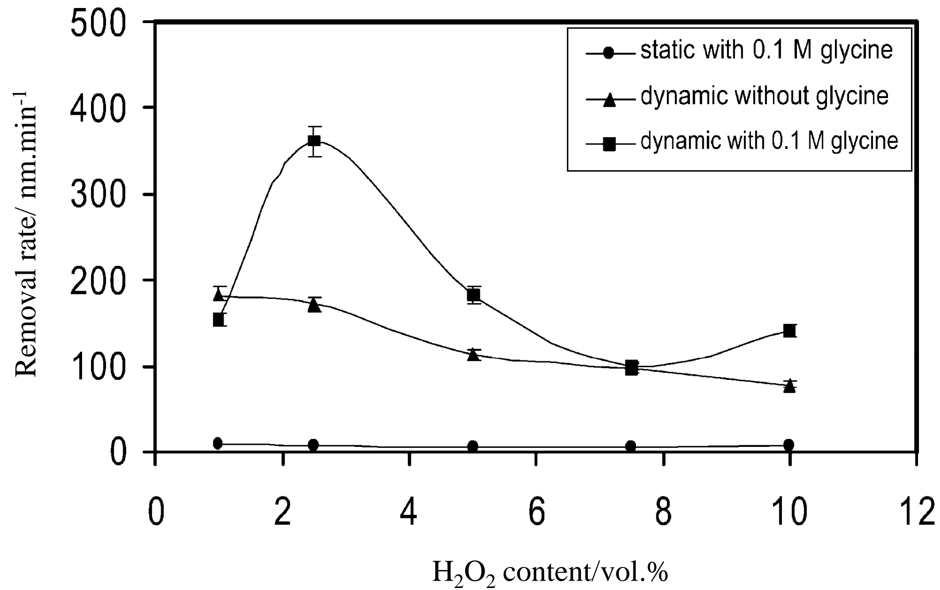

Figure 6: Variation of removal rate for different H_2O_2 concentrations [16]

Chen *et al*. [18] found the dissolution rate to increase with H_2O_2 and the passivation of copper to take place at its highest concentration. Moreover, the $Fe(NO_3)_3$ resulted in the absence of copper passivation. The dissolution of copper in both H_2O_2 and $Fe(NO_3)_3$ increases at high

rotation speeds. Gorantla *et al.* [19] proposed that the surface chemical reaction occurs when citric acid was added a complexing agent, with and without H_2O_2 in acidic and alkaline solutions. A high concentration of citric acid inhibits passivation of copper in H_2O_2 and results in an increase in the dissolution of copper [20].

Ein-Eli *et al.* [21] investigated the electrochemical behavior of copper with and without BTA in the absence of H_2O_2 in a Na_2So_4 based solution. They found that when BTA was added to this solution, copper undergoes a strong passivation below 0.2 V (SCE) and the protective layer of BTA was damaged by localized corrosion attacks above 0.2 V. The role of interaction effects of an oxidants and inhibitors in Cu CMP study using X-ray spectroscopy and secondary-ion mass spectroscopy showed that the presence of glycine in H_2O_2 leads to Cu-glycine complex. This resulted in the dissolution of copper. The BTA addition to this solution of H_2O_2 and glycine leads to Cu-BTA complex , causing decreased removal rate at pH 2 in 5% H_2O_2 , 0.01 M BTA, and 0.1 glycine [22]. Gorantla *et al.* [23] used different additives to investigate the importance of OH^- in the H_2O_2 slurry during Cu CMP. They found that the removal rate depends upon the interaction of different additives with Cu^{2+} and the pH of the slurry during the CMP process. Tsai *et al.* [24] investigated glycolic acid to improve the polishing rate, which also decreases the difficulty in post cleaning by electrostatic repulsion. The alkaline-based slurry having uric acid as an inhibitor and H_2O_2 as an oxidizing agent increased the polishing rate with passivation [25]. In acidic slurry, increase in the OH^- radicals in the slurry increases the removal rate, but it decreases on a further increase of OH^- radical after adding oxalic acid [26].

2.3 Abrasive:

Lin *et al*. [27] reported that finer and softer abrasives result in higher finish with less removal rate in the case of NiP/Al substrate. Gopal *et al*. [28] studied colloidal behavior of alumina abrasive through zeta potential and particle cluster distribution using different additives and agglomerate size distribution measurements. After the addition of glycine at a pH below 4, agglomeration reduction takes place due to Cu-glycine complex. However, a decrease in the

agglomerate size about 100-400 nm occurs when 0.2 wt% of H_2O_2 was added to the slurry [29]. The transition alumina particles [30] of 20 nm were studied as a futuristic abrasive in the CMP process. Its use in CMP results in superior finish and better planarity on a tantalum and thermal oxide layers.

2.4 Polishing pad:

Polishing pad acts as a carrier for a slurry transport, and the abrasives are embedded in the pores for material removal during polishing. It is generally made up of two layers i.e. a polishing layer and a substrate layer bonded together with an adhesive, which can be a hot-melt adhesive or pressure sensitive adhesive. In industries, the IC 1000 pad has a stacked layer of Suba IV, which is used for polishing.

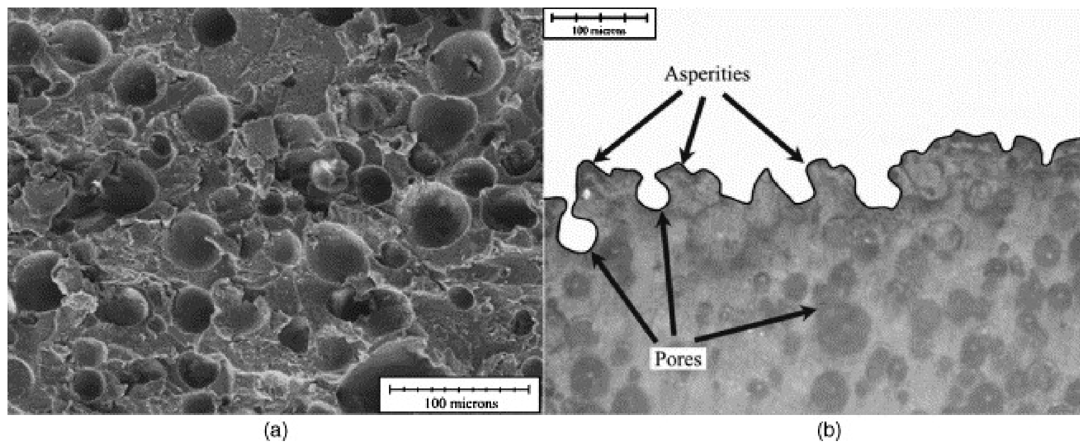

Figure 7: SEM of surface and cross section of a unpolished pad [31]

IC1000/ Suba pad has a superior slurry transport which results in good compressibility. This leads to uniform MRR and good planarity compared to the IC1000 pad. Figure 8 shows a comparison of the stacked IC1000 and Suba pad (top views and cross sections).

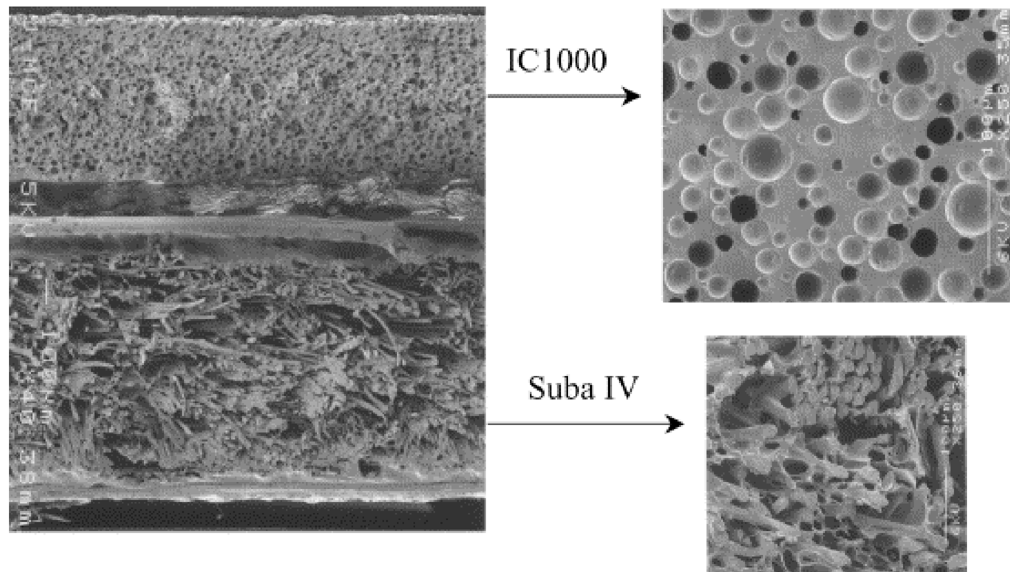

Figure 8: Cross-section (SEM) of IC1000/suba stacked pad [32]

Stavreva *et al.* [33] discussed the impact of the IC1000/suba pad on good planarity, which leads to a decrease in Cu dishing and SiO_2 thinning. During polishing, wear of unconditioned pad takes place due to rolling and fatigue caused by the high friction force and continuous polishing. However, in the case of the conditioned pad, pad wear caused by abrasion [34]. Three different kinds of conditions were used to study the properties change in the suba and the IC1000 pad. The first condition was soaking the pad in water for 5 hrs, secondly, increasing the pad temperature, and thirdly, pad conditioning. The shear modulus of the pad decreases, while the material removal rate remains unchanged during the soaking of the pad in water. Figure 9 shows the rate of decrease in the shear modulus in the case of IC1000 is higher than the Suba pad in the same temperature range. However, in the case of an increase in the temperature of the pad, reduction in the shear modulus and increase in the MRR takes place. However, the MRR is maintained and the planarization efficiency decreases after conditioning [35].

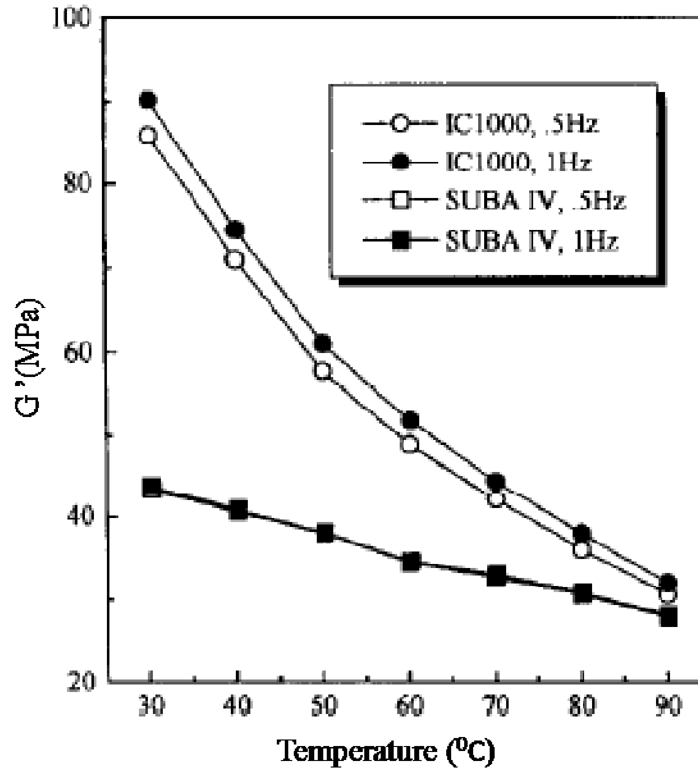

Figure 9: Dynamic shear modulus of Pads [35]

Byrne *et al*. [36] applied the finite element method (FEM) model for predicting the pad wear for studying planarization. They assumed flat pad geometry and consistent pad properties across the pad- contact. From this, they found that Von Mises stresses was low in the center of the wafer and increased 40% at the outer radius of the wafer as the pad wear. Different investigations were conducted for analyzing the pad property. The thermal analytically study of the soft and hard pads used four techniques i.e. dynamic mechanical analysis (DMA), thermal modulated differential scanning calorimetry (TMDSC), thermal gravimetric analysis (TGA), and thermal mechanical analysis (TMA) at different temperatures and at different times [37]. By DMA, a decrease in the storage modules at about 31-50% at a typical CMP temperature range of 25 ^{0}C -50 ^{0}C was shown.

Figure 10 shows the DMA scans and TMA runs for the hard pad with a 31% reduction in dynamic storage modulus (G'). No dramatic change in the coefficient of thermal expansion was observed in a typical CMP temperature range of 25 ^{0}C -50 ^{0}C.

From the TMA test, they concluded that the temperature of the hard pad should not decrease below 25 ^{0}C and not increase above 50 ^{0}C for a stable coefficient of expansion, while for the soft pad temperature, it should not increase above 85 ^{0}C. Additionally, they concluded that the elastic modulus of the soft pad is not affected in a typical CMP temperature range. The mobility or storage modulus increases with conditioning, which increases the performance of a hard pad [37]. Also, step height has an impact on planarization. When the step height was high, the pad did not touch the lower surface, even if it became rough or deformed thereby maintaining efficiency. However, as the step height was reduced with an increase in slurry temperature, the softer fiber of the pad increased efficiency. Also when the step height was further reduced, efficiency decreased because of pad deformation.

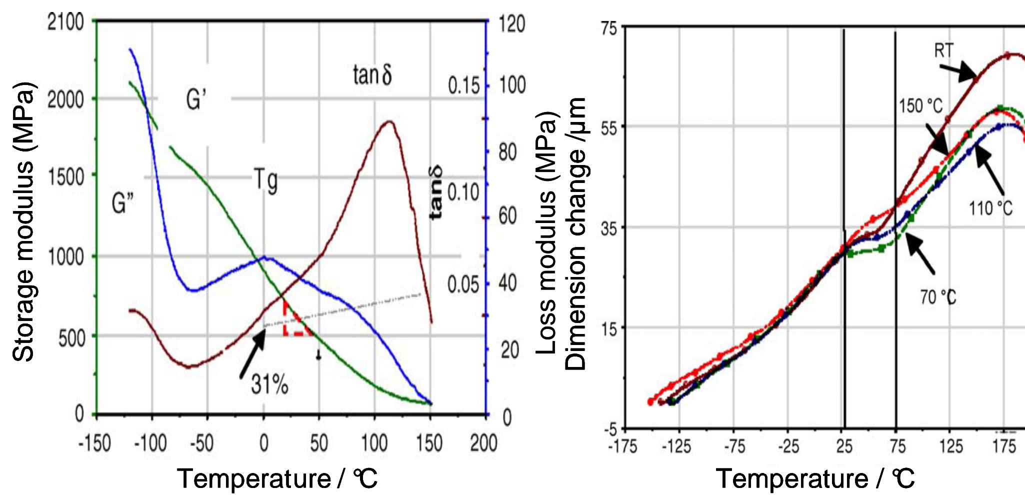

Figure 10: DMA and TMA run for hard pad [37]

Different types of pad characterization techniques were used to measure the pad shape before and after polishing. McGrath *et al.* [31] applied the contact i.e. stylus type profilometer and non-contact techniques i.e. white light interferometry (WLI) for studying microscale deteriotion of the IC/suba pad using roughness as a parameter.

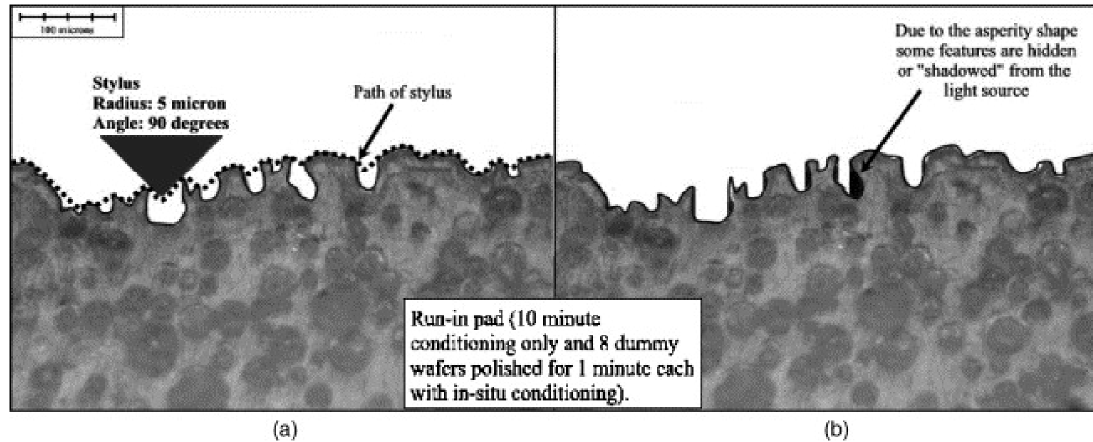

Figure 11: a) Path as mapped by 10 μm and 90 μm stylus. b) Pad surface mapped by WLI [31]

The stylus based technique was found to be inadequate for measuring pad features compared to WLI. The WLI images were plotted to investigate the asperity heights or scale before or during the polishing process for a better understanding of the wear phenomenon of the pad. Bearing parameters such reduced peak height (R_{pk}), core roughness depth (R_k), and reduced valley height (R_{vk}) displayed the asperity height which was not clear in the case of the average roughness parameters (R_a). This WLI based technique distinguishes between different conditions of the pad, which was not possible earlier [31].

The scanning electron microscope (SEM), white light interferometry, and attenuated total reflectance Fourier transform infrared method were used to measure the pore geometry, roughness of the pore height, and chemical changes in the pad after polishing [32] . They found by WLI, the pore of the used pad was smaller and shallower compared to the new pad. By using the IR spectrum, no chemical shift was found, which explains the absence of a chemical change in the pad after polishing. It indicated that physical and mechanical changes in the pad are prominent during polishing.

Hooper *et al.* [38] conducted roughness analysis to study the conditioning of the pad in the CMP process. The roughness of the pad decreases with polishing due to the flow of worn out pad material into the pores. Moreover, they concluded that the pad wear was more in the case of

higher conditioning density. Zantye *et al*. [39] used a new metrology and characterization technique for a newly developed polishing pad. The pad was made of polyolefin having a surface coating of ceramic (TEOS) using PECVD. The new pad was chemical resistant and an excellent adhesive compared to polyurethane, which can be used without conditioning. SEM was used for surface and cross section analysis. The properties were measured by nanoindentor having an indentation of 1200 nm. An X-ray photoelectron spectrometer was used for characterizing the surface modification using a base pressure of 10^{-10} torr. Also, the coefficient of friction (COF) was measured using a wear test by Kiedon 445 static COF tool. The polyolefin pad coating time was proportional to the elastic modulus and hardness resulted due to increased thickness. They showed an increase in the COF increases the wear rate. The mechanical properties of the soluble particles (WSP) based on nonporous pad with a porous pad (IC1000) were compared with temperature [40]. A nonporous pad, such as IC1000 pad was found to be densely cross- linked leading to higher decomposition at a higher temperature. The storage modulus of the WSP was high.

Yoshida *et al*. [41] studied the relation of pad roughness with the material removal rate at different ceria sizes. The removal rate was higher at a maximum pad roughness and with a decrease in crystalline size. Also, abrasive free technology appeared as the next viable option in CMP. A fixed abrasive pad in which the abrasives were embedded in the pad instead of in the slurry was studied, resulted in the exclusion of complex cleaning processes using deionized water. The material removal at the start was found to be less, compared to the conventional CMP process.

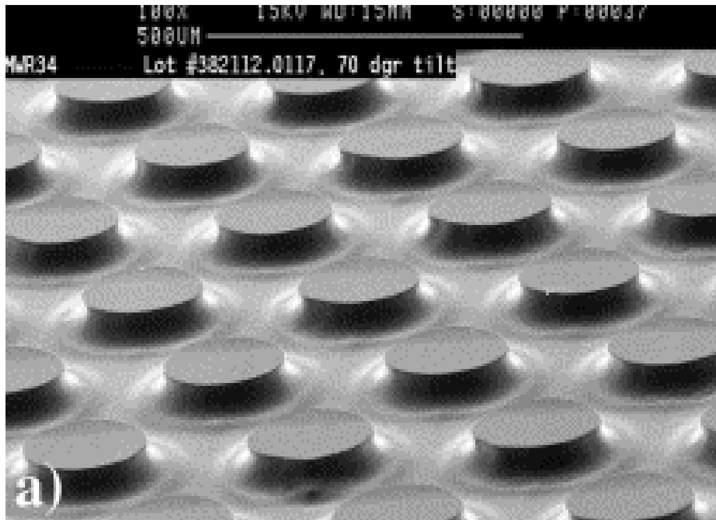

Figure 12: SEM of a fixed abrasive pad [42]

Nguyen *et al.* [43] studied the four different CMP processes to investigate the MRR, planarization efficiency, and step removal. These processes were conventional CMP with high and low abrasive content, abrasive free CMP, and fixed abrasive pad-based CMP process. There were two types of material removal in the CMP, i.e., lateral removal and top down removal. The top-down removal was independent of the feature size and pattern density, while the lateral removal (round off corner of feature) was dependent on the feature size and pattern density. They explained that the lateral removal of a fixed abrasive pad in the field area and the small copper feature were the same as compared to a conventional CMP, i.e., good planarity.

The fixed abrasive pad was used to study the material removal dependency in the case of Cu CMP [42]. Figure 12 shows the SEM of a fixed abrasive pad. The use of the fixed abrasive pad resulted in reduced polishing time with small dishing, independent of pattern density, and feature size by using optimized slurry having 15% volume H_2O_2 and pH of 3. The hydrophilic polymers, having a property of swelling and expanding with water, were studied for making fixed abrasive pads. This property of the pad results in self-conditioning of the pad by the frictional force between the pad and the wafer. This leads to the removal of a weaker layer, maintaining material

removal compared to conventional CMP [44]. Figure 13 explains the above self conditioning mechanism of the hydrophilic based pad.

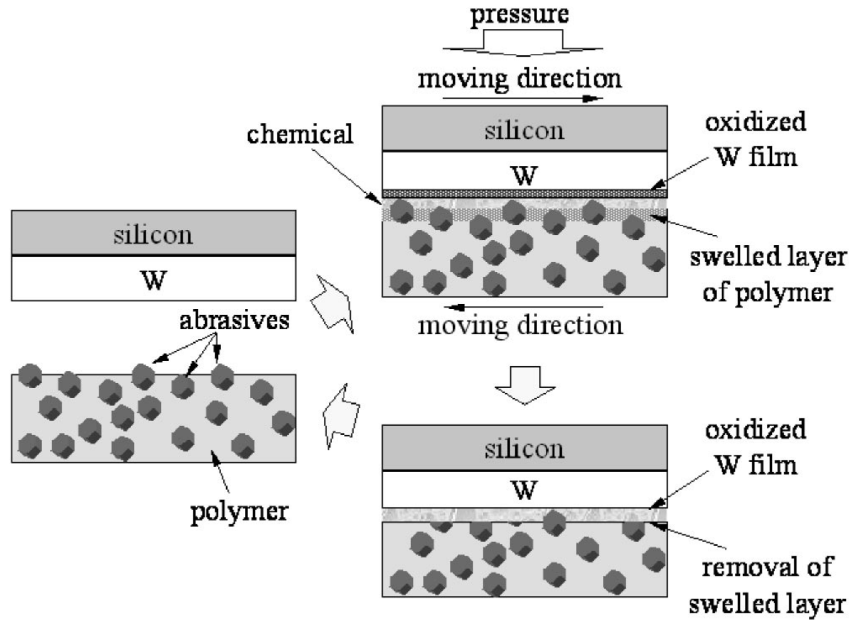

Figure 13: Polishing mechanism of tungsten CMP using hydrophilic polymer based pad [44]

Pad conditioning maintains the MRR by means of asperities conditioning before polishing. This leads to higher material removal as compared to after polishing [45, 46]

2.5 Temperature:

The temperature plays an important role in the CMP process. The temperature change leads to changing of the properties of the pad and slurry which are very sensitive to it. The increase in temperature of the slurry results in decrease in the elastic modulus of the pad and a higher material removal rate. The increase in temperature leads to a decrease in the hardness of the metal oxide layer causing an elastic deformation of the layer [47]. Generally, in the CMP process, heat is generated by the rubbing action of the pad on the wafer surface. This rubbing action or abrasive wear is of two types i.e. two-body abrasive or three-body abrasive wear [48]. In a two-body abrasive wear, the abrasive present in the slurry merged on the pad surface and acts rigidly like a cutting tool on the wafer surface. However, in the case of three-body abrasive wear, the abrasive

slides or rolls freely over the wafer surface. The three-body process is ten times slower than the two-body process. Therefore, it was concluded that the abrasive action in the CMP process is of a two-body type [48].

Figure 14 shows the relation of the temperature with respect to the relative velocity and pressure. In the CMP process, the temperature change is inversely proportional to the pH value of the slurry. The removal rate is greatly affected by the heat dissipation at the interface due to various changes it brings in the polishing pad. The variation in physical properties and the chemical kinetics of the polishing pad are the major changes crucial in the CMP process.

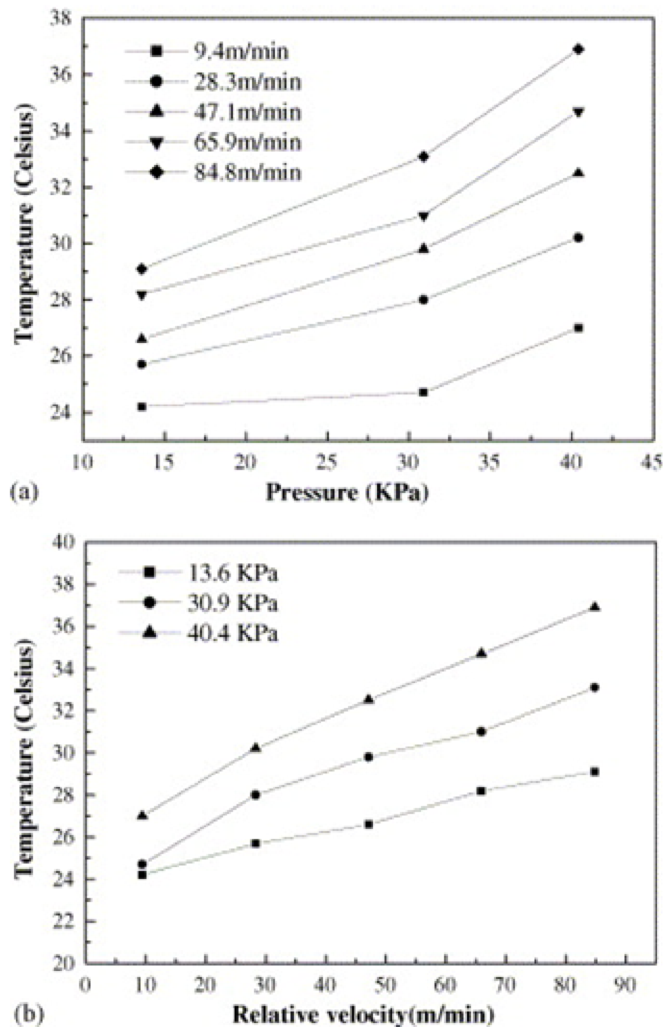

Figure 14: Variation of temperature with relative velocity and pressure [48]

An increase in the temperature of the slurry during polishing results in an increase in the coefficient of friction and material removal rate (using two different pads made of polyurethane). This resulted in an increase in the area of the contact of the pad-wafer interface causing increased shear force at the interface [49]. Figure 15 shows the coefficient of friction data during the CMP process at different temperatures [49]. The increase in temperature also results in an increase in the metal dissolution rate, dishing of the surface, and metal loss [49]. Figure 16 shows the change in dishing with temperature. The interaction of temperature affects the mechanical properties of the wafer. They found that increased slurry temperature results in an increase of the modulus and hardness of the polished copper surface due to work hardening. The rise in temperature causes a decrease in the hardness of the pad asperity, thereby the contact area between the pad and the wafer is increased.

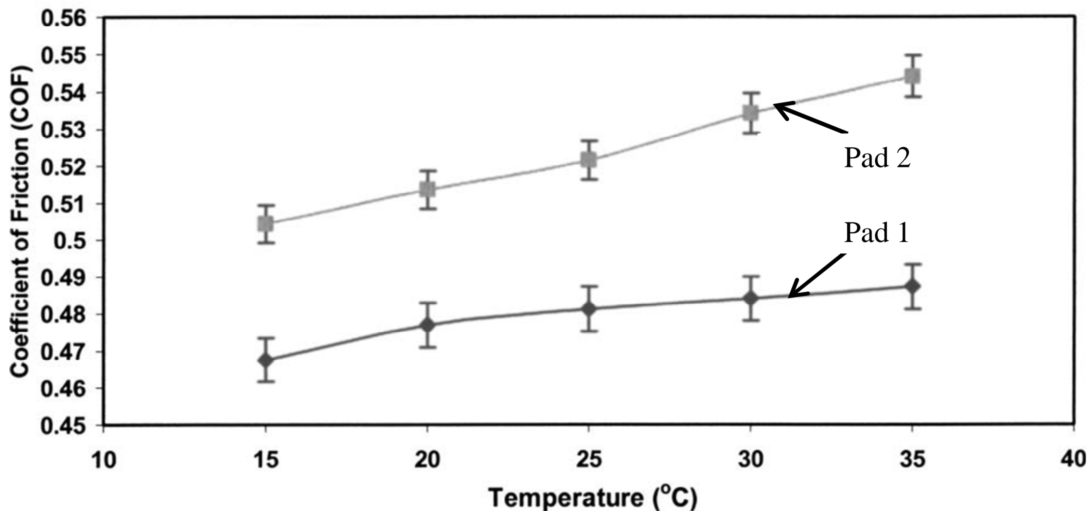

Figure 15: Variation of coefficient of friction with temperature [49]

Figure 17 shows increase in the contact area with increase in temperature. This states that the real contact pressure is proportional to an increase in temperature. This leads to a reduction in the removal rate as the pressure is decreased, which caused a reduction in the indentation of the abrasives [50]. Additionally, a shift in the chemical equilibrium state is observed due to a change in the temperature. The temperature rise leads to an increase in the particle size (due to increase in

kinetic energy). This causes the dispersed particle to colloid with each other, which further results in scratches on the film [50]. The pH of the slurry decreases with increase in temperature. The shift in the equilibrium state causes a change in the pH value with temperature because the equilibrium state is affected by absolute temperature.

Figure 18 shows that the variation of pH with temperature. The pH decreases from ~ 11 at $20\,°C$ to $\sim$ 9.3 at $70°C$. By a direct measurement under the substrate using a specially designed carrier, it was found that the temperature under the substrate was higher compared to the pad temperature [51]. In the case of oxide layer, an increase in the wafer temperature leads to an increase in a removal rate. The linear relationship between the temperature and removal rate of the oxide layer was found in Ref [52].

The uniformity of the oxide removal was increased due to reduced wafer temperature variation at a constant temperature of slurry and a densed grooved pad compared to a densed ungrooved pad. Mudhivarthi *et al.* [53] investigated the variation of dissolution rate in electrochemical machining and found an increase in the removal rate due to an increase in the interfacial temperature using electrochemical, and X-ray photoelectron spectroscopy. They concluded that at higher slurry temperature, oxidation of the surface occurs at higher rates in the slurry solution. This leads to higher material removal rate with no significant change in roughness. The non-uniformity occurs due to increased oxidation rate at higher slurry temperature [54].

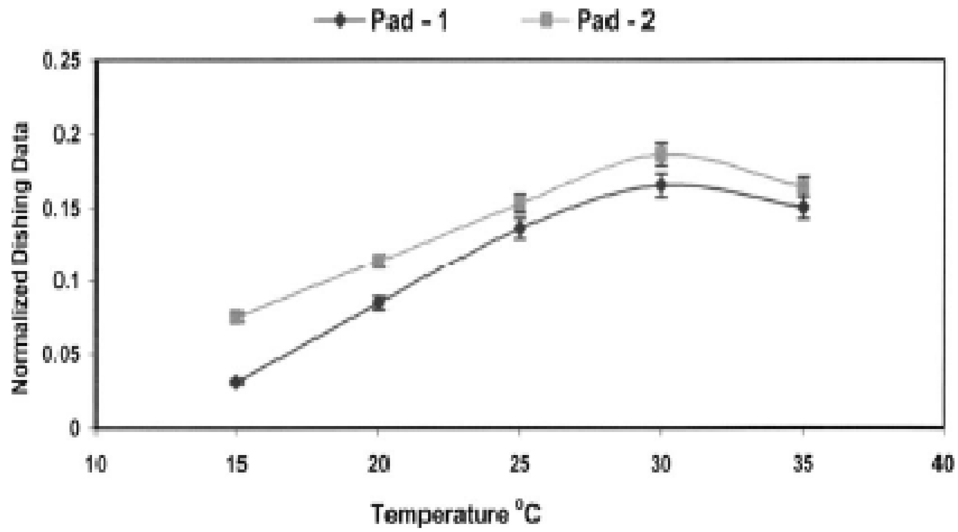

Figure 16: Effect of temperature on dishing [49]

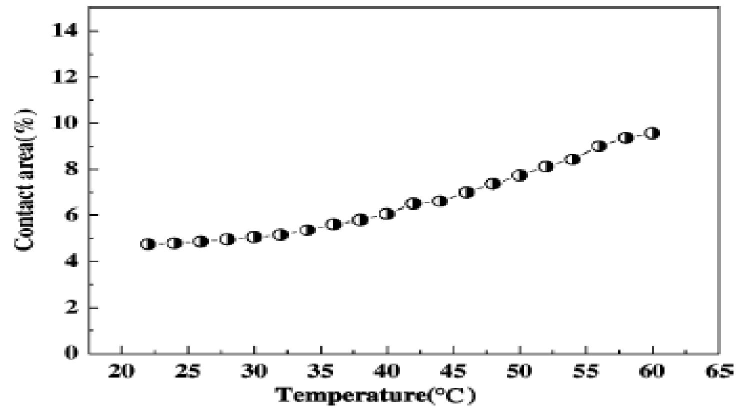

Figure 17: variation of real contact area with respect to temperature [50]

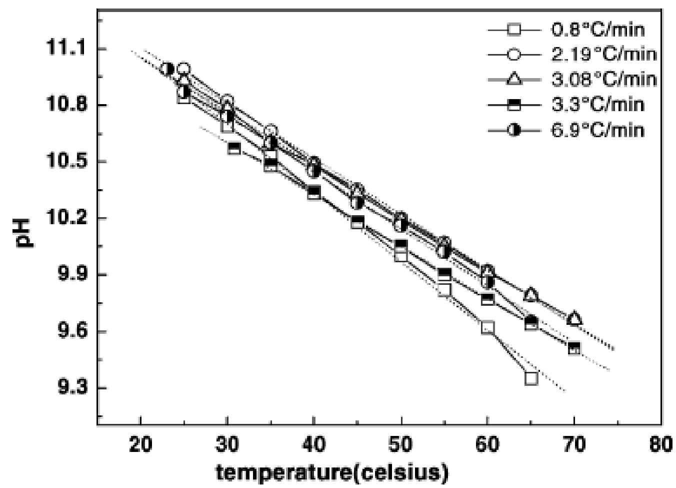

Figure 18: Variation of pH value with temperature [50]

2.6 Analysis of vibrations in CMP process

Figure 19 shows the CMP process vibration signal obtained during the polishing process. Initially at the start of polishing, asperities in the pad contacted with the wafer, which leads to vibration in an abrasive environment caused by an uneven friction [55]. However, as polishing proceeded, friction between the asperities and the wafer reduces as the roughness of the pad and the wafer decreases.

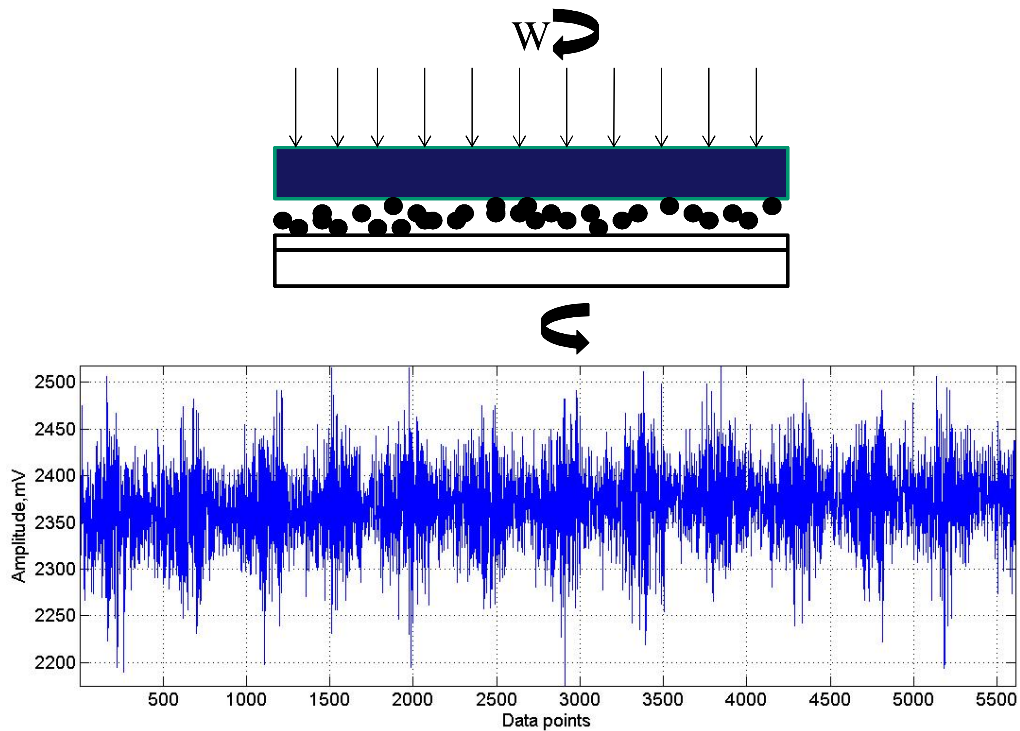

Figure 19: Vibration in chemical mechanical polishing

2.7 CMP Modeling:

According to Preston [56], the material removal rate in polishing of an material can be found empirically as the product of applied pressure and the relative velocity, which can be written as

$$\frac{d\xi}{dt} = k_p p v_R$$

Where $\frac{d\xi}{dt}$ the removal rate or polishing rate, p is the nominal pressure, v_R is the relative velocity, and k_p is the Preston constant i.e. which depends on the polishing surface roughness, elasticity, and chemistry at the slurry- interface. Various modified Preston equations were developed because of the following problem with the Preston equation i.e. gives a zero removal rate at zero relative velocity, fails to show that removal rate depends more on velocity than pressure and includes only mechanical synthesis with no chemical synthesis. Luo *et al.* [57] presented the following Preston equation

$$R = (KP + B)V + R_c$$

K = Preston coefficient

P = applied downward pressure

B = constant

V= Relative velocity

R_c =Purely chemical removable rate

This equation takes into account the variable for a purely chemical reaction of the slurry during the process and the other variable for a greater dependence of MRR on the relative velocity. Furthermore, it was stated that the thin layer formed on the surface does not follow the Preston equation correctly. For the case of a large PV, a constant is fitted in the Preston equation [58]. Wang *et al.* [59] proposed a removal rate model using a combined solid and fluid mechanics.

$$R.R = M(P,V)P^{5/8}V^{1/2}$$

Chen *et al.* [60] used dimensional analysis for modeling MRR using process and machine parameters where RR is the removal rate, DF is the downward force, BP is the back pressure, TT is the platen or pad rotational speed, and TR is the carrier rotational speed. The equation is given as

$$RR = A \times (DF/BP)^2 (TR/TT)^b$$

A modified Preston equation including an Arrhenius relationship was derived to study the effect of the pad temperature on ILD and copper s [61]**.** They combined a thermal factor in the Preston constant k which takes into account the information regarding thermal dependent and inter-layer independence of copper of CMP.

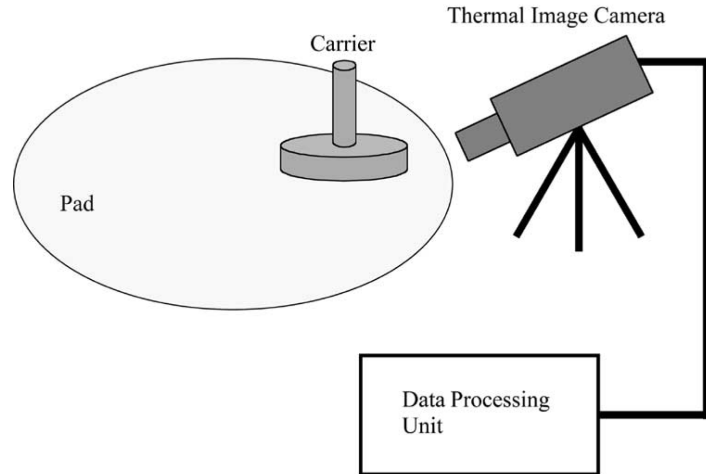

Figure 20: Infrared set-up for measuring the temperature at the -pad interface [62]

A MRR model based on solid-solid contact mode was studied on an assumption of plastic contact over -abrasive and abrasive-pad interfaces. It included various material parameters, namely, wafer hardness, pad hardness, pad roughness etc with process parameters i.e. pressure and rpm. The basic equation of this model is as follows [63]

$$RR = \rho_{\omega} NV$$

Here ρ_{ω} is the wafer density, N is the number of active abrasives, and V is the material removed by a single abrasive grain. The coefficient of friction between the pad and the metal interface was more when compared to the pad and dielectric layer. The slope of temperature rise in the case of pad-metal interface was found to be higher compared to the pad-dielectric interface. A regression-based pad temperature model was developed for predicting the endpoint detection using kinematic energy at the pad- interface [62]**.** They identified the onset of change when the error between the five continuous second order regressions was large and that change ended when this error was less for second order regression. Figure 20 shows the setup for measuring temperature

using an infrared camera. Li *et al*. [64] developed a model which showed a decrease in a material removal rate caused by the decrease in the temperature at higher flow rates. They showed that the rise in temperature of wafer was approximately twice as compared to pad. A dynamic model was presented for the material removal rate combining CMP process parameters and the energy flow mechanisms [65]. In the CMP process, most of the heat is carried away by the slurry flow and redistributed over the pad by radial convection. A thermal model of the heat generation, transport and heat exchange was developed on a flat and concentrically grooved pad. It was reported that the temperature of the is twice the pad temperature during polishing [66]. Lin *et al.* [67] applied an axisymmetric quasic-static analysis for the explanation of the CMP model. They used a minimum total potential energy and axisymmetric elastic stress-strain relation for that model. In that model, the slurry pressure was neglected, and the four layer structures were used for the model. They found that Von Mises stresses were uniform at the centre, followed by a slight decrease and a very steep increase at the edges (see Figure 21).

Yoshio *et al.* [68] devised a relationship for the material removal rate using the energy conservation law after modifying the Preston empirical relationship. They took into account the normal and shear components of the down force. A MRR model based on the assumption of

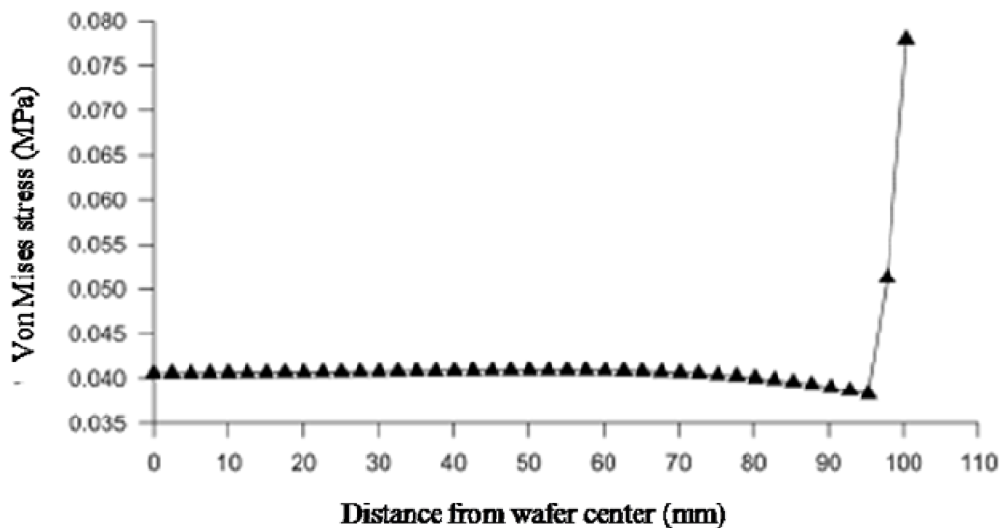

Figure 21: Variation of Von Misses stresses with distance from center [69]

perfectly plastic contact between the wafer and the abrasive in the oxide CMP was presented [69]. A wear model based on an elastic model was presented to model the MRR in Si CMP. This model relates MRR with the material properties. Further, they concluded that an increase in the pressure and pad rotational speed lead to an increase in the removal rate. However, carrier rotation speed, back pressure, and slurry flow does not play a prominent role in the material removal rate [70].

Chapter 3: Sensors in chemical mechanical planarization (CMP)

3.1 Vibration Sensors:

Vibration sensors are used for detecting defects in various manufacturing processes. Research is on-going for its applications in the semiconductor industry. Researchers at the Sandia National labs monitored the polishing process using piezoelectric accelerometers placed in the horizontal and vertical position [71]. The horizontal position was found to be more appropriate for capturing the dynamics of the CMP process than the vertical position. They also suggested the application of accelerometer at low rpm of the platen and carrier as other factors dominate the acceleration signals at higher rpm. Figure 22 shows the implementation of sensors on the polishing head using a slip ring [72].

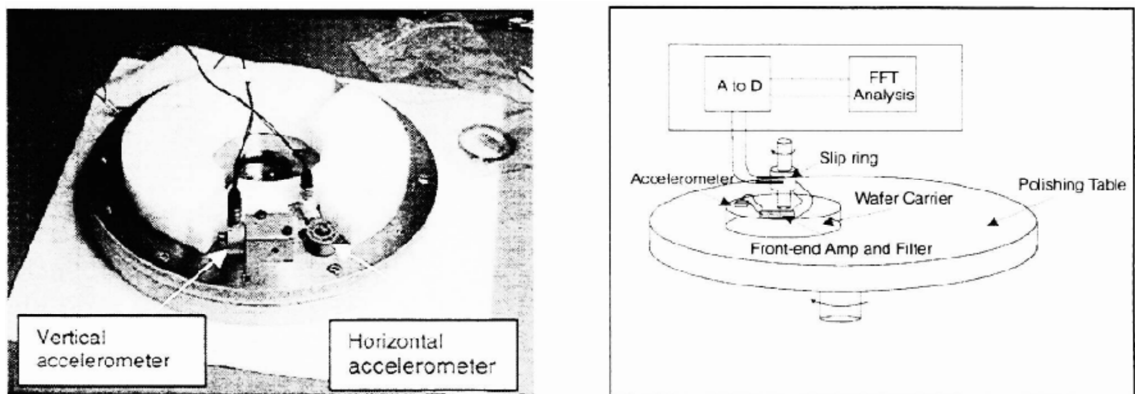

Figure 22: Acceleration sensor implementation and procedure [72]

Kojima *et al*. [72] at Fujitsu implemented a vibration signal based monitoring system for end point detection as well as for monitoring of other polishing abnormalities, such as peeling, slipping. Various issues related to the sources of mechanical vibration, such as floating structure of polishing head, head rotating shaft connecting material, change of material of the retainer ring i.e. noise were investigated. However, they have not monitored the vibration along other two axis as vibrations monitored along these axis may be more significant. Figure

23 (a) and (b) shows the vibration-based monitoring system which includes a signal conditioning unit, such as an amplifier, AC/DC [72] .

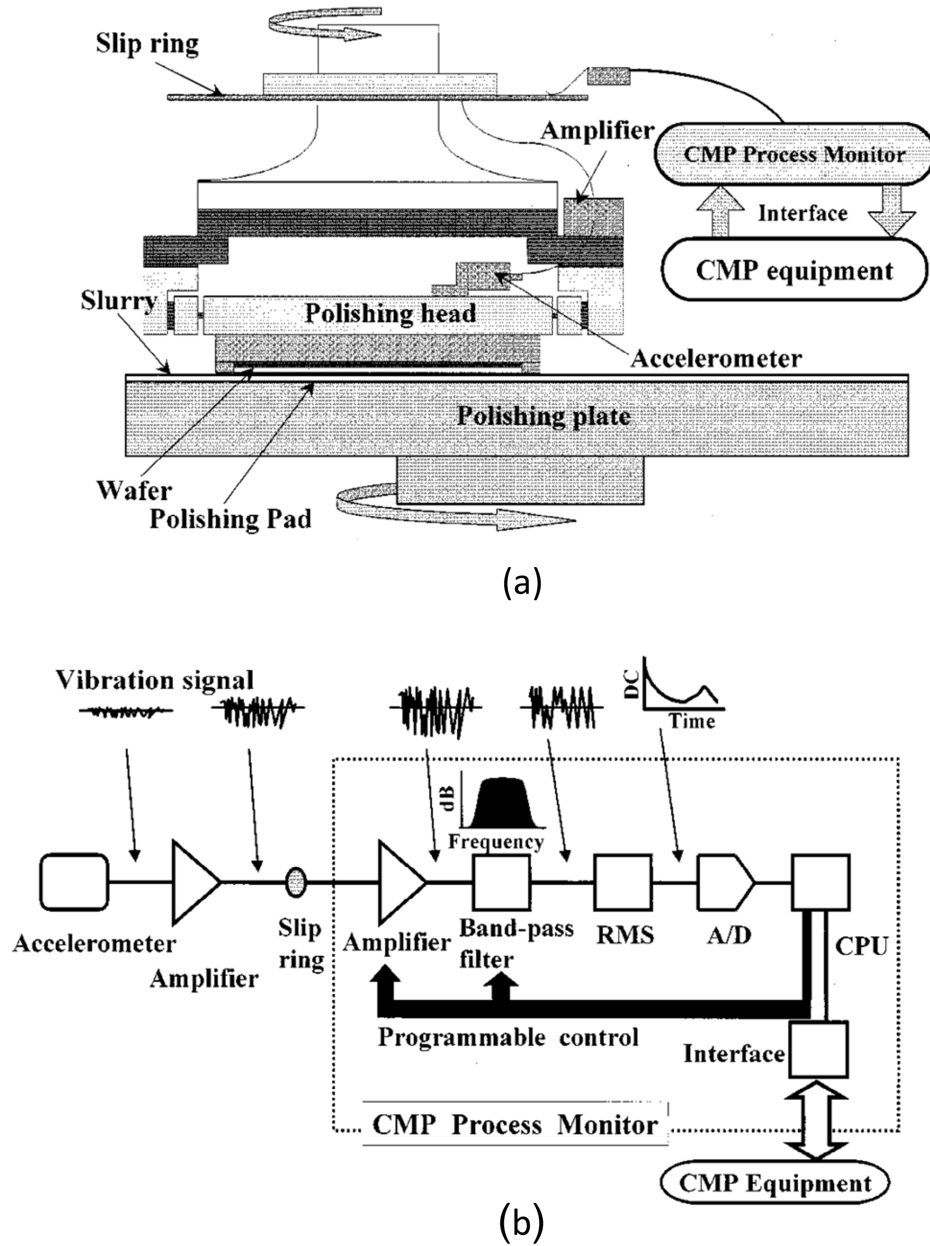

Figure 23 (a) and (b): Vibration signal based monitoring system [72]

Fukuroda *et al*. [73] developed an *in situ* monitor technique for detecting the uneven surface, pad wear, and uniformity at the surface of wafer. They demonstrated different polishing events using accelerometer signals through signal processing technique. Using the vibration monitoring system [73], they showed that the spectra signal decreases as polishing proceeds (See Figures 24).

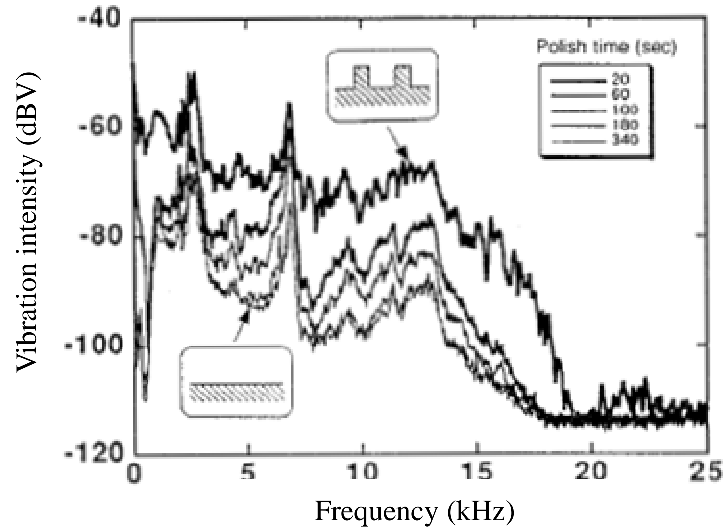

(a)

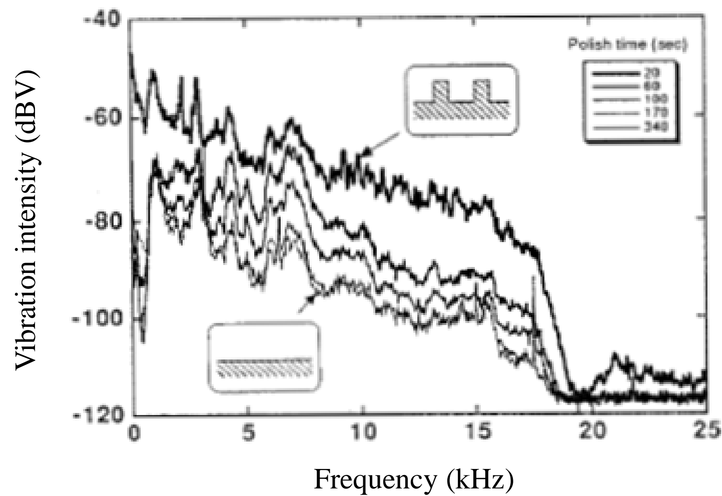

(b)

Figures 24 (a) and (b): (a) Horizontal and (b) Vertical components of the vibration spectra of a polishing head [72, 73]

Additionally, they implemented this monitoring system for copper CMP in which they used it to monitor the end point detection, which is more complex as compared to other issues, such as dishing and erosion [74]. They reported that the monitoring system can detect various abnormalities even during the change in the initial film thickness, slurry flow rate, and polishing rate. They detected the end point in polishing to be in vibration band range in the range of about 5 kHz to 15 kHz [73] under various polishing conditions. Figure 25(a) and (b) show the vibration intensity change under various conditions.

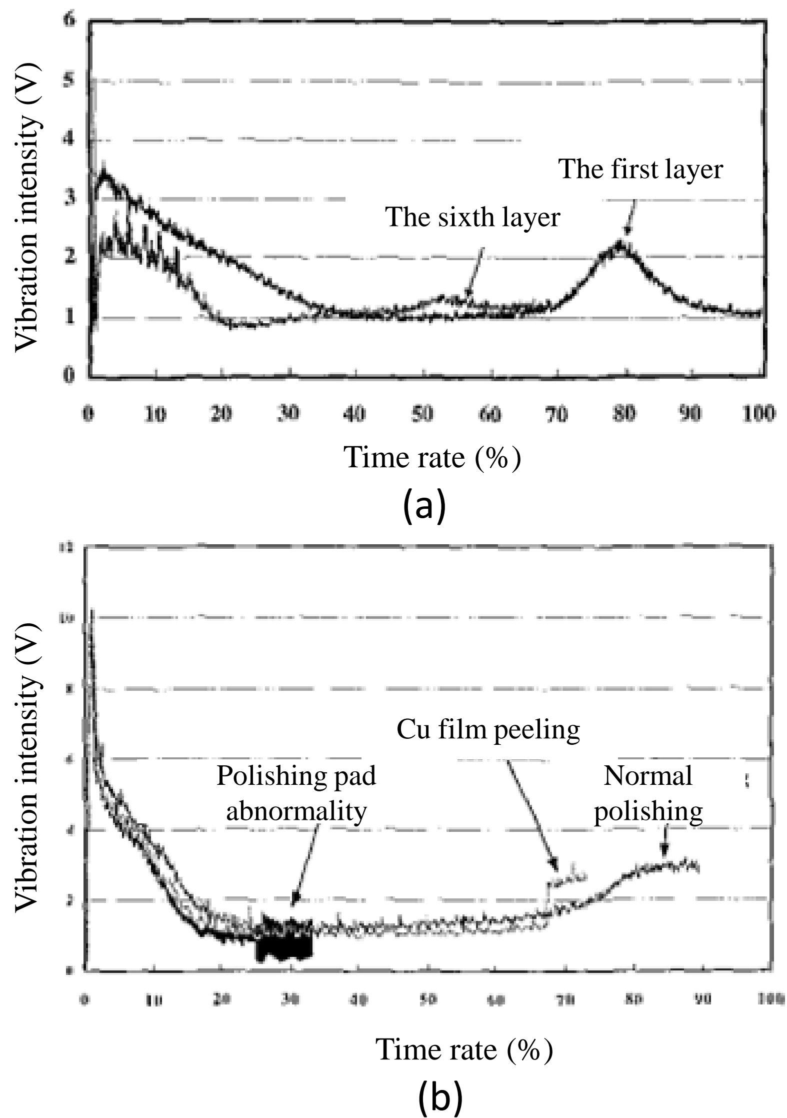

Figure 25 (a) and (b): Vibration intensity change detection during (a) copper multilayer polishing and (b) under different defect exposures [74]

Bukkapatnam *et al.* [75] developed a sensor based modeling approach to model MRR using various nonlinear techniques to demonstrate the nonlinearity of the CMP process. Using this technique, they bypassed the problem associated with empirical technique namely modeling was with low predictability. Also various statistical features, such as mean, skewness, and nonlinear features, such as, embedding dimension, time delay, maximum Lyapunov exponent etc. were used for the above modeling technique. Phatak *et al.* [76] used the multi-sensor based modeling approach to track slurry variations during Cu CMP through wireless and wired vibration signals. It may be noted that the analysis was performed offline. The PCA based regression analysis was successful in tracking the variation in slurry parameters with high predictability compared to the statistical model. This model was used for predicting optimum process parameters and MRR.

Maury *et al*. [77] used a vibration sensor to monitor the endpoint by vibration signals. Figure 26(a) shows the vibration sensor arrangement in the CMP apparatus. The vibration sensor is mounted on the wafer carrier to sense the vibration in the horizontal and vertical directions. The presence of an oxidizing agent in the slurry oxidizes the conductive layer. This layer is abraded by the abrasives in the slurry leaving behind the metallic layer. The exposed metallic layers exhibit different material properties, namely, the hardness and coefficient of friction. This result in a change in the frequency of the vibration related to that layer. This change in the frequency was then detected and monitored by the vibration sensor.

Kramer *et al. [78]* used seismic sensor for monitoring the conditions of consumables using seismic signals. Figure 26 (b) shows the seismic sensor attached to the drive assembly of the conditioning unit. In this, various consumables, such as, the conditioner, pad, slurry, and components of polishing head were monitored for the process stability. The seismic signals are indicative of the vibrations. They were monitored from the drive assembly for estimating the status of the consumables. Also, the acquired signals at each time point of the predefined

polishing conditions were used for estimating the lifetime of the consumables. Based on the seismic signals, the process conditions were controlled for process stability.

Pattengale *et al.* [79] used an accelerometer for CMP endpoint detection through spectral analysis . Figure 26 (c) shows the accelerometer-based arrangement in the CMP apparatus. In this, the accelerometer was coupled to the machine frame, and mounted under a platen of the CMP apparatus. The accelerometer measured vibration signals. An electrical signal proportional to the process vibration was received by the spectrum analyzer. The change in the amplitude or frequency of one or more frequency components was detected for end-point detection, i.e., when the metal above the layer was polished. Additionally, the process conditions in response to this change were modified for an effective control of the process.

Lim *et al*. [80] used vibration sensor to monitor the pad condition through vibration signals. Figure 26 (d) shows the accelerometer mounted on the supporting arm of the pad conditioner. The vibration signals from the conditioning arm were correlated with pad wear for monitoring the pad conditioner. The temporal signals were transformed to the frequency domain using Fast Fourier Transform (FFT) for analyzing the process in the frequency domain. The negative feedback loop was applied for real time monitoring of the pad conditioner by controlling the number of the sweep and head pressure of conditioning device. The process conditions were terminated where the amplitude of the abnormal peak increases to the maximum value.

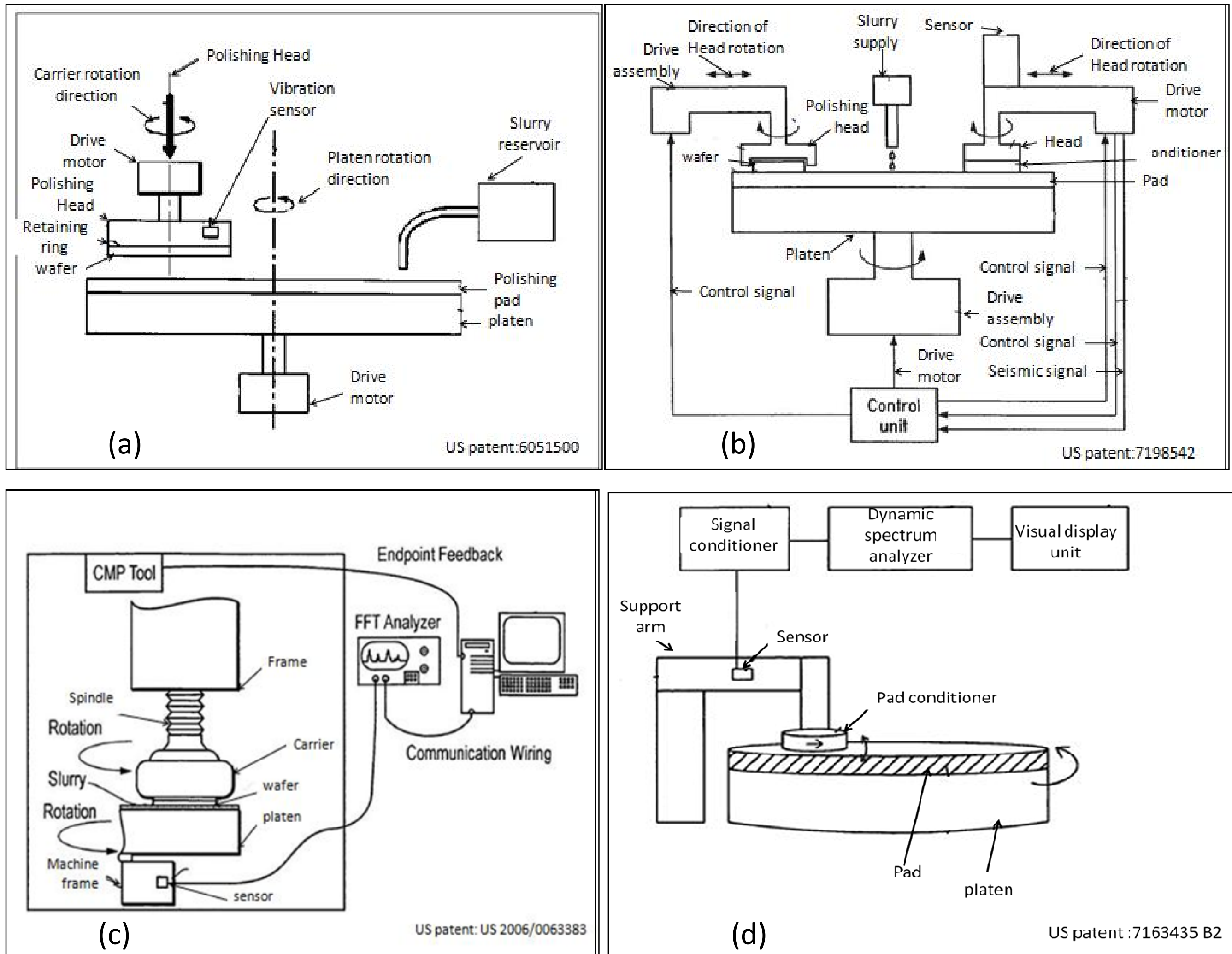

Figure 26: Vibration sensor monitoring systems in CMP [77-80]

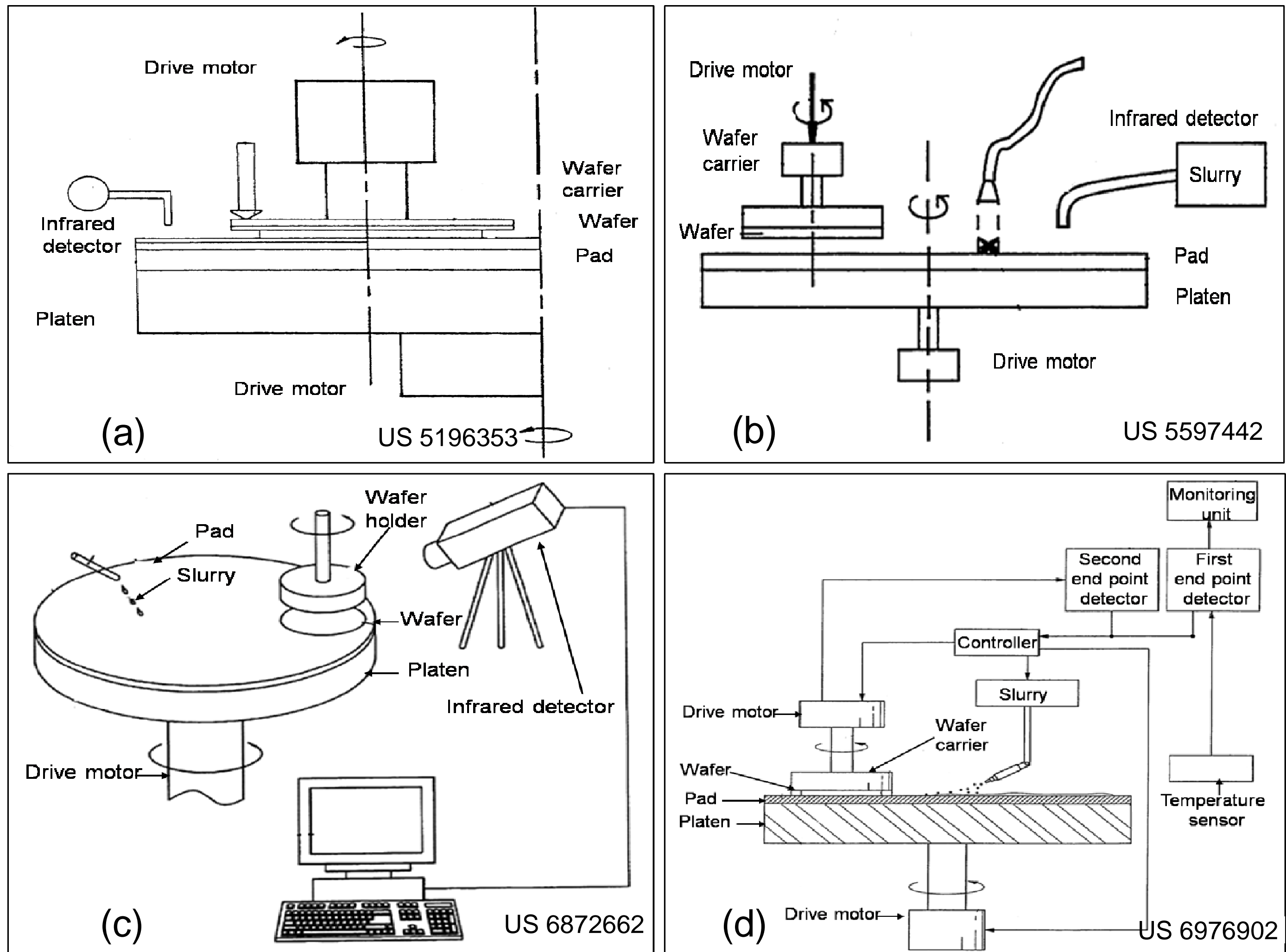

Figure 27: Thermal monitoring systems in CMP [81-84]

3.2 Thermal sensors:

Heat is generated by friction between the pad and the abrasive in the CMP. This is manifested by increase in the temperature. Sandhu *et al.* [81] established an CMP process control by thermal image of the . Figure 27 (a) shows the thermal monitoring arrangement using infrared detector in the CMP apparatus. The rise in temperature at different points on the wafer has resulted due to change in the coefficient of friction. The real time infrared image of the wafer was developed by periodic scan of the temperature using the thermal imaging camera mounted to the platen. The endpoint of the process was detected by the rise in temperature when the first layer was polished.

Chen *et al.* [82] established an i*n-situ* endpoint detection by thermal monitoring of the pad. Figure 27 (b) shows the thermal monitoring arrangement of the pad. Endpoint of the process was detected when the temperature at a selected position on the pad decreases $2°C$ below the maximum temperature reached. Endpoint was detected when the pad temperature decreased below the maximum temperature of the pad at a slurry temperature of 20 °C to 22 °C. Figure 28 shows the variation of the pad temperature with time during the polishing process. The increase in pad temperature initially is due to friction. The maximum temperature is due to local high pressure in between the pad and the rough topography of the wafer and endpoint is the event where the topography of the surface is smoothed. With further in polishing time, the temperature of the pad reduces after the endpoint.

Hocheng *et al.* [83] determined the endpoint detection of the CMP process using temperature changes. The temperature of the environment and the temperature at one point of the pad were measured by an infrared camera. Then a curve was plotted using temperature difference between the environment and pad temperature. Figure 29 shows the variation of the temperature slope during the polishing process. The total slope of the curve includes three slopes, namely, first constant slope, second non-constant slope, and third constant slope. The dots in the curve represent the rise in the temperature at one portion of the pad while the line represents the rise in

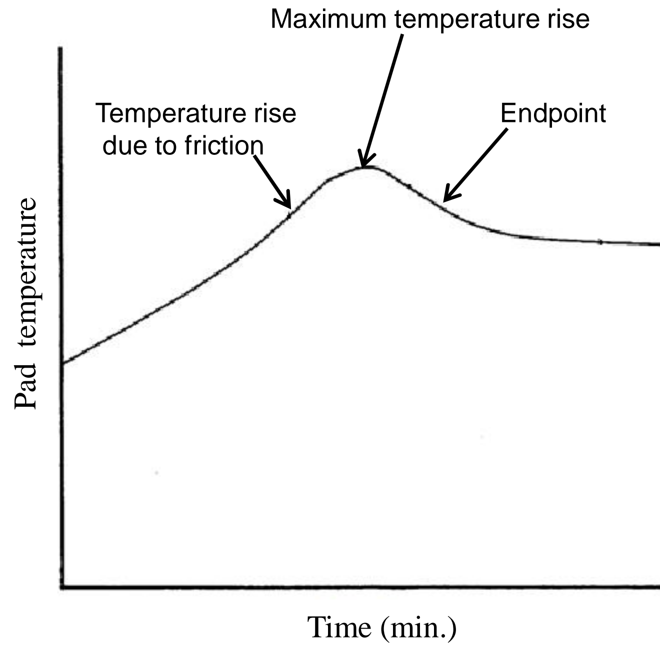

Figure 28: Variation of pad temperature with polishing time [82]

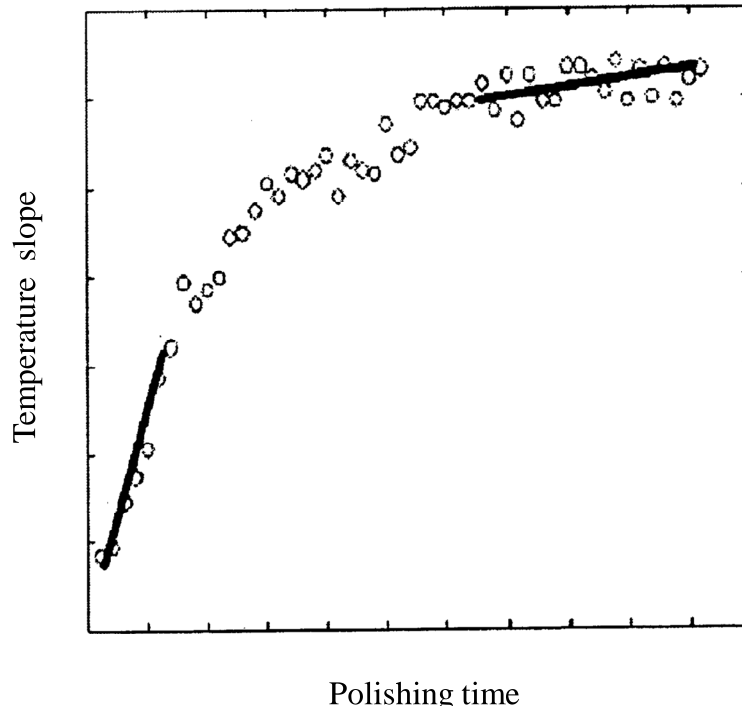

Figure 29: Variation of temperature slope with polishing time [83]

the temperature of the area of the pad. The endpoint was detected by the turning point between the first constant value slope and second constant value slope.

Koo *et al.* [84] used the multisensor arrangement for endpoint detection of the CMP process. In this, temperature of the slurry was measured by the sensor attached to the bottom of the carrier head and temperature of the pad was measured by an opening on the table meant for measurement. During the polishing process, frictional force is generated that leads to a steady increase in the temperature of the pad or at a constant level due to this frictional effect. However, there occurs a sudden increase in the temperature when the first layer was polished. Figure 30 shows the variation of temperature with time during a multilevel polishing illustrating the endpoint detection in the CMP process [84] . Point P is the point describing the endpoint detection point or where first layer is polished and after that the second layer is going to be polished that leads an increase in the frictional force. This results in increased temperature of the wafer or the pad.

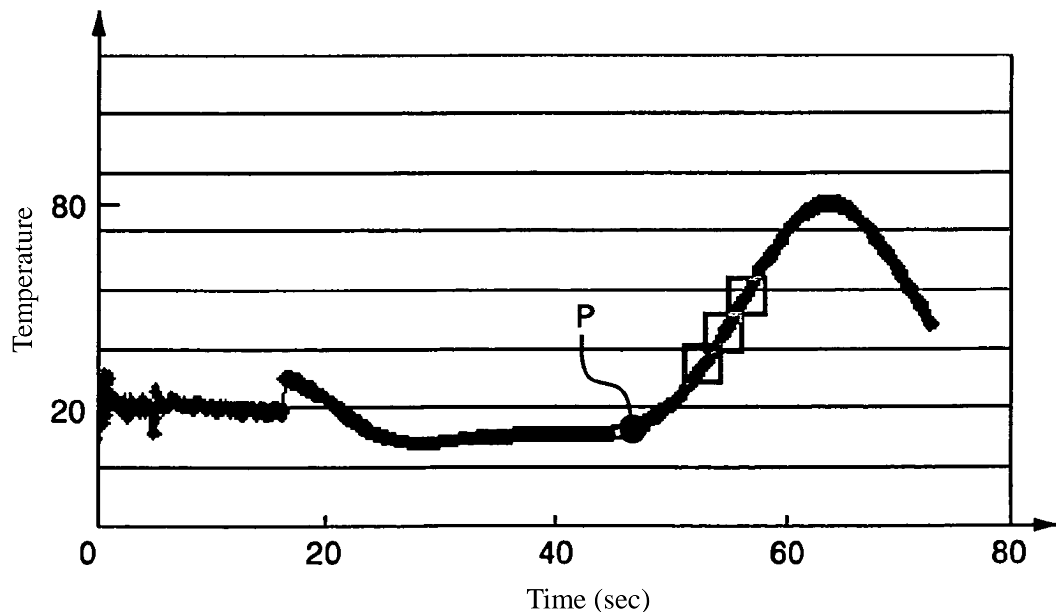

Figure 30: Variation of temperature with time in multilevel polishing [84]

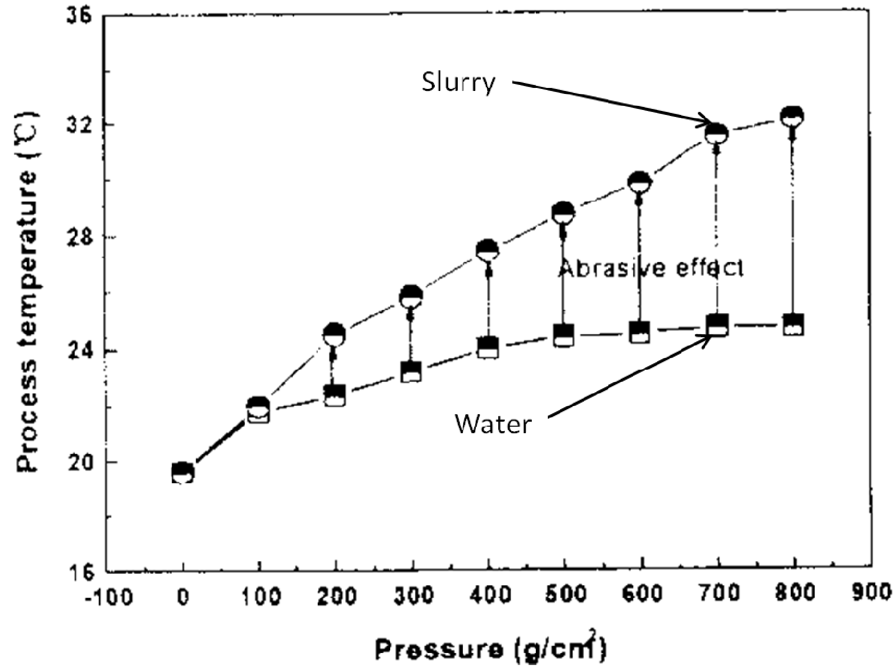

Figure 31: Variation of temperature with pressure for slurry and water in CMP process [85]

3.3 Acoustic emission sensor (AE):

AE sensors find applications in many manufacturing processes from abrasive to abrasive-free processes, including, machining, grinding, lapping, and polishing [86] [87]. This sensor has the widest range of sampling rate compared to other sensors. Figure 32 shows the AE sensor integrated in a Toyoda ultra-precision float polishing machine (Model SP46) based on CMP apparatus. The sensor is attached in the middle of the platen.

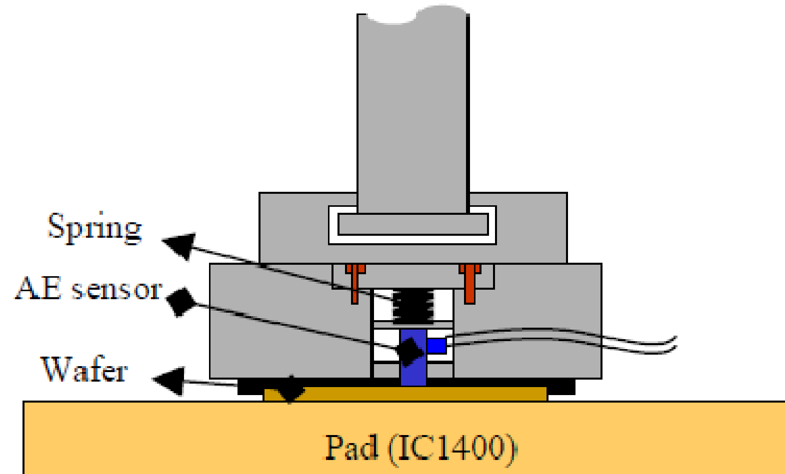

Figure 32: AE sensor arrangement in the CMP process [88]

Tang *et al.* [89] used AE sensor for monitoring and characterizing the CMP process. This was used to monitor the scratches generated during the process. A three-stage polishing regime, namely, loading stage, self-accommodation stage, and equilibrium-stage during the polishing process using AE signal. The loading stage was the stage when wafer contacts the pad, self accommodation-stage occurs due to unsteady state of friction caused by the geometry of contact during the start of polishing, and equilibrium stage was the stage where stabilization in material removal and surface roughness were established. Figure 33 shows this polishing regime in CMP. The first regime lasts 2-3 seconds, the second regime lasts for about several tens of seconds and at the third regime, a constant level and variance can be observed in the signal. Figure 34 shows the AE signal with numerous spikes obtained when 1μm size diamond grits are added to the slurry intentionally to cause scratching.

Using the AE sensor, Hocheng *et al.* [90] developed a regression model for the end point detection (EPD) using energy features from the AE signal. A decrease in the signal energy was observed when the metal layer was polished. Choi *et al.* [88] used AE sensor to track variation in slurry chemistry during the polishing process. Three distinct variations were observed in the signal with variation in the slurry content. Figure 35 shows the AE signal during polishing. At

the start of polishing with water, the RMS of the AE signal was 1.67 V followed by a decrease in the signal to 1.2V after adding glycine as a complexing agent. Further transition in voltage was observed at 1.1 V after re-oxidation with H_2O_2.

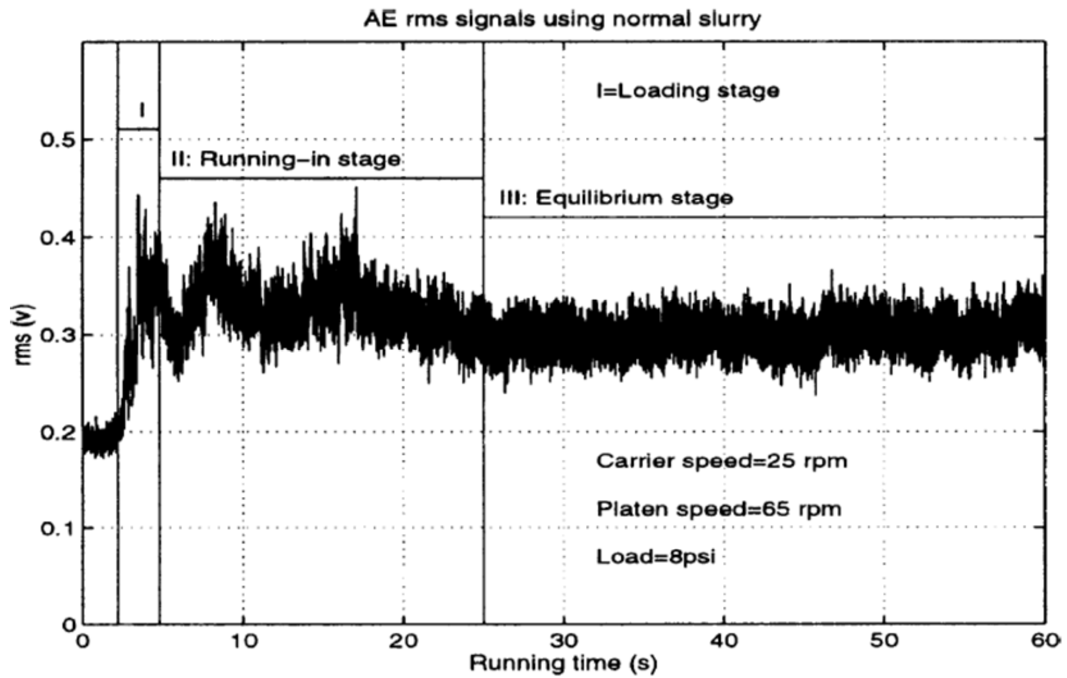

Figure 33: AE signal during polishing [89]

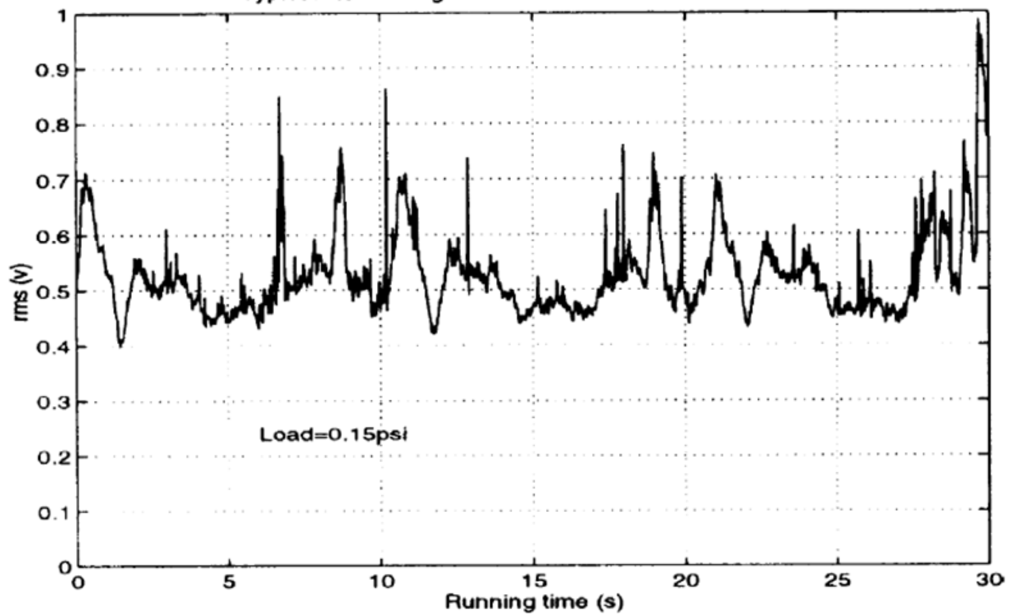

Figure 34: AE signal obtained when micro scratches were formed [89]

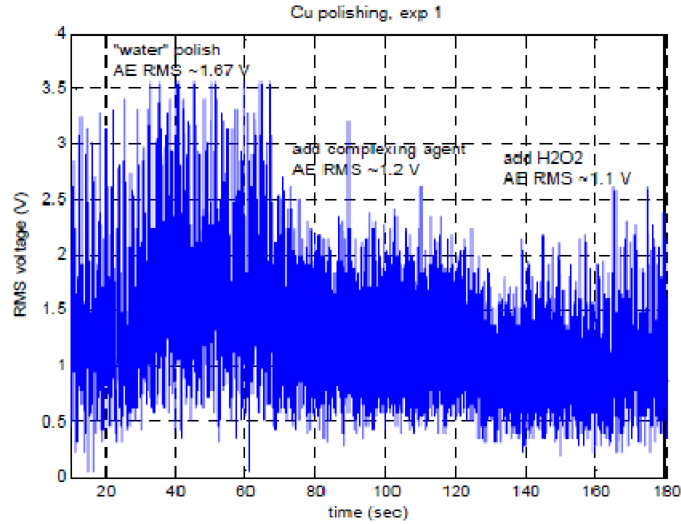

Figure 35: AE signal without abrasive [88]

Ganesan *et al.* [91] studied the delamination defects in CMP using wavelet- based strategy on AE sensor signal. Wavelet-based multiresolution was applied for monitoring the CMP process. Figure 36 shows the cumulative energy of AE signal at 16 levels of decomposition. The out of control signal's cumulative energy was higher than in control of AE signal. Also, the energy in both cases was significantly higher, up to 6 levels.

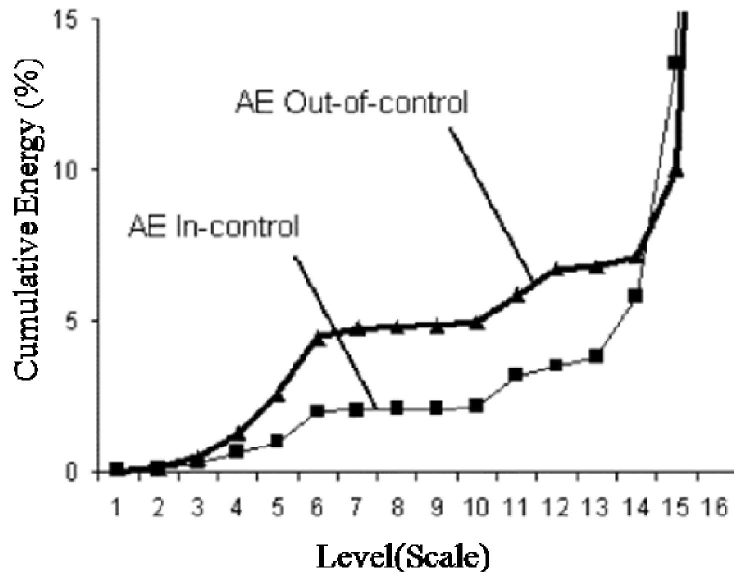

Figure 36: Cumulative energy for 16 levels for in-control and out-of-control AE signal [91]

Table 1: Patents on vibration sensors in CMP

	US Patent No.	Issue date	Inventor	Assignee	Title	Brief Description
1.	6051500	18 Apr. 00	Maury *et al.*	Lucent Tech.	Device and method for polishing a semiconductor substrate [77]	A multilayer CMP was described in which the process vibration was detected by a vibration sensor. A change in the signal was described as the layer gets polish.
2.	7198542B2	3 Apr. 07	Kramer *et al.*	AMD	Method and system for controlling the CMP by using a seismic signal of a seismic sensor [78]	A CMP control system was described for the detection of condition of consumables in polishing. Also status of the conditioner used can be detected by the system. The seismic sensor was used to detect the process vibration in the system.
3.	6431953B1	13Aug. 02	Carter *et al*.	Cabot, IL	CMP process involving frequency analysis based monitoring [92]	A CMP control using an algorithm was described. In this, the signals from different sensors were used to control the online process by means of power spectrum. Any change in amplitude or frequency will help in detecting pad wear. Frictional force was measured by strain gauge.
4.	7163435 B2	16 Jan. 07	Lim *et al.*	TSSP Ltd	Real time monitoring of CMP pad conditioning process [80]	A monitoring arrangement was described in which the accelerometer was attached to the conditioning arm for monitoring the pad wear. By spectrum analyzer, abnormal peak of the frequency was analyzed for monitoring.
5.	2006/0063383	23 Mar. 06	Pattengale *et al.*		CMP process endpoint detection method by monitoring and analyzing vibration data [79]	End point detection arrangement was described in which the accelerometer was attached to the CMP tool. It included a computerized system in which a encoded frequency was detected real time during the polishing for an end point.
6.	5904609	18 May 99	Fukuroda *et al.*	Fujitsu Ltd.	Polishing apparatus and polishing method [93]	A failure detection system was being described for preventing the breakage and jumping of wafer by detecting abnormal vibration signal. The Vibration sensor was attached to rear of substrate holder.
7.	6634924 B1	21 Oct. 03	Ono *et al.*	Ebara Corp.	Polishing apparatus [94]	A polishing machine with a signal analyzing method was described in which the vibration signal transmitted through the radio was used for pad wear and polishing endpoint by comparing the signal during the polishing with the initial signal.

Table 2: Patent on AE sensors in CMP

	US Patent No.	Issue date	Inventor	Assignee	Title	Brief description
1.	6709314	23 Mar. 04	Kaushal *et al.*	AM, CA	Chemical mechanical polishing endpoint detection [95]	A method for detecting the transition in layers of polishing by monitoring acoustic energy using acoustic emission is described. The acoustic energy was converted to electrical signal which was further filtered before converting to frequency spectrum. The end point was detected by comparing the frequency spectrum with the previous frequency spectrum
2.	6379219	30 Apr. 02	Oba	SLET, JP	Chemical mechanical polishing machine and method [96]	A controlled polishing mechanism based on delay time of two elastic wave signals from work piece was described. A control by spectral analysis was done through maintaining a signal magnitude from different sensors.
3.	6488569	3 Dec. 02	Wang et al.	FSU,US	Method and apparatus for detecting micro-scratching in semiconductor wafers during polishing process[97]	CMP apparatus in which the AE sensor was attached close to wafer for monitoring surface defect i.e. scratches. Increase in amplitude threshold was used to monitor surface characteristics.
4.	6424137	23 Jul. 02	Sampson	STM Inc.	Use of acoustic spectral analysis for monitoring/control of CMP processes [98]	An online technique based on spectral analysis was described for detecting scratches during polishing. A band of frequency was being monitored to determine uneven vibration before any damage to wafer.
5.	7377170	27May 08	Ganesan *et al.*	USF	System and method for the identification of chemical mechanical planarization defects [99]	A moving window based strategy against delamination for monitoring the polishing process was described. A dyadic signal was decomposed up to the 6th level and energy of coefficient was calculated by daubachies wavelet of fourth order. The threshold limit was assigned for calculating significant energy through the wavelet coefficient.

6.	6910942B1	28 June 05	Dornfield	UCA	Semiconductor CMP process and End point detection method and apparatus [100]	A system was described in which a sudden drop of AE signal was used as a end point of polishing. Also explained that the signal at the start was due to brittle abrasion and at the endpoint was due to the particle dielectric abrasion and particle metal abrasion.
7.	5240552	31 Aug. 93	Yu et al.	Micron	CMP of a semiconductor wafer using acoustical wave for in-situ end point detection [101]	A monitoring system for detecting the thickness and endpoint through acoustic emission sensor was described. The received signal was compared with the directed signal for thickness monitoring.
8.	6494765 B2	17 Dec. 02	Gitis *et al.*	Center for tribology Inc	Method and apparatus for controlled polishing [102]	A CMP process control arrangement comprising a multiples sensors namely AE sensor, force sensor, and temperature sensor mounted on the rotating head was described. The simultaneously obtained signals were processed and analyzed by the control unit

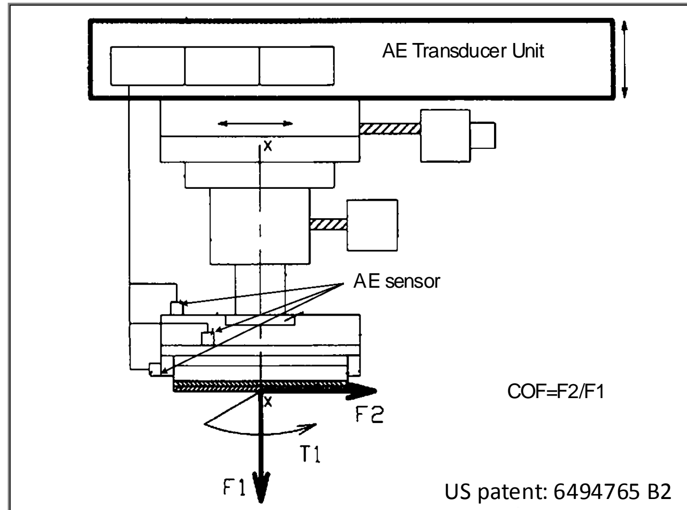

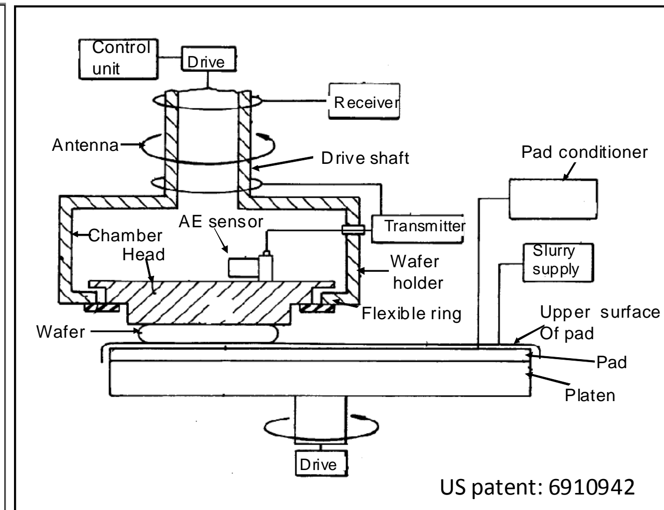

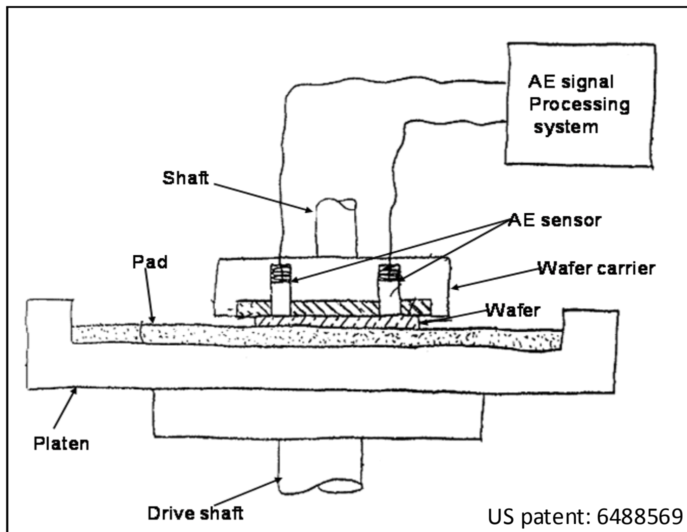

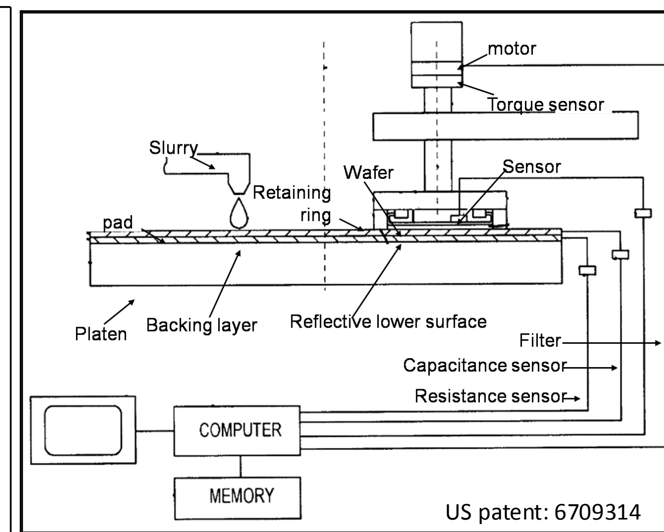

Figure 37: AE sensor monitoring systems in CMP [97, 100, 102, 103]

Table 3: Patent on sound sensors in CMP

	US Patent No.	Issue date	Inventor	Assignee	Title	Brief description
1.	5245794	21 Sep, 93	Isi	AMD	Audio end point detector for chemical mechanical polishing and method therefore [104]	A method for detecting the acoustic wave produced due to rubbing action and converting that into acoustic energy in the range of 30 Hz to100 Hz was described. A phase loop system was applied for detection of set frequency.
2.	5222329	29 June, 93	Yu	Micron	Acoustical method and system for detecting and controlling CMP depths into layers of conductors, semiconductors and dielectric materials [105]	A microphone was positioned a distance away from the wafer to sense the acoustic wave. This contactless based arrangement was used to determine the end point detection in CMP i.e. thickness of the polished layer removed. This signal detected was amplified and analyzed by a spectrum analyzer.
3.	6494769	17 Dec, 02	Sinclair *et al.*	AM	Wafer carrier for chemical mechanical planarization polishing [106]	A wafer carrier was developed in which the microphone was mounted inside the cavity just sticking the wafer plate. In this way, the sensor was at the rear of the wafer in contact. Also, the endpoint detector was adapted to measure the relative surface of the wafer.

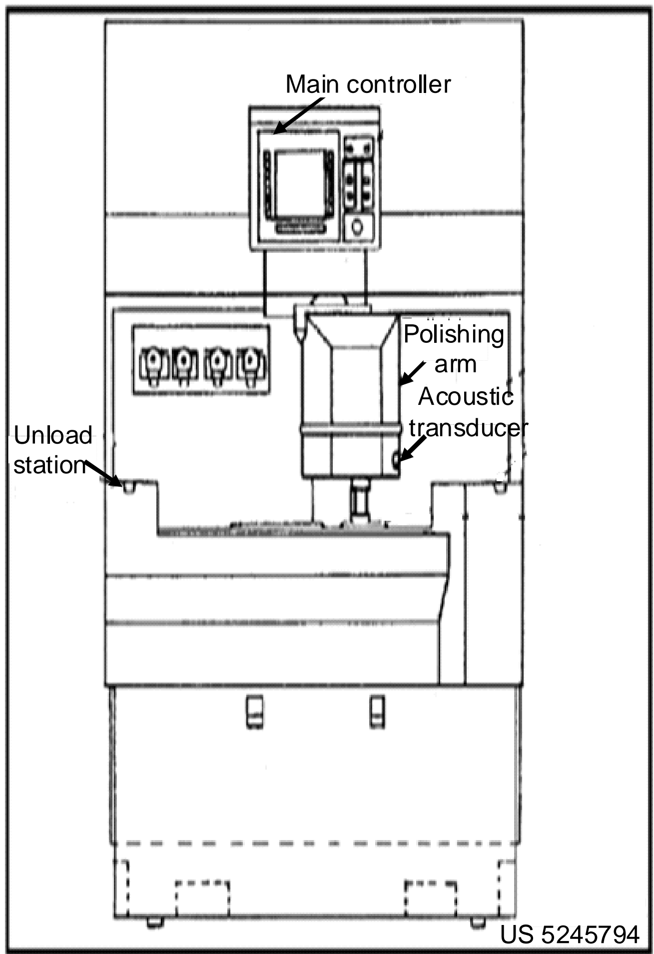

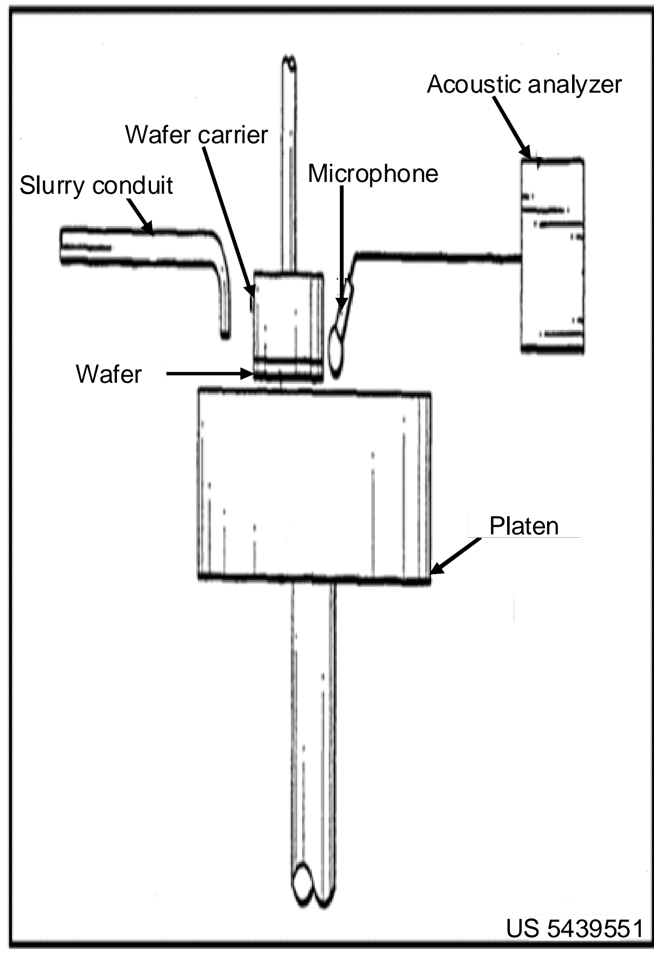

Figure 38: Acoustic or sound sensor monitoring systems in CMP [104, 105]

Table 4: Patent on temperature sensor in CMP

	US Patent No.	Issue date	Inventor	Assignee	Title	Brief description
1.	5196353	23 Mar. 93	Sandhu *et al.*	Micron	Method for controlling a CMP process by measuring a surface temperature and developing a thermal image of wafer [81].	A thermal arrangement was described for measuring the temperature of wafer using the infra red detector. The endpoint detection was detected by the sudden change in wafer temperature, when the new layer was exposed.
2.	5597442	28 Jan. 97	Chen *et al.*	TSMC	Chemical mechanical planarization (CMP) endpoint method using measurement of polishing pad temperature [82]	A temperature monitoring system for EPD was described. The infra red detection device was used to monitor the pad temperature at the abraded region.
3.	5643050	1 July. 97	Chen *et al.*	ITRI	Chemical/Mechanical polish (CMP) thickness monitor [107]	A thickness monitor arrangement using temperature measurement at controlled slurry temperatures between 10°C to 30°C was described. The temperature of the wafer or pad versus time was plotted to monitor thickness. The removed thickness was derived using computer stored integration coefficients. These coefficients were specific for slurry chemistry and pattern density.
4.	6872662	29 Mar, 05	Hocheng *et al.*		Method for detecting the endpoint of a chemical mechanical polishing (CMP) process [83]	The infrared detection device was described was used to measure pad temperature for an end point detection system for CMP. The endpoint was detected by slope variation of the temperature curve. The curve was plotted using numerical method like linear regression methods using the temperature difference measurement between atmosphere temperature and pad temperature.

5.	6976902	20 Dec.05	Koo *et al.*	Samsung	Chemical mechanical polishing apparatus [84]	Multi sensor based EPD was employed. In this, temperature sensors for slurry, wafer, and pad temperature were used as first detector whereas load current, voltage and resistance of carrier head motor was used as the second detector. In the second invention, the second detector was replaced by an optical detector which detects light illumination on the wafer and reflected from the wafer.

Chapter 4: Problem statement

In the CMP, the key process parameters, namely, down force, rpm, slurry flow rate play an important role in achieving good planarization with good material removal rates. Earlier work deals with the monitoring of the process using different sensors, such as, vibration, acoustic emission, friction, and temperature to study the polishing process using wired and wireless sensors [76]. However, the scope of the modeling of the process performance variables (MRR, roughness and WIWNU) through sensors fusion has not been explored. Recently, an investigation using a using a single type of wired and wireless sensors was reported [76]. A CMP process is a complex nonlinear process with some 36 input variables. Due to uncertainty of the CMP process, use of one sensor alone for predicting the process may not be inadequate. Wireless technology is now widely used for various applications. This study is undertaken to quantify the process by sensor fusion modeling through vibration and temperature sensor using regression analysis. Also, most of the models in the literature are on MRR. However, MRR is not a direct output parameter in the CMP process. Surface roughness and WIWNU of the wafer are direct output parameters for the monitoring process. Till now, there is no such model to track roughness in the CMP process.

In this investigation, a sensor fusion model was proposed using data obtained from a full factorial design of CMP experiments on copper samples. This model is used to quantify the roughness and material removal of the process without the need for wired sensors. This technique helps in tracking the variation of process output using wireless temperature and vibration sensors. Response surface methodology was applied to

estimate the key process parameters with output variables using various sensor features, such as, statistical, frequency, and recurrence quantification based features. The sensor is located underneath the copper sample for maximizing the accuracy of the process signals. Two vibration and two temperature sensors are attached for monitoring the process dynamics during the polishing process. Wireless sensor fusion approach is found to be more accurate compared to single sensor modeling using linear and nonlinear statistical techniques. The sensor fusion model is able to estimate the roughness of the copper sample and MRR in the CMP process for real time monitoring using various statistics-based features, time-frequency features, nonlinear features, and temperature features.

Chapter 5: Initial CMP Studies

5.1 Submerged Face-up CMP:

Research on face-up CMP process has been undertaken by many researchers from university, national laboratories and industry [108] [109]. Recently at OSU, we developed a wireless sensor-based monitoring system for face up CMP. Figure 39 shows the CMP apparatus. It consists of a mini-milling machine to run the shaft or pad arrangement, and a fixture for holding the wafer. In the initial set up, the diameters of the wafer and the pad were the same i.e. 4 inches in diameter. Figure 40 shows the top and front views of the submerged face up CMP apparatus. The inside component of the tank had a slot made for locating the sensors. The plastic base plate was made to hold the tank (8″ x 8″ x 4.5″) during the polishing process.

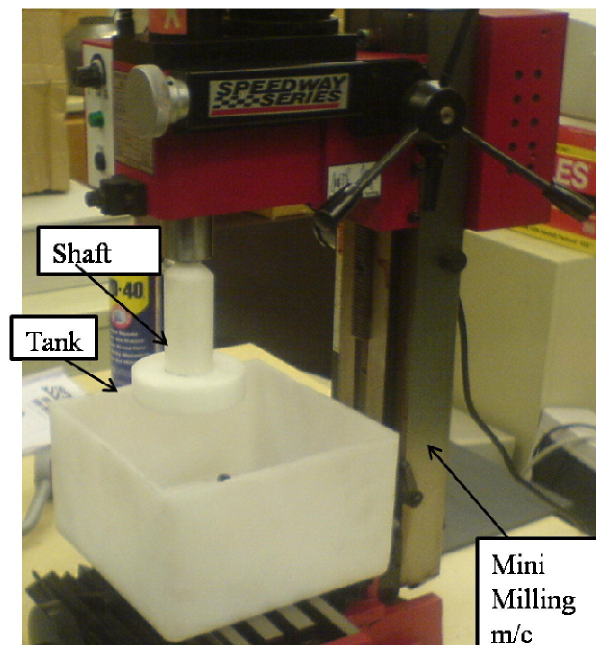

Figure 39: CMP polishing machine

Copper disc was used as a wafer in this arrangement. The materials of the apparatus were chosen very carefully. For example, polyethylene tank was used because of its resistance to most inorganic chemical environments. The shaft was rotated in the anticlockwise direction.

CMP polishing was conducted under different conditions. We monitored vibration, sound, and temperature signals using sensors attached under the wafer. Most of the literature on CMP vibration monitoring was based on capturing the vibrations of the carrier holder or holder during polishing. The present system is different in that the sensors are attached underneath the wafer [71] [72]. The slurry used for polishing condition is colloidal slurry of silica having abrasive size of 70-90 nm, which is alkaline in nature.

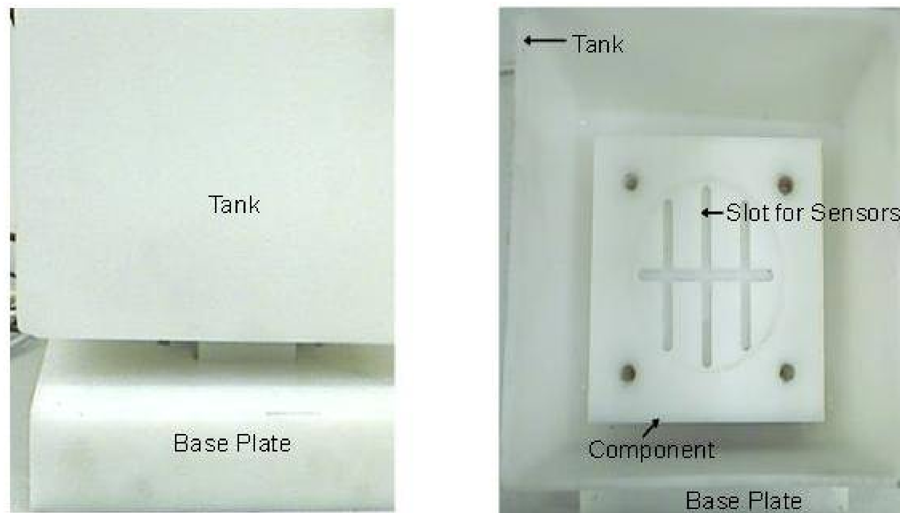

Figure 40: Front and Top views of the face-up CMP apparatus

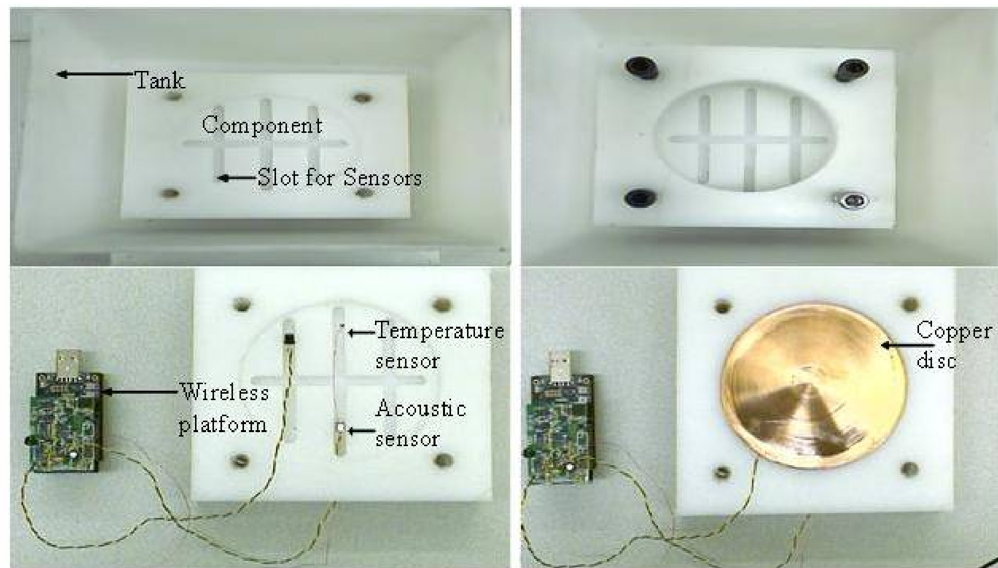

Figure 41: Sensors arrangement in the face-up CMP apparatus

Figure 41 shows the arrangement of sensors in the CMP arrangement. Our system incorporates wireless MEMS technology for the polishing process. In this apparatus, wafer was submerged in slurry contained in the tank. The wafer is tight fitted in the circular slot using a bolt. A base plate was used to support the tank during the polishing process. The signals obtained from the polishing process were analyzed to identify various frequencies associated with the process. Initially, the shaft was run at 75 and 90 rpm. Figure 42 shows the temporal vibration signals and their power spectrum, respectively, obtained from the process at a sampling rate of 500 Hz. The vibration signals obtained at 90 rpm from the process was found to be nonlinear. From the power spectrum, a wide band from 110-140 Hz was observed. Figure 43 shows the sound signals from the polishing process at a shaft speed of 70 rpm. In the case of the sound sensor, at 75 rpm, the signal contained noise. A frequency band at 150 Hz can be seen from the plot.

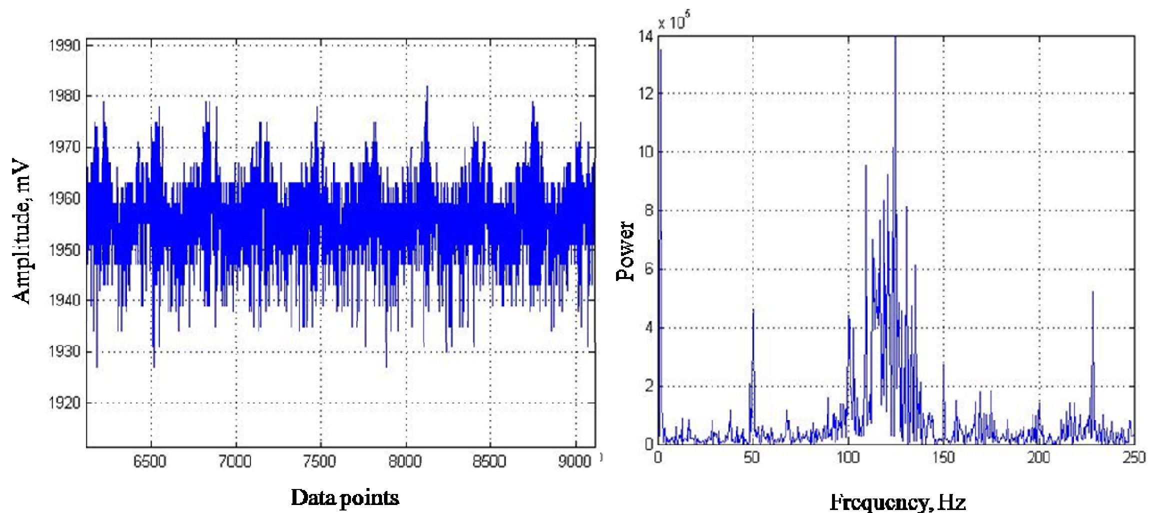

Figure 42: Vibration signals at 95 rpm, 500 Hz

Statistical features, such as mean, standard deviation, maximum, minimum of the frequency band of the process signals were extracted. However, some concentric rings and scratches were observed on the surface due to pad rotation only. A motor arrangement was then used to provide rotation to the wafer carrier. A load cell was mounted on the base plate holding the tank to

determine the load acting during polishing. This load cell was aligned with the axis of wafer carrier.

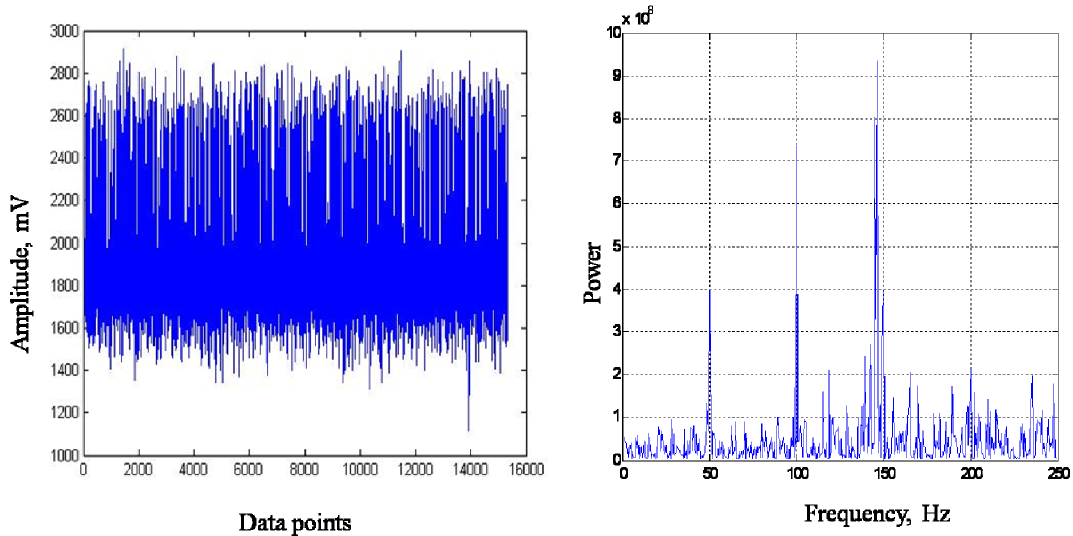

Figure 43: Acoustic/sound signals at 75 rpm, 500 Hz

Figure 44 shows the modified arrangement of the face up CMP apparatus. A Teflon shaft was attached to the milling machine spindle using an end mill holder ( ). The wireless platform was attached to the shaft holder by means of a T-bolt clamp. Initially, colloidal silica slurry was used for polishing.

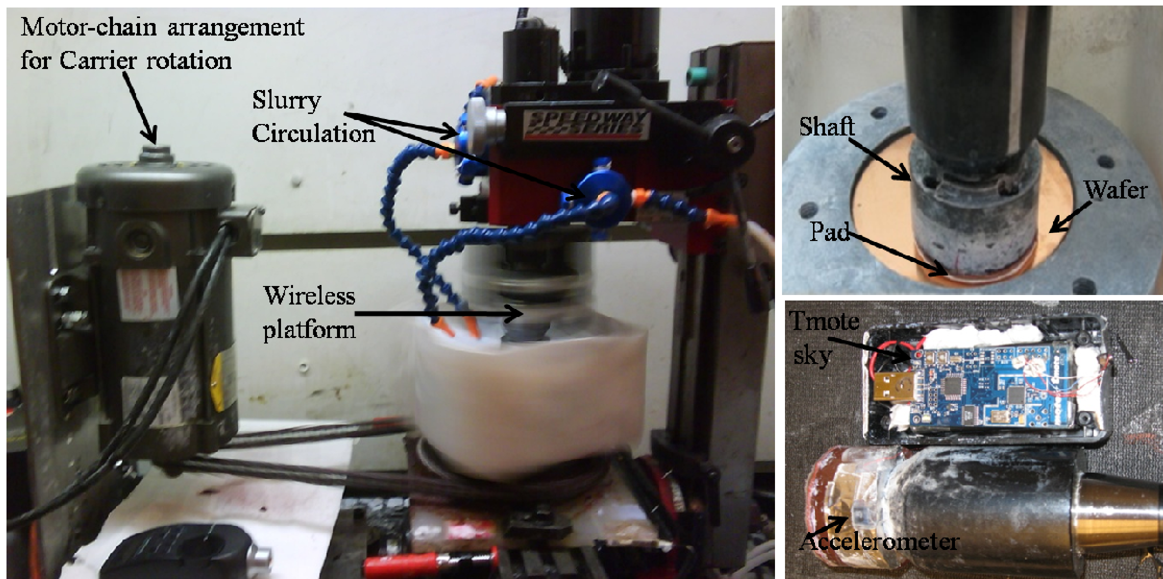

Figure 44: Face up CMP with wireless sensor

Different types of pads were investigated to optimize the polishing process. A copper cup was bonded to the shaft with an adhesive. A pad was attached to the cup using an adhesive for measuring its temperature. Figure 45 shows the copper cup arrangement for CMP. In this, a slot was made in the shaft for measuring the temperature of the pad. In this system, MEMS-based vibration sensor was attached to the shaft and the temperature sensor was attached to the rear end of the pad.

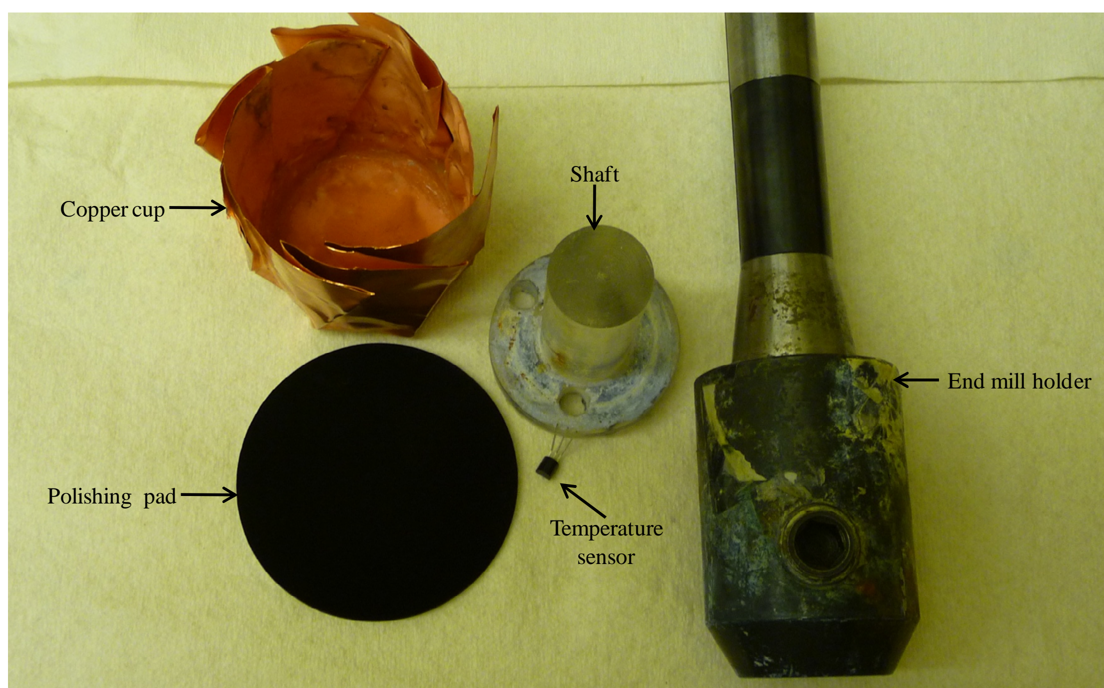

Figure 45: Copper cup arrangement for temperature signals in CMP

This system was able to capture, pad vibration and temperature during the polishing process. Figure 46 shows the temperature signal of the pad obtained under the following conditions: Suba pad, 400 rpm for the shaft, 40 rpm for the carrier, and 30 lb load using colloidal silica-based slurry. The temperature rises rapidly with time reaching towards a steady state temperature. The net temperature rise was 6 ℃ over 4 minutes. Figure 47 shows optical images of the as-received

and polished copper wafers used in multistage polishing. Initially, the as-received wafer had defects, such as pits, scratches. After polishing, these defects were removed.

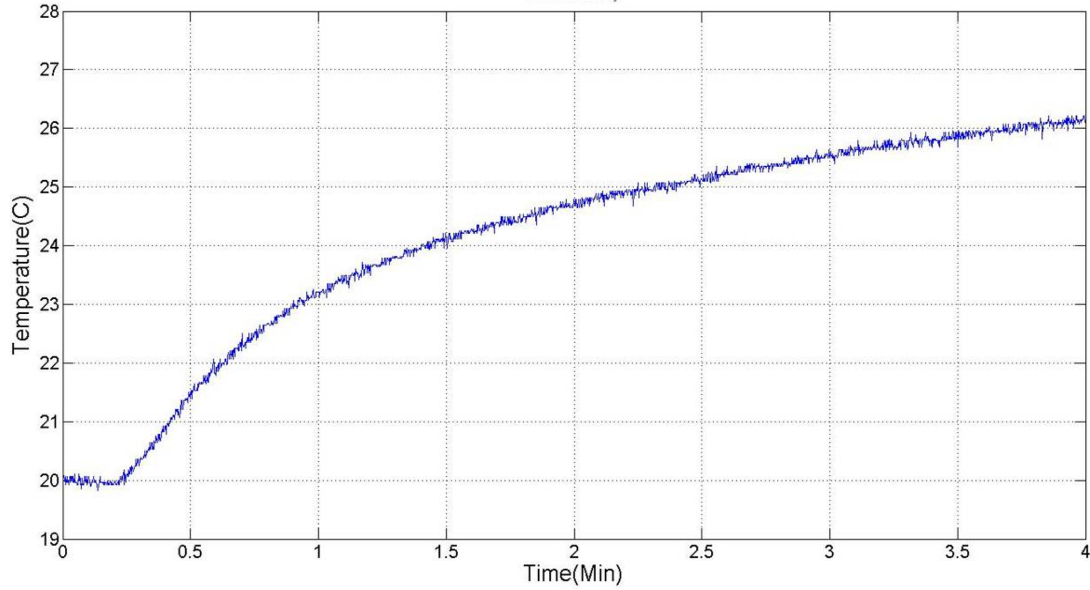

Figure 46: Pad temperature signal

The average roughness (Ra) of the polished wafer was 35 nm. Table 5 shows the conditions used during various stages of multistage polishing. The pads used were Suba IV, FBP, and microcloth. In order to obtain a defect-free surface from polishing, the loads were reduced, and the rpm were increased after each polishing step. The scratches or pits were removed in the first stage, a matty surface finish was observed in the second stage, and in the third stage mirror finish surface was obtained. Other different multistage steps were performed using different pads.

Table 5: Multistage polishing process in a colloidal silica slurry

Stage	Pad Type	Load (lb)	Wafer rpm	Pad rpm	Polishing time (min.)
1	Suba IV (Hard Pad)	35	40	500	30
2	FBP (Medium pad)	25	50	700	30
3	Beuhler MicroCloth (Soft pad)	15	75	700	15

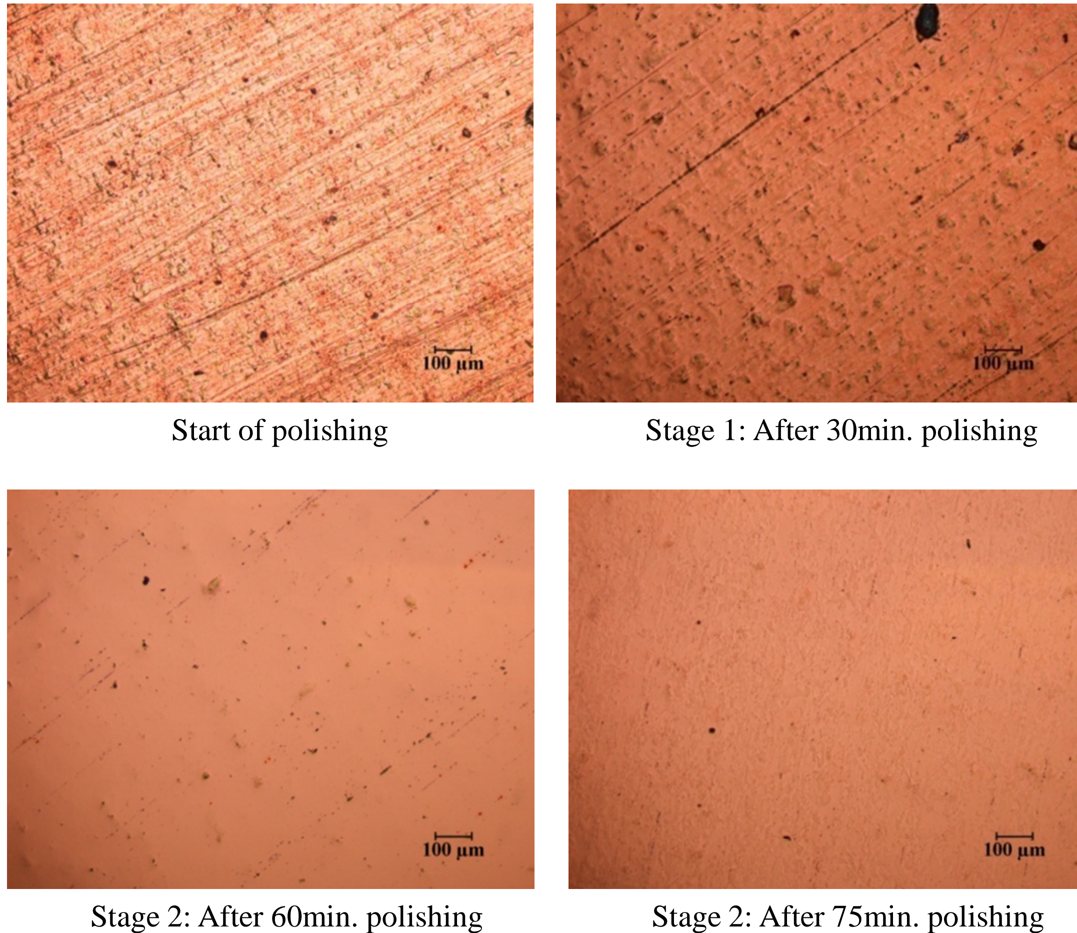

Start of polishing | Stage 1: After 30min. polishing

Stage 2: After 60min. polishing | Stage 2: After 75min. polishing

Figure 47: Optical image of copper wafer using multistage polishing using a face-up CMP polishing apparatus

Figure 48 shows the IC 1000 pad used for polishing the copper disc at a carrier speed of 50 rpm and the shaft speed of 375 rpm at 20 lb load. Wear of the pad was observed after polishing. The color of the pad changed from white to a dark color at the end of polishing due to wear and impurities. Figure 49 shows the FBP 3000 pad after polishing at 20 lb load under the same polishing conditions. The color of the pad changed from light green to a dark color due to impurities and asperities removed after polishing. Wear of the pad was observed after polishing. The polishing conditions were optimized for polishing of the wafer in 45 minutes. A multistage polishing technique was used to obtain the mirror finish surface using colloidal silica slurry. In this, three different kinds of pads were used for polishing copper discs. The hard pad IC1000 was

used initially for high material removal, Suba IV pad in the middle for intermediate polishing and FBP 3000 at the end for mirror finish. Colloidal silica slurry was used in these experiments.

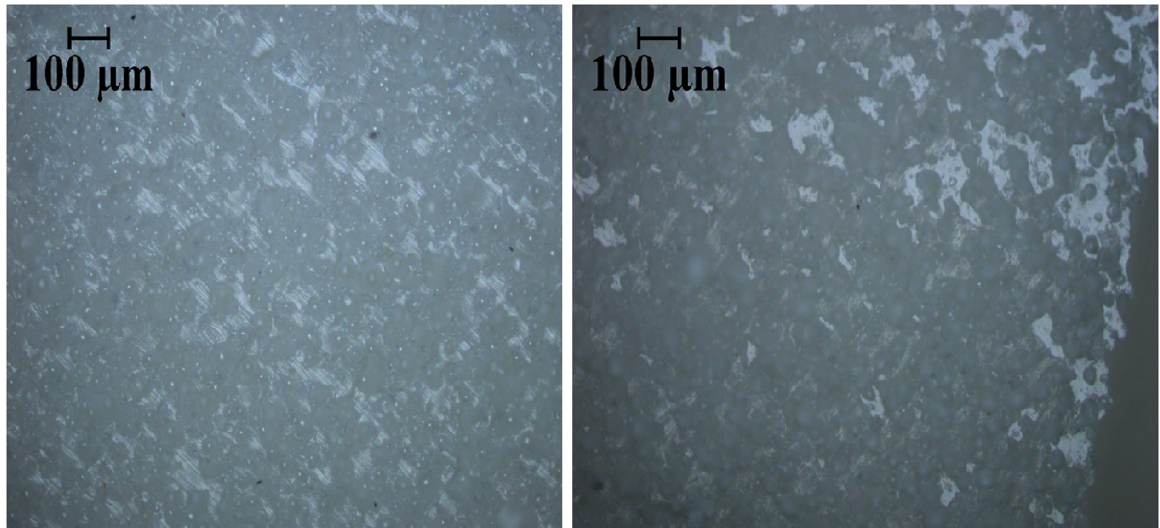

Figure 48: IC 1000 pad before and after 25 min. of polishing time with colloidal silica slurry (1:2)

Figure 50 shows the signal obtained from the CMP polishing process under the following process conditions, i.e., chemomet pad, shaft speed of 300 rpm, and carrier speed of the 50 rpm. An alumina slurry concentration of (1:3) was used. The vibration sensor signal was sampled at 500 Hz frequency. The power spectrum shows that the signal includes many frequencies. The power spectrum was further studied for analyzing the process during polishing time intervals. Figure 51 shows the power spectrums for the above polishing conditions. The variation in the power spectrum of the vibration signal for alumina-based slurry was observed at 10 minutes of the polishing time. The amplitude of the frequency band (from 230-235 Hz) decreased with time [see Figure 51]. Power spectrum analysis was made to study the frequency of the CMP process. The vibration signals were very sensitive to machine vibration as well.

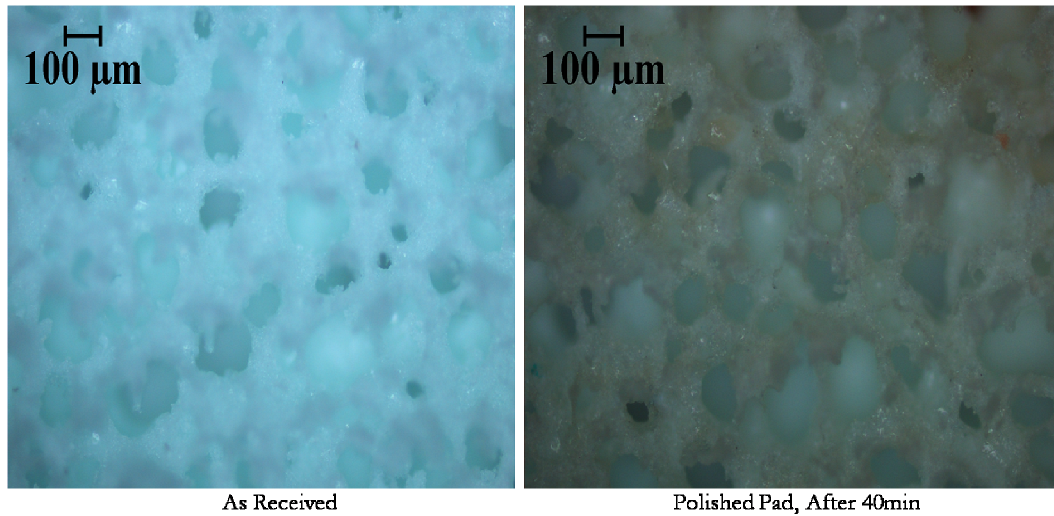

Figure 49: FBP 1000 pad before and after polishing

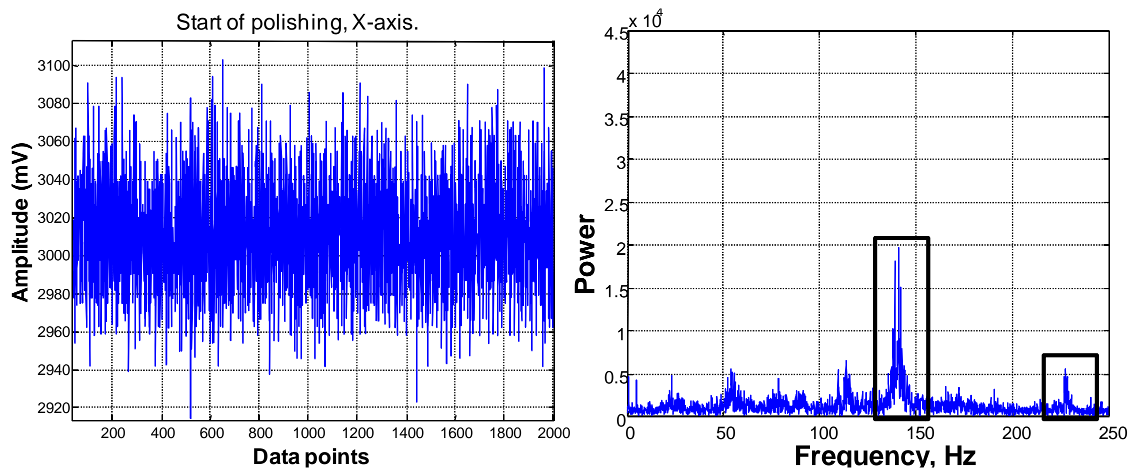

Figure 50: Vibration signal and Power spectrum at 50 lb load

Initially, experiments under different conditions were conducted for the frequency spectrum analysis of the CMP process signals. From this study, it was concluded that the signal includes shaft frequency, chain frequency, and their interactions. Figure 52 shows the power spectrum obtained under the above polishing conditions. The study was made to determine the frequencies of the process under a constant polishing condition.

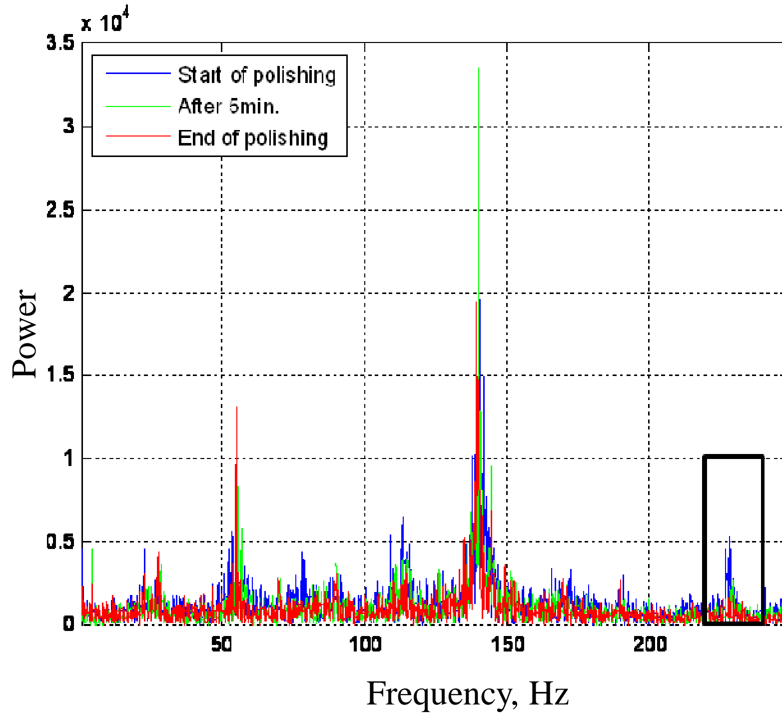

Figure 51: Power spectrum during the polishing process

Table 6: Process frequency band at various conditions

No.	Condition	Frequency band
1.	Wafer carrier rotation without contact	95-105 Hz, Vibration due to motor
2.	Wafer carrier in contact with wafer	185-200 Hz, Process frequency band
3.	Shaft spindle rotation without contact	No significant band
4.	Shaft spindle rotation in contact with the	95 -105 Hz and 150-160 Hz
5.	Wafer carrier and shaft spindle rotation only	No significant band
6.	Wafer carrier and shaft spindle rotating during polishing	95-105 Hz and 150-160 Hz

The shaft and carrier rpm were 400 and 40 rpm, respectively under a 30 lb load using (1:2) colloidal silica slurry. The vibration signal was sampled at 500 Hz. Frequencies below 60 Hz were coming from the motor. Table 6 shows the process frequency analysis obtained from Figure 52. The signals were taken under different conditions, such as shaft rotation only,

polishing with shaft rotation only (no motor rotation), motor rotation only, polishing with motor rotation only (no shaft rotation), shaft and motor rotation (no polishing), and polishing with shaft and motor rotation. From the first and second conditions of the shaft rotation, it was concluded that power spectrum band from 95-105 Hz was the frequency band associated with shaft vibration and 150-160 Hz band was the frequency band associated with the CMP process.

Tests were conducted in dry and wet environments for vibration analysis of the CMP process. The vibration signal was sampled at 850 Hz. The polishing conditions were 400 rpm shaft rotation, 40 rpm motor rotation and a 30 lb load. Figure 53 shows the vibration signals under different conditions. Figure 53 (a) shows the signals under dry conditions and polishing, Figure 53(b) shows the signals under wet polishing conditions, Figure 53 (c) during polishing with slurry, and Figure 53(d) when slurry quantity was increased. In the case of dry polishing, when there was no slurry or water, one continuous signal was observed without any variation [Figure 53 (a)]. However, when polishing was conducted in water [Figure 53b], continuous band in the signal was observed for a longer interval in the polishing. When water was removed, and slurry was added, a continuous band was observed in a small interval. These results are attributed to the abrasive action during polishing. Figure 54 shows the power spectrum analysis at different loading conditions. The sampling rate of the wireless platform was 850 Hz. Three loading conditions were chosen for the vibration signals, namely, 30 lb, 20 lb, and 10 lb. The shaft and motor rpm were fixed at 400 rpm and 50 rpm. The frequency band from 40-70 Hz was from the motor. The mean of power band from 170-185 Hz was plotted. The drop in power from 30 lb to 20 lb was two times more than the drop from 20 lb to 10 lb. A qualitative study was made for the CMP process through vibration signals. From the above, it was evident that vibration signals were very sensitive to the process which includes the slurry condition and the loading condition. It was concluded that the vibration signal can be beneficial for monitoring the process.

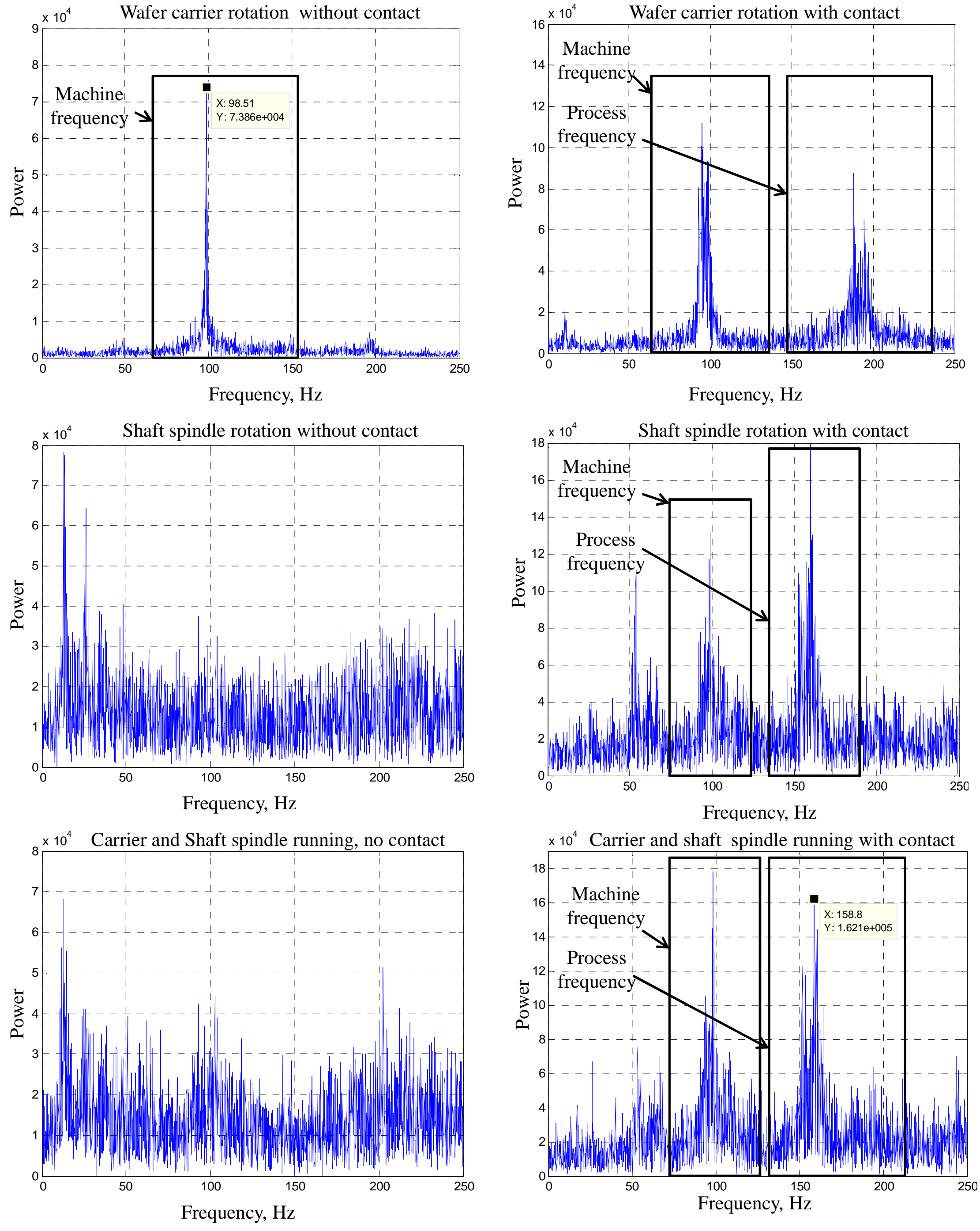

Figure 52: Vibration frequency power spectrum for analysis

However, there was some uncertainty associated with the experimental set up described in Section 5.1. Therefore, a DOE-based quantitative study was made using bench top polisher for regression analysis modeling of Ra and MRR of the wafer.

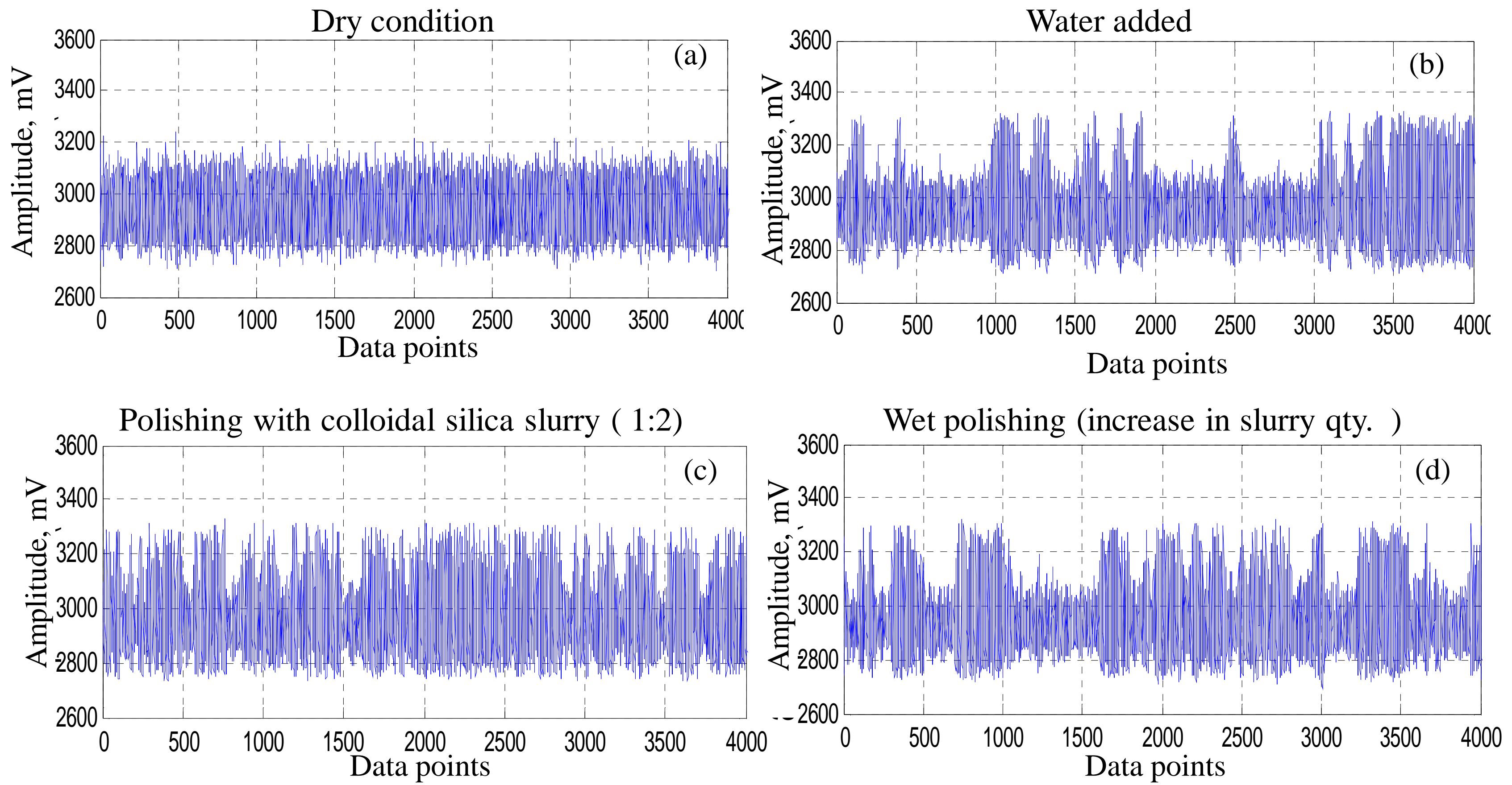

Figure 53: Vibration signals under dry and wet polishing conditions

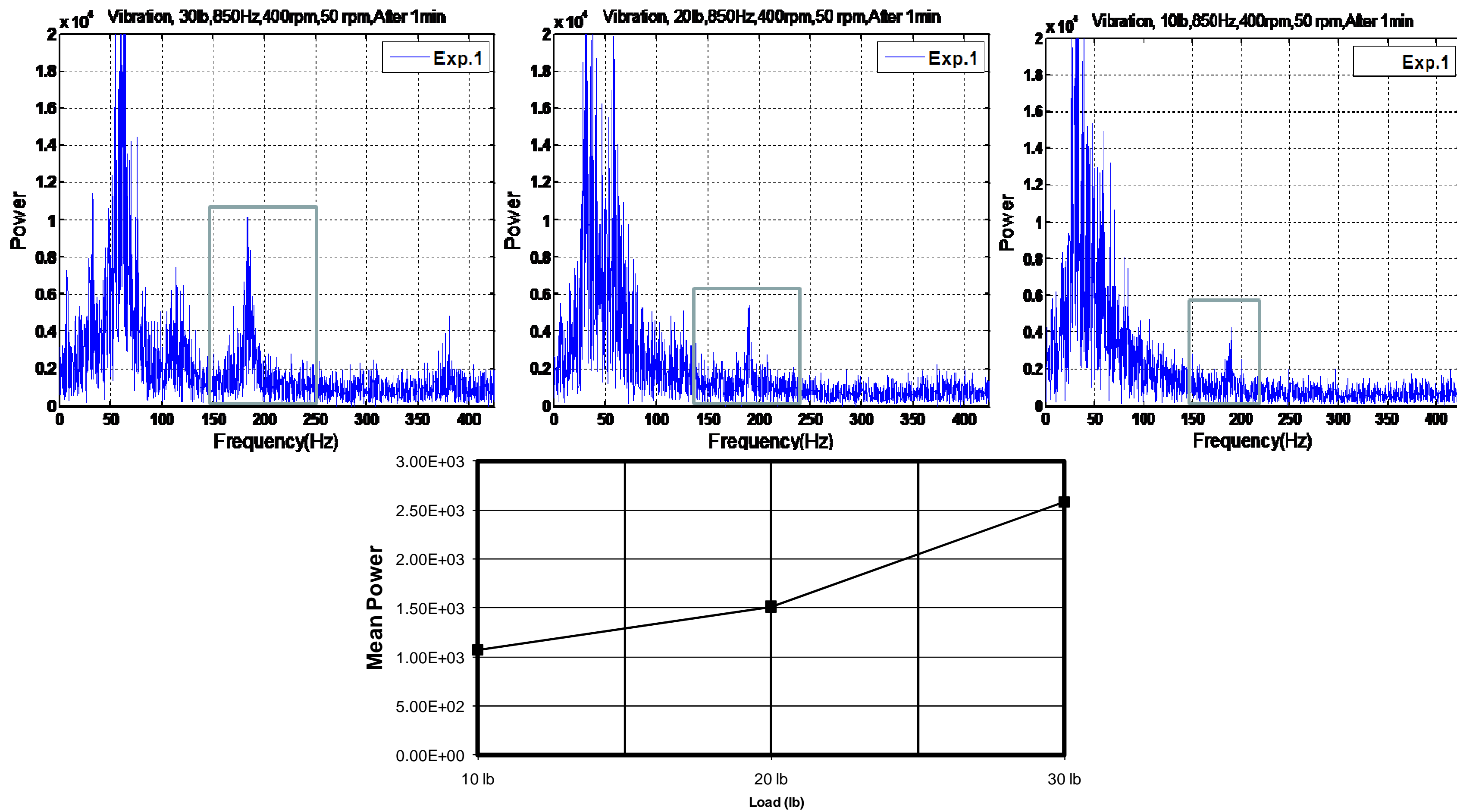

Figure 54: Power spectrum at different loading conditions under constant spindle speed of 400 rpm

Chapter 6: Experimental Apparatus and Design of Experiments

6.1 CMP polishing apparatus:

Figure 55 shows a Buehler polishing machine (EcoMet® 250/AutoMet® 250 Family) used for CMP polishing studies. It is also used as a transmitter base for the sensors. Figure 56 shows a desktop computer as a receiver or base for the signal collection which was used for studying the CMP process. This machine contains an upper and lower main housing. The upper housing is equipped with an air cylinder arrangement. The lower housing is equipped with a platen of 8" diameter with a platen speed of 10 to 500 rpm operated by a high toque motor of 1 Hp. The machine is equipped with a sample holder having multiple openings of different sizes for polishing samples. Each opening is mounted with aluminum lip for flexible mounting of the samples. The sample holder is driven by a drive shaft rotated by an electric motor. The applied load varies from 1 lb to 10 lb. The load was applied on the copper sample through the finger tip. Polishing was done by the application of down force on the sample through the actuation of pressure cylinder against the pad rotation in a slurry environment. Consistent repetitive pressure is retained due to well controlled air activated cylinder. The sample and the pad were rotated in opposite directions. The diameter of the sample holder is slightly less than then platen diameter. An adhesive pad was bonded to the bimetallic plate which intern was mounted on the platen. A wireless sensor network was used to sense the temperature and vibration signals. Two copper samples of tellurium copper (copper alloy, Alloy C14500) with 1.6" diameter were polished simultaneously in each experiment. MEMS sensors were attached at the rear of the sample to study the dynamics of the process. An alumina slurry (0.05 µm grain size) and napped Microcloth pad from Buehler were used in the experiments. A 1.6" diameter disc was prepared to cover the top of the copper piece from the slurry. The slurry was filled in the beaker for polishing. The

peristaltic pump was used to pump the liquid from the beaker to the pad using hoses and for slurry recirculation. Another beaker was placed at the outlet from where slurry is circulated using the pump. The pump was run by a dc power source for uniform electric current. The wireless platforms were tightly packed inside the plastic boxes by means of thermocol.

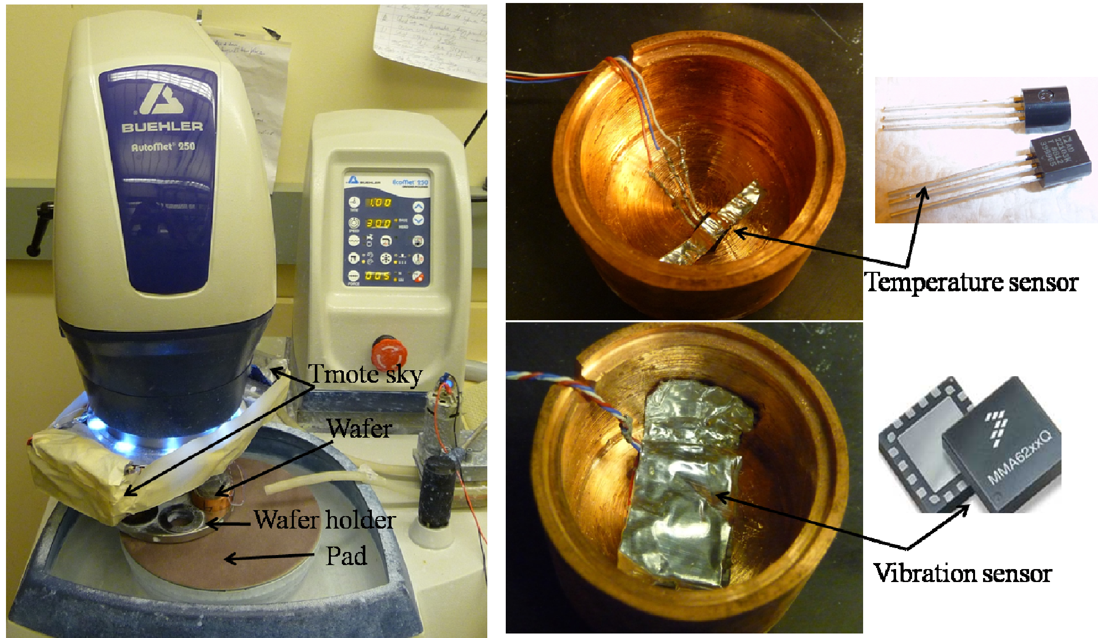

Figure 55: Transmitter base i.e. Buehler polishing machine for vibration and temperature signal

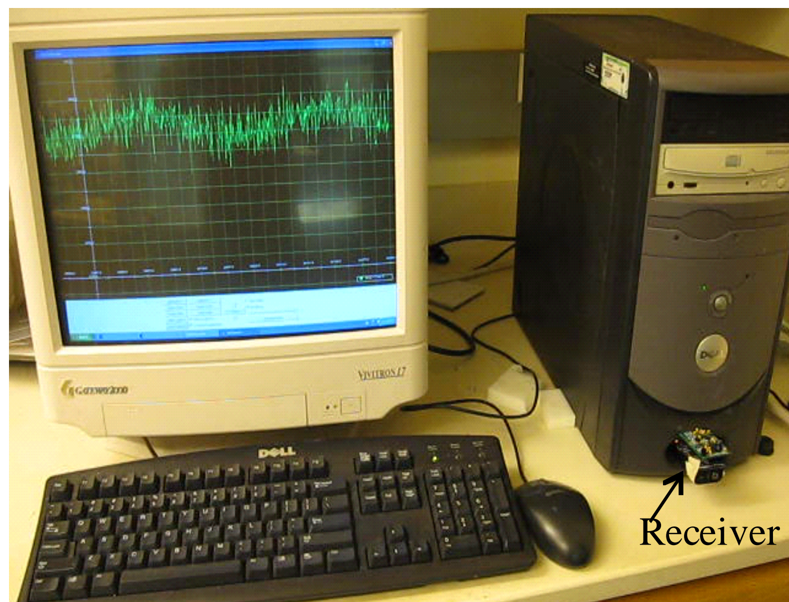

Figure 56: Receiver base for vibration and temperature signals

The wireless platforms inside the boxes were mounted to the machine cylinder by means of a shaft collar.

6.1 Wireless Sensor:

Figure 57 shows the Tmote sky based wireless platform from MOTEIV for signal collection. Tmote sky has Zigbee-based system architecture. The main components of the Tmote sky are the 8 MHz Texas Instrument MSP430F1611 microcontroller (10k RAM, 48k Flash) and the CC2420 chipcon's radio interface. TinyOS, an open source platform, was used to run NesC based program for programming wireless platform in the cygwin environment. The software was installed in the Windows Xp operating system. The java application-based oscilloscope window was used for the display and saving of the signals. The MEMS sensor from 'FREESCALE' was used for the vibration signal and IC sensor from 'ANALOG DEVICES' was used for temperature monitoring. The vibration signals were sampled at 500 Hz and temperature signals were sampled at 4 Hz. Three wireless platforms were attached to the spindle. Two platforms were attached with two vibration sensors, and the third Tmote sky was attached to the two temperature sensors. The slurry temperature was measured by a thermocouple before and after polishing. The sensors were attached to the workpiece by means of an electric wire to the wireless platform. Some of the features of tmote sky are as follows [110]:

- 250 kbps 2.4 GHz IEEE 802.15.4 chipcon wireless transceiver
- Integrated ADC, DAC, supply voltage supervisor, and DMA controller
- Integrated onboard antenna with 50 m range indoors/ 125m range outdoors
- Ultra low current consumption
- Fast wakeup from sleep ($< 6\mu s$)
- 16-pin expansion support and optional SMA antenna connector
- TinyOS support: Mesh networking and communication implementation

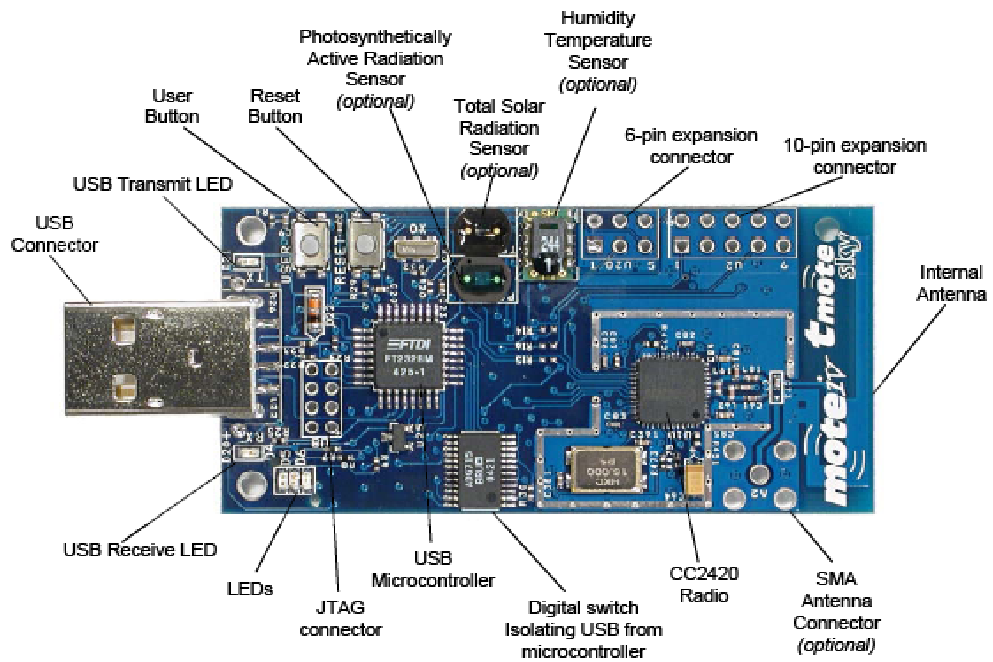

Figure 57: Tmote sky-based wireless platform

Figure 58: Sartorius weighing balance machine

6.2 Design of experiments (DOE):

Table 7 gives details of the factors used in the full factorial design of experiments. Three factors (load, rpm, and slurry ratio) at two levels (high, low) were investigated to study the process dynamics with the sensors. After each experiment, the copper sample was cleaned in an ultrasonic cleaner for 2 minutes. It was then dried by air pressure before measuring its weight. The material removed and the roughness was measured after drying. Averages of five points were chosen for roughness (nm). The material removal was measured after each run using a precision weighing balance. Figure 58 shows the Sartorius weighing balance machine (Model 1712 MP8). The resolution of the instrument is 0.1mg. Experiments were conducted randomly to study the process dynamics without any uneven interaction. The roughness of the copper sample was measured by ADE Phase Shift MicroXam, Optical laser interference microscope (see Figure 59). It is a non-contact surface metrology system for measuring the roughness of test pieces. The resolution of the apparatus is 0.1 nm. It is used for mapping three dimensional surface profiles with the measurements made in three modes, namely, quantitative, visual and confocal modes using optical interferometry.

Table 8 shows the levels used in the full factorial design. For load and rpm, the high and low level were (10 lb and 5 lb) and (500 rpm and 300 rpm), respectively. Before polishing, each sample was mechanically hand polished to an average roughness of 350-380 nm with a 600 grit size sand paper. Each experiment was conducted with a new pad, copper sample, and a new slurry concentration. Each run was divided into four parts, i.e., 30, 60, 90, and 120 sec. Each sample was mounted with a temperature and a vibration sensor. Response surface methodology was used for obtaining a regression model to estimate Ra, MRR, and Preston constant from the sensor signals features. These tests were carried at a constant speed (60 rpm) of the spindle. The MRR was the material removal rate in a particular run having initial weight of W_{n-1} and initial time of t_{n-1}.

Figure 59: MicroXam, Optical laser interference microscope

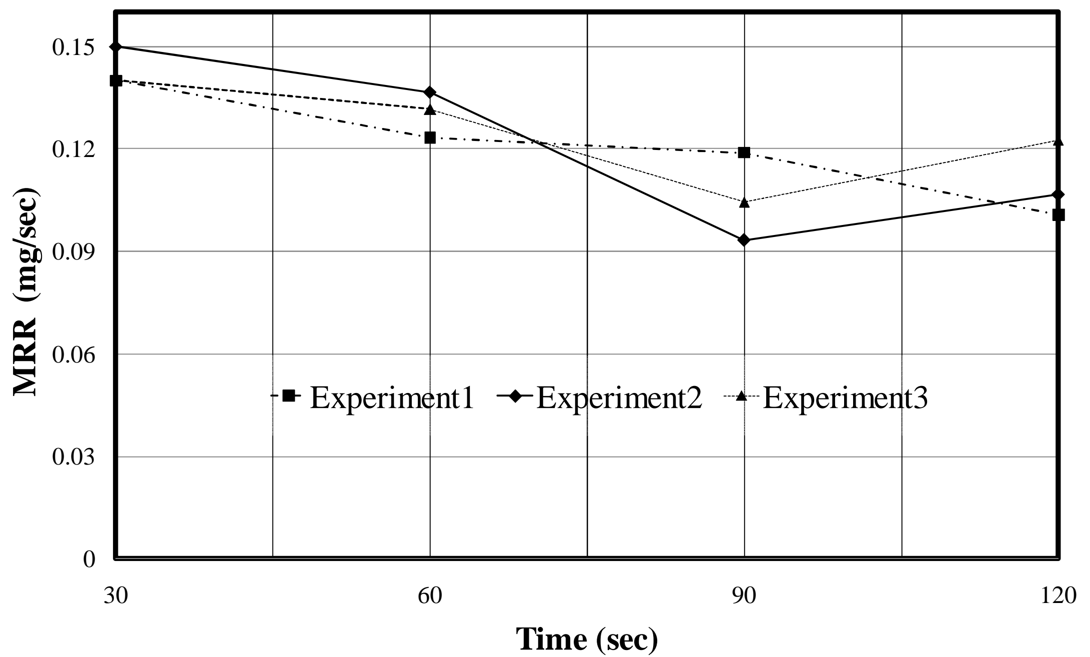

Figure 60: MRR repetition for Run R1 (see Table 7 for details)

Table 7: Full factorial design of CMP experiments

Run	Load, lb	Rpm	Slurry ratio
R1	10	500	1:3
R2	10	300	1:3
R3	5	500	1:3
R4	5	300	1:3
R5	10	500	1:5
R6	10	300	1:5
R7	5	500	1:5
R8	5	300	1:5

Table 8: High and low level in CMP experimental design

Level	Load, lb	RPM	Slurry ratio
High	10	500	1:5
Low	5	300	1:3

Figure 60 shows the MRR for two repetitions calculated under the following condition of 500 rpm, 10 lb, and ratio of colloidal alumina slurry 1:3. During this repetition, the signals were captured and analyzed for the reproducibility of the process. The trends of MRR were the same in all the repetitions. The MRR was measured in mg/sec. The images and 3D surface profiles were captured by ADE Phase Shift MicroXam, a surface-mapping microscope. Figure 61 (a) and (b) shows the optical microscope images of the copper sample at run R1 condition at the start and end of polishing. At the start of polishing, the optical image was full of scratches and pits, which was removed in subsequent polishing after 2minutes.

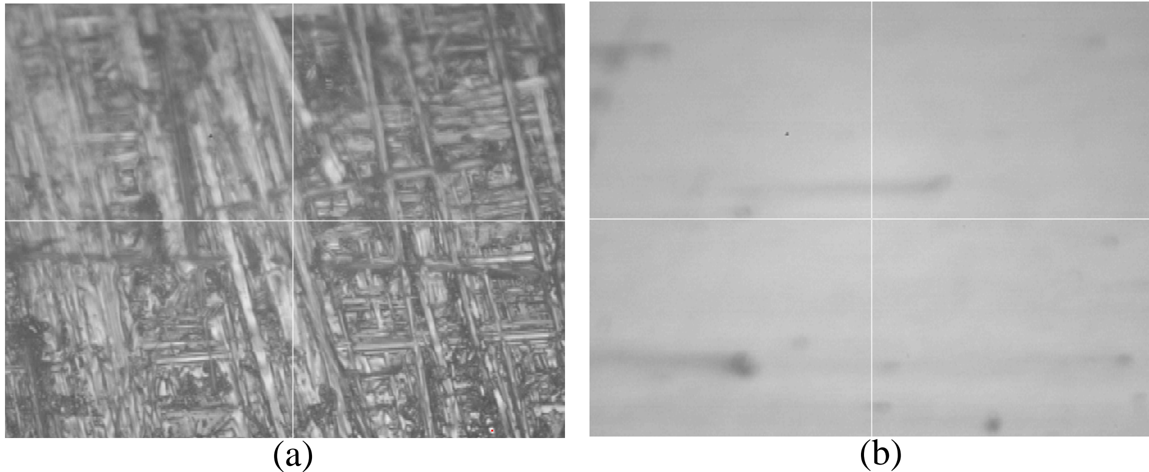

Figure 61: Microstructure of copper sample before and after polishing

Figures 62(a) and (b) shows the 3D surface profile of copper. After 2 minutes of polishing, the observed image was flattened with a surface roughness of 4 nm. Various defects like scratches and pits marks were removed after polishing. Figure 63 shows the time series of signals under two different loading conditions (10 lb and 5 lb) at the same rotational speed (500 rpm). The slurry ratio in both the conditions was same. It was observed that the signal's amplitude in the case of the high load was more [see Figure 63 (a)] compared to the low load [see Figure 63 (b)].

Figure 64 shows the power spectrum of run R2 conditions where the load is 10 lb, platen speed 300 rpm, and slurry ratio (1:3). The frequency band was from 120 to 130 Hz which is the processing frequency band after 15 sec of polishing. Also, the highest peak in the power spectrum was observed at 126.2 Hz.

Figure 65 shows the power spectrum after 90 sec of polishing. The power of the signal decreases towards the end of polishing. The dyadic length for the power spectrum was 2048. Figure 66 shows the temperature profiles and material removed during polishing using a microcloth pad. The rotational velocity of the platen and carrier were 300 rpm and 60 rpm respectively. The load applied was 10 lb. polishing was done at 30 sec, 60 sec, 90 sec and 120 sec. The material removed for 30 sec and 60 sec of polishing was 2.9 mg and 4.8 mg respectively. These experiments were conducted using a new pad and new slurry.

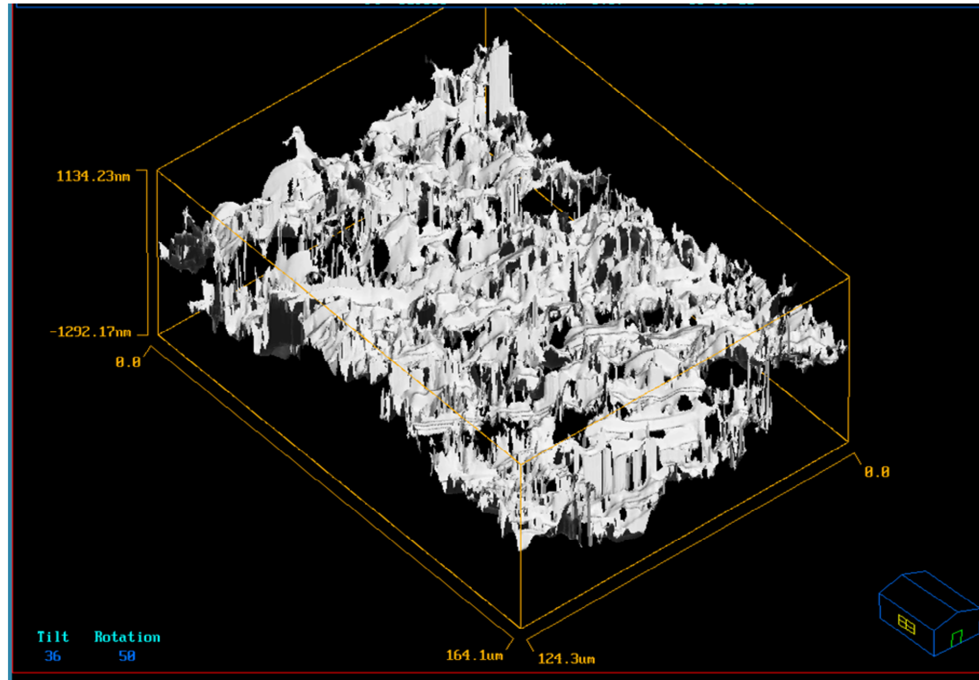

(a) Start of polishing, 431nm

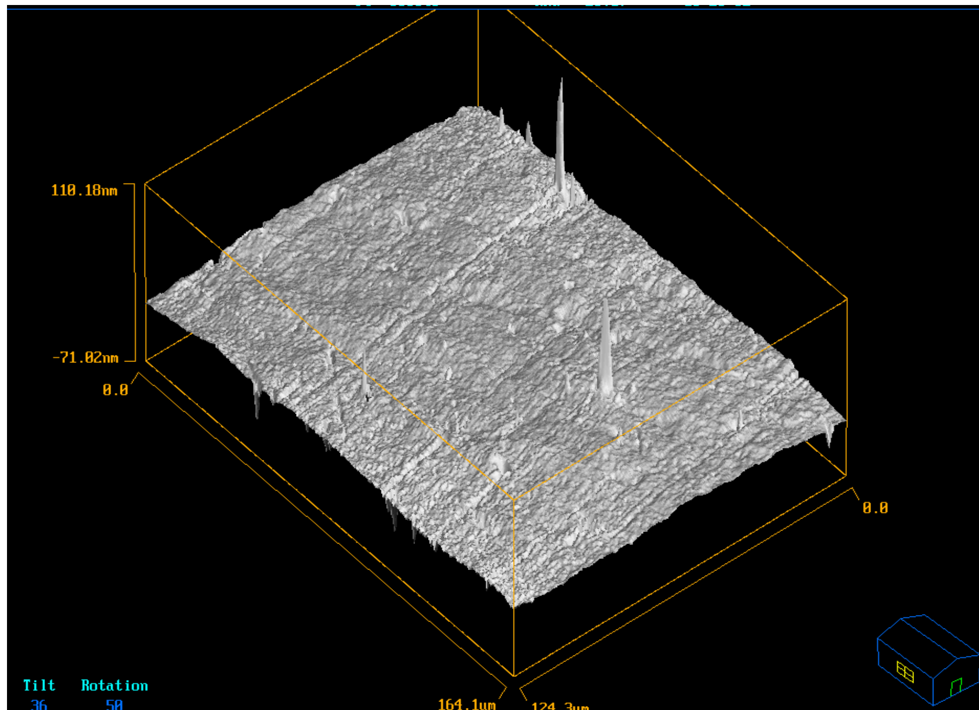

(b) 2min. of polishing, 4nm

Figures 62 (a) and (b): 3D surface profiles of the sample before and after polishing

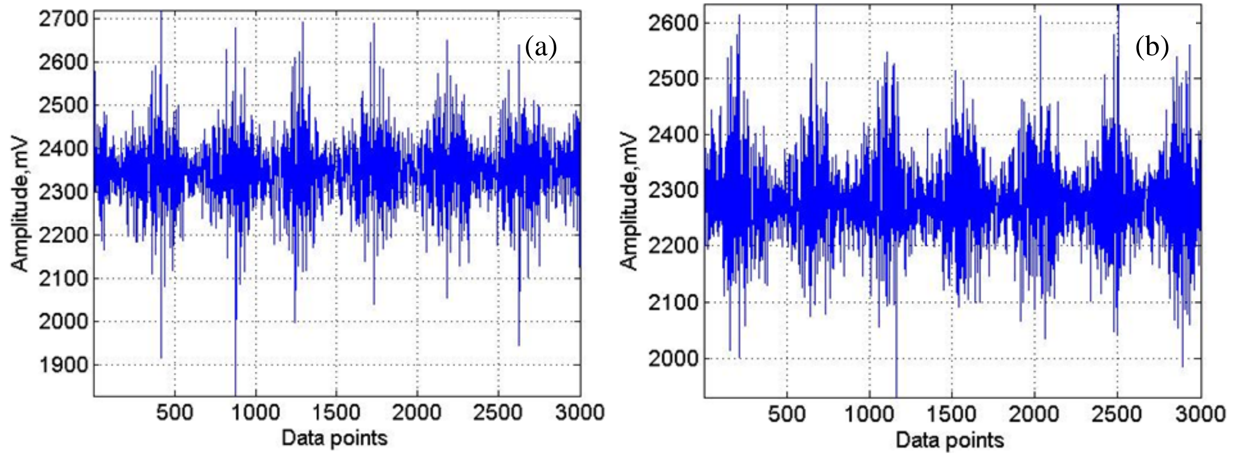

Figure 63: Comparison of time series of the signals under two different loading conditions of (10 lb and 5 lb) and same platen rotating speed of 500 rpm

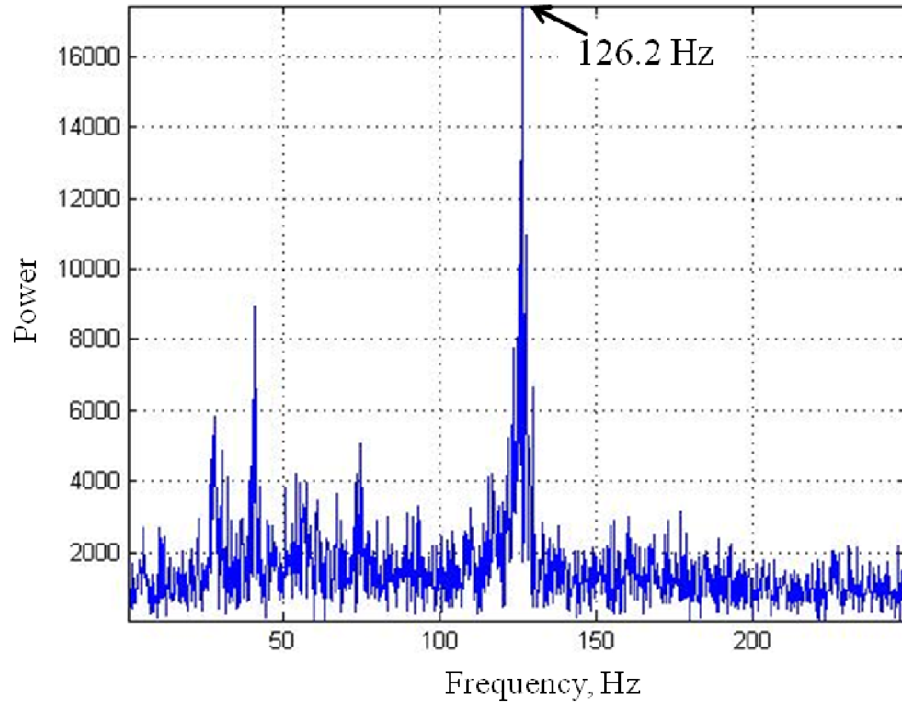

Figure 64: Power spectrum at 30 sec under Run R2 conditions [see Table 7]

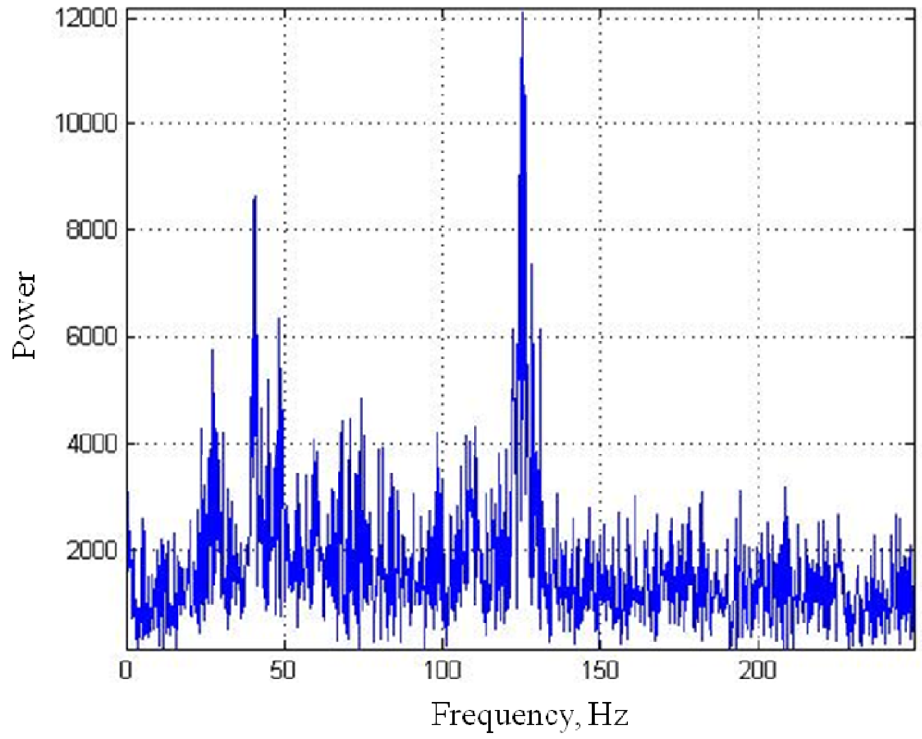

Figure 65: Power spectrum at 120 sec under Run R2 condition [see Table 8]

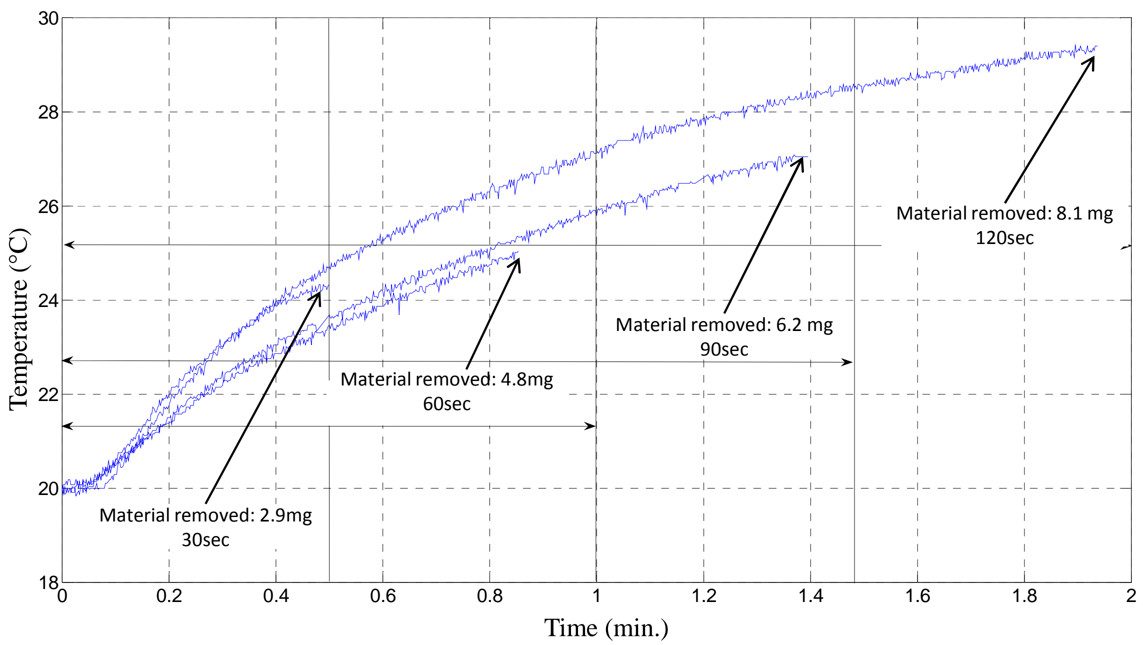

Figure 66: Temperature profiles with time during CMP polishing (platen rotational speed: 300 rpm, load: 10 lb, and pad: Microcloth)

Chapter 7: Feature Extraction and Process Dynamic Visualization

Time series analysis has been used in the past for visualization and analysis of the process in the time domain. With the evolution of the Fourier transforms, it became easier to analyze the process in the frequency domain. However, most of the signals from the CMP polishing are nonlinear. Consequently, this method appears to be inadequate for analyzing the process. The short time Fourier transform (STFT) has also been used for analyzing the process in the time and frequency domains. The wavelet analysis was found to be powerful enough for the denoising and real time condition monitoring.

Ganesan *et al*. [111] developed a sequential probability ratio test (SPRT) method based on a wavelet for real time monitoring of the polishing condition. They conducted CMP process monitoring by multi- resolution and multiscale analysis using the Daubechies wavelet on AE signals. It was successful in detecting the delamination defects.

Furthermore, multiscale Bayesian SPRT was developed for monitoring the non-stationary CMP process signals having multiple characteristics [112]. A modeling of the cutting process using wavelet and recurrence analysis was described in Ref. [113]. A recurrence quantification analysis (RQA) features based on recurrence and Morlet wavelet was used for analyzing the dynamics of the cutting process. The system showed periodic oscillation at low and high speeds when compared to intermittent motion and was confirmed by recurrence and Morlet wavelet analysis. It was explained that the curved and micro- patterns have resulted due to non-stationarity in the phase and frequency [114]. Recurrence occurred, when the integer multiple of the sampling interval matched with another period's integer multiple. The origin of a curved macro pattern was described using modulated and non-modulated sinusoid. Vazquez *et al.* [115] used the recurrence analysis for comparing between chaotic acoustic and chaotic pressure signal from bubble flow.

Sensor features extraction: Various features, including linear and nonlinear features were extracted to model the surface roughness of the polished copper samples. This includes statistical, energy and RQA based nonlinear features. Matlab code was written for extracting the features from the signal.

7.1 Statistical features:

The statistical features extracted using the Matlab for modeling roughness (Ra), MRR, and Preston Constant were mean, standard deviation (std.), variance, kurtosis, skewness, and mean peak to peak amplitude. In the following equations for statistical features, where y is the data points, n is the total number of points (n=1…j) and μ is the mean.

$$Mean, \mu = \frac{\sum_{j=1}^{n} y_j}{n}$$

$$Standard\ deviation\ (std), \sigma = \sqrt{\frac{1 \sum_{j=1}^{n}\ (y+\mu)^2}{n}}$$

$$\text{Variance (var)}, \sigma^2 = (y-\mu)^2$$

$$Kurtosis\ (krt) = \sum_{j=1}^{n} \frac{\left(y_j - \mu\right)^4}{n\sigma_2^4}$$

$$Skewness\ (skew) = \sum_{j=1}^{n} \frac{\left(y_j - \mu\right)^3}{n\sigma_2^3}$$

In addition to the above statistical features, the coefficient of variance i.e. (mean/std) feature was also calculated.

7.2 Time series visualization:

Figure 67 (a) and (b) shows the vibration signals obtained through the wireless channel at 5 lb load and 500 rpm rotating space at the start of polishing and after 2 minutes of polishing. The signal was observed to be burst in nature and the amplitude of the signal decreases in the

polishing process. This complex signal was formed mainly of two bands. The initial study was conducted to study the MRR, Ra with the vibration signals at a constant slurry concentration. Each run was carried out on a 1.6” copper sample. This test is carried with a ‘Microcloth pad’ from ‘Buehler’ at a constant 60 rpm of the spindle. The runs were conducted randomly to study the process dynamics without any uneven interactions of the factors.

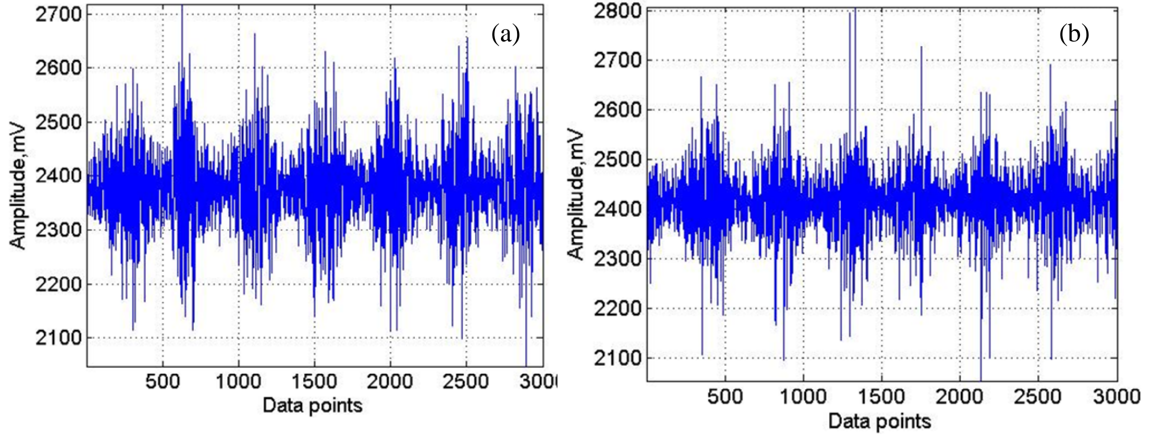

Figure 67: Vibration signal during the polishing process during the (a) Initial and (b) After 2 min of polishing under load 5 lb

7.3 Energy features:

The energy features of the spectrogram were used to extract the features for the short wave varying over a short period of time. The energy features of the short time Fourier transform (STFT) of the signals were extracted using Matlab. $\mathrm{X}(\tau, \omega)$ is the STFT of the $x(t)\ \omega(t-\tau)$

$$\text{Short time fourier transform, STFT} = \mathrm{X}(\tau, \omega) = \int_{-\infty}^{\infty} x(t)\ \omega(t-\tau) e^{-j\omega t} dt$$

Here, $\omega(t)$ is the window function centered around zero, $x(t)$ is the signal for transformation, ω is the frequency, and τ is the time index. Figure 68 shows the time series, the spectrogram, and the power spectrum of the vibration signal studied at platen rpm of 300 rpm and load 10 lb. The energy band from 120-130 Hz was taken for extracting energy features. Energy α was defined for the energy of the red segments while Energy γ was defined for energy between the red segments. In Matlab, the following command was used

Y= [S, F, T] =spectrogram(x, window, noverlap, nfft, fs).

Here, Y returns the STFT of the signal vector x i.e. 3000 data points, window size taken was 128, noverlap was the number of segments which each segment overlap i.e. size taken is 120, nfft was the dyadic length taken as 1024, and fs was the sampling frequency i.e. 500 Hz. In STFT matrix, S was the vector having a short time Fourier transform matrix of signal, F was the vector of a rounded frequency, and T was the time vector at which spectrogram was computed.

7.4 Time-frequency visualization:

Different conditions were investigated to study the dynamics during the polishing process. Wireless sensor-based technology has been applied in many processes, but so far, it was not applied to CMP process for a clear understanding of the process-machine interactions. In an earlier investigation, MEMS based wireless vibration sensors were used to compare with the wired sensor earlier for monitoring slurry chemistry effects on MRR [76]. The following conditions are required for vibration based monitoring i.e. the machine used for polishing should be stable and care should be taken for the positioning of the sensor for studying the process. The vibration-based sensor monitoring is complex because of the abrasives particles interacting during the polishing process. Figure 69 shows the spectrograms in Run R2 condition during 2 minutes of polishing with one repetition. The energy at the end of the polishing process decreases.

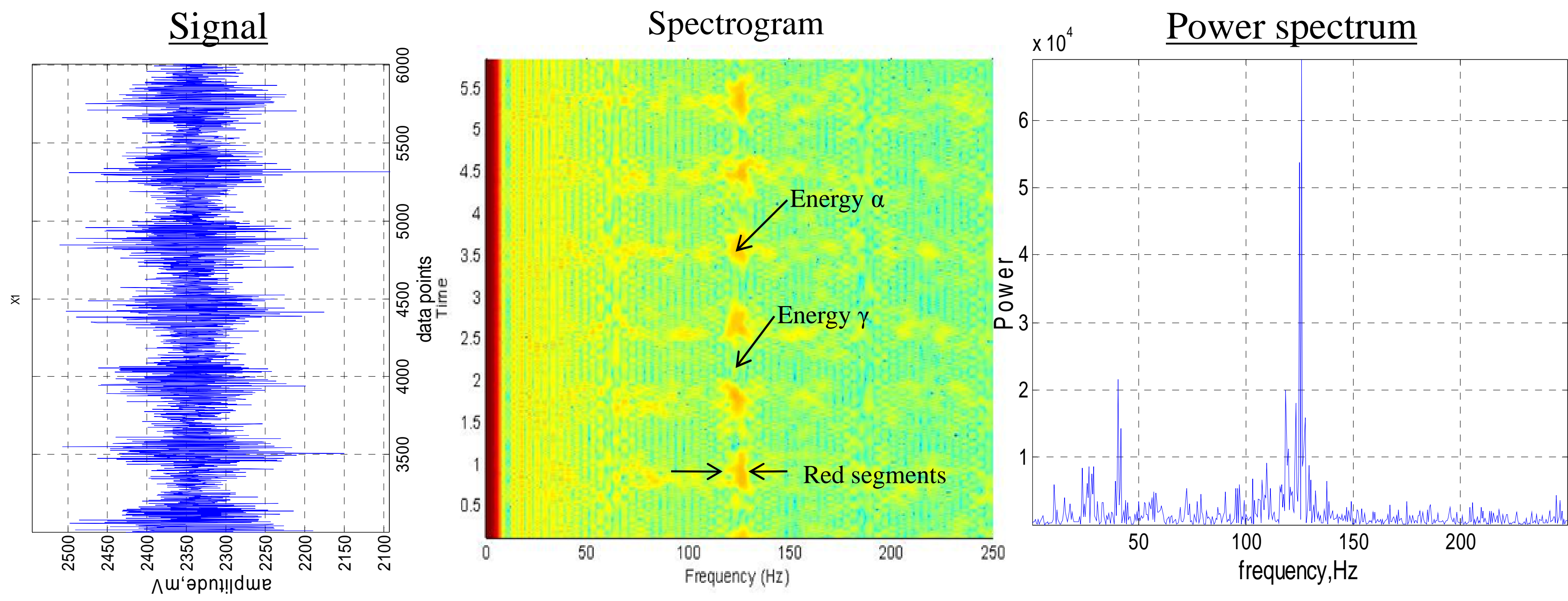

Figure 68: Time-frequency representation of the vibration signal at 300 rpm, 10 lb and slurry ratio 1:5

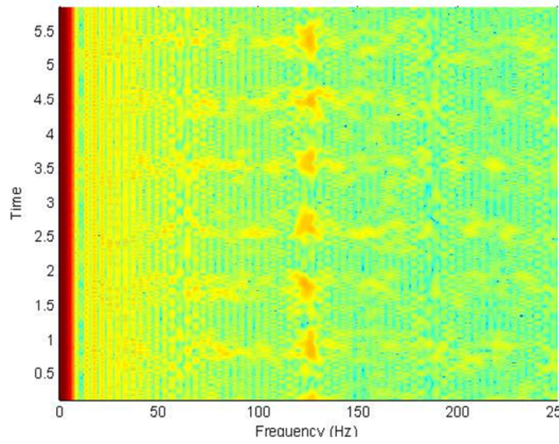

Start of polishing

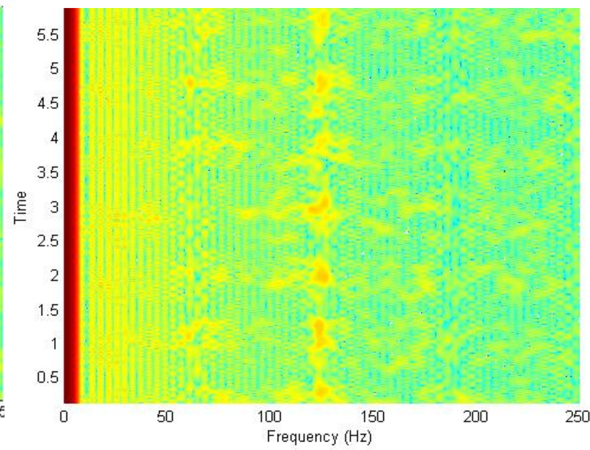

Middle of polishing

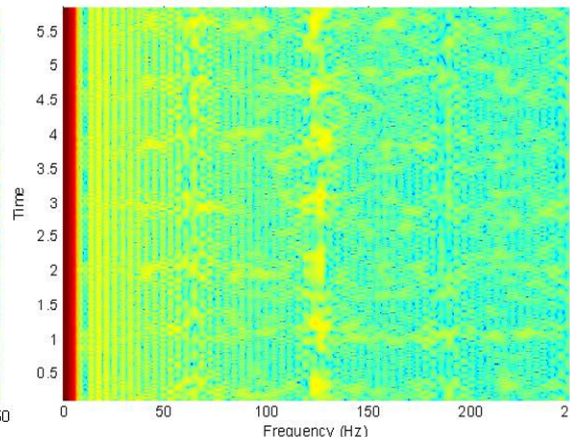

2min. of polishing

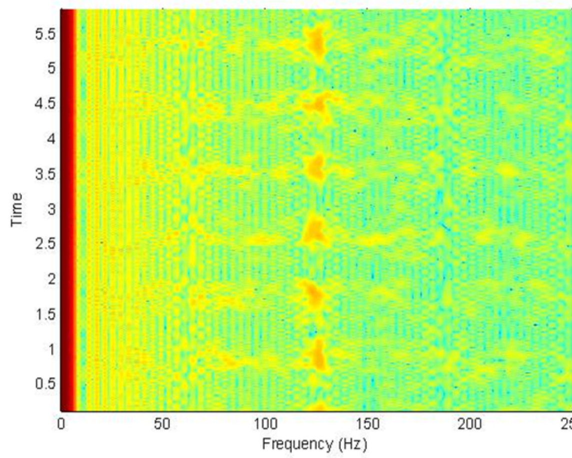

Start of polishing

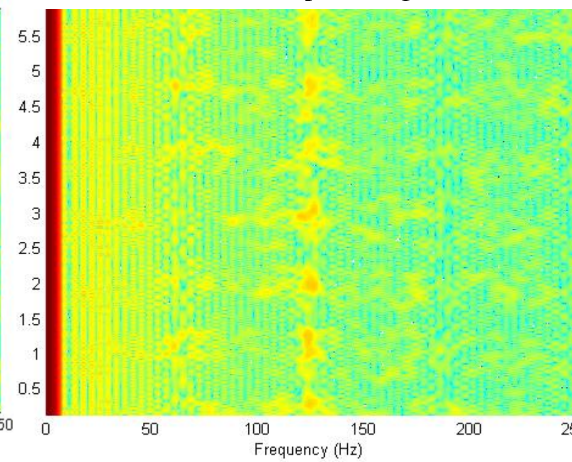

Middle of polishing

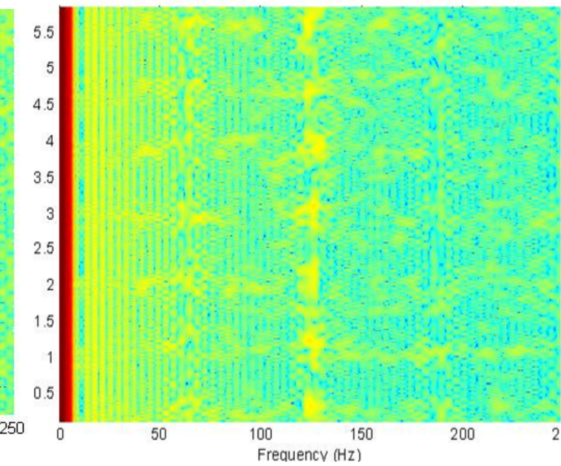

2min. of polishing

Figure 69: Spectrogram under Run R2 conditions with two repetitions [see Table 7]

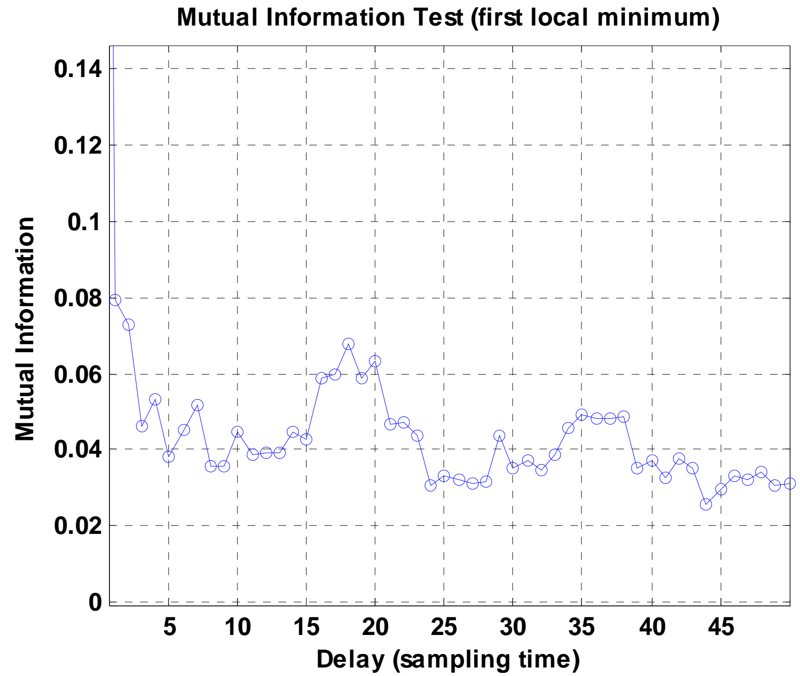

Figure 70: Time delay portrait with time delay 3 under Run R2 conditions at the start of polishing (See Table 7)

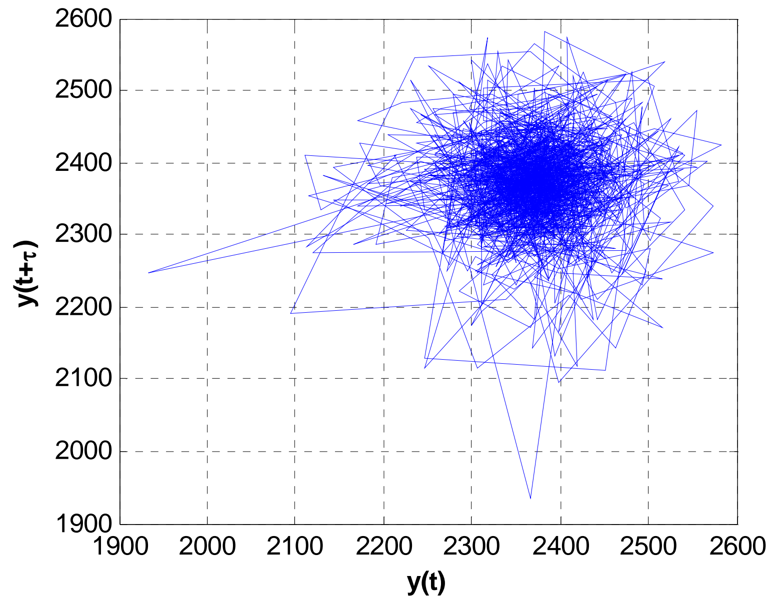

Figure 71: 3D Phase space portrait under Run R2 conditions at the start of polishing (See Table 7)

7.5 Nonlinear features:

Bukkapatnam *et al.* [75] studied the process dynamics of the polishing process for monitoring the MRR at different process-machine conditions using a lapping machine. The process studied was found to be stochastic in nature and bursts in the vibration signals were observed. The present study was done to study the Ra and the MRR with vibration signals at a constant slurry flow rate. Mainly, there were two parameters required for a recurrence plot, namely, time delay and dimension.

7.5.1 Mutual information: Information on the Time delay coordinates was required for plotting the phase space portrait of the signal. The mutual information is better than autocorrelation for finding the time delay [116]. Figure 70 shows the time delay plot for 1500 points using a mutual information algorithm. The time delay for Figure 70 is 3, where the first local minimum takes place.

7.5.2 False nearest neighbor [FNN]: This method is used for finding the dimensionality of the nonlinear system [117, 118]. It was found that the process was 6 dimensional at the start of polishing.

7.5.3 Recurrence quantification analysis (RQA): Eckmann *et al.* [119] presented a recurrence plot based on Lorenz attractor for describing the hidden parameters or dynamics of the process which was difficult to find with other analysis. RQA is a nonlinear data analysis tool which is used for the purpose of quantification of recurrent plots of a dynamic system based upon a structure on a small scale. It is used for studying the nonlinear dynamics of the processes, such as heart beat dynamics, blood pressure, muscle fatigue, protein molecular dynamics, and financial time series [120]. Recurrence analysis is used for investigating the out hidden recurring patterns, non-stationarity, and structural changes [121]. It enables visualizing of the dynamic systems through phase space trajectory. The total number of data points taken for the recurrence plot and RQA

analysis was 1500. Phase space portrait is the space in which all the possible states of the process can be represented. Figure 71 shows the phase space portrait of the vibration signal of 1500 data points for Run R1. Generally, for a phase space trajectory having k number of points, recurrence is described by a matrix

$$R_{i,j}(\varepsilon) = \Theta\left(\varepsilon - \|x_i - x_j\|\right), \quad i,j = 1, \dots k \qquad [121]$$

In recurrence matrix, ε is the threshold distance, Θ(x) is the Heaviside function having value 0 at $x < 0$ and value1 at $x > 0$. The back diagonal line is the line of identity.

RQA was introduced by Zbilut and Webber Jr. in 1992 [122]. The phase space trajectory is plotted using the embedded theorem. For recurrence analysis, proper care should be taken for selecting the threshold. If the threshold (ε) is too small, recurrence will be merely results due to noise fluctuation, leading to an increase in the area under the curve. However, if it is taken too large then every other point in it will be in the neighborhood of the other point which causes recurrence in hidden form structure, leading to a decrease in the area under the curve[123]. Also, 5% of the phase space diameter should be chosen for threshold measurement. Nichols *et al.*[124] used RQA features for damage detection in structures using algorithms. The algorithm was based on one feature to detect damage detection without any assumption compared to FEM. Three recurrence quantifiers used were recurrence, determinism, and entropy. Recurrence showed a higher value when the damage occurred, and the entropy was less sensitive at a large threshold. Various recurrence quantifiers are as follows [122]:

a) Recurrence rate (Recrate): It is the percentage of dark points in the threshold recurrence plot. It also includes the probability of the recurrence at a particular rate. It describes the amount of recurrent points that will cover the recurrent plot. The recurrent rate for a given window size(W) can be explained as follows:

   Recurrence (%), REC=100*(number of recurrent points in the triangle) / (W (W-1)/2)

b) Determinism (DET): It is the percentage of all the dark points that will be aligned or predicted. It describes the percentage of recurrent points that lie above the diagonal line segments.

   Determinism (%), DET=100*(No of points in diagonal lines)/ (No of recurrent points)

c) LMAX: It is the length of the longest diagonal line segment in the plot. It states that a small LMAX describes a more chaotic or a less stable signal, while a higher LMAX describes the repeated or periodic signal.

d) Entropy (Shannon entropy) (ENT): It considers the signal complexity and distribution of the line length. It enables in finding out the probability (P_{bin}) of the diagonal line which has same length by frequency distribution. Its units are given by bits/bin. For the periodic signal, the entropy is 0 bits/bin

$$ENT = -\sum (P_{bin}) \log_2 / (P_{bin})$$

e) Trend (TND): It describes the barrier of the recurrence plot towards its edges. It is the quantification of the paling of recurrent points away from the diagonal. It tells about the system stationarity. If the system is periodic, then its value will be near 0. It is calculated as the slope of the line-of-best-fit through REC as a function of orthogonal displacement from the main diagonal.

f) LAM: It describes the fraction of recurrence points which will be forming the vertical lines rather than diagonal lines in the case of the LAM.

   LAM (%) = 100(Number of points in the vertical lines/Number of recurrent points).

g) Trapping time (TT): It defines the average length of vertical lines in the recurrence plot. It explains the mean time the system traps at a particular state.

7.5 Nonlinear dynamic visualization:

For RQA based features extraction, data of 20 sec was divided in three parts of 1500 data points taken from the beginning, the middle, and the end. Then the average of all these features

was taken for analysis. Table 12 shows the RQA based nonlinear features of a particular run. Figure 72 shows the recurrence plot having high frequency components. For the recurrence plot, no de-noising of the signal is required. At the start of polishing, a clear high frequency segment can be seen in the recurrence plot, but at the end of polishing, these high frequency segments decreases showing the end of polishing. The average roughness of the sample at the start of polishing was 350 nm. Figure 73 shows the recurrence plot at the end of polishing. The energy of the signal decreases at the end of polishing which is shown in the faded segment in the recurrence plot. The roughness of the sample at the end of polishing was 15 nm.

Table 9 shows the process parameters, such as load on the sample (lb), rpm of the carrier, slurry ratio, slurry temperature rise, and change in pH at the conditions in run R1 (see Table 7). Table 10 shows various sensor signals based statistical features, namely, mean of the signal, variance of the signal, and maximum of the signal etc.

Table 11 shows various vibration features, such as energy, peak to peak amplitude (PTP) of the signal, and thermal features like net temperature rise and temperature rise rate under run R1 conditions (see Table 7). The time-frequency features i.e., energy α and energy γ were extracted from the spectrogram in the frequency range from 120 to 132 Hz. The energy α was the energy of the red segment, and energy γ is the energy in-between the two red segment in the spectrogram. Table 12 shows various nonlinear recurrence quantification analysis (RQA) based features under run R1 conditions. This includes dimension and time delay of the signals. As discussed in section 7.3.3, the periodic signal has zero entropy. In RQA, the entropy was above four; therefore, the signal is not periodic in nature.

These sensor features with process parameters were then used for sensor based modeling. Sensor features extracted were modeled in Minitab 15 using a response surface methodology. R^2 stands for goodness of fit or coefficient of determination, and adjusted R^2 is the modified version

of R^2 which increases only when new variables are introduced in the model [125]. R^2 (Pred.) describes how well and accurate the model predicts response for new observation.

$$R^2 = \frac{\text{SSR}}{\text{SST}}$$

Here, SSR stands for the sum of square of the regression, and SST is the total sum of the squares. The total number of variables is 32. Both R^2 and Adjusted R^2 show how well the model fits the data.

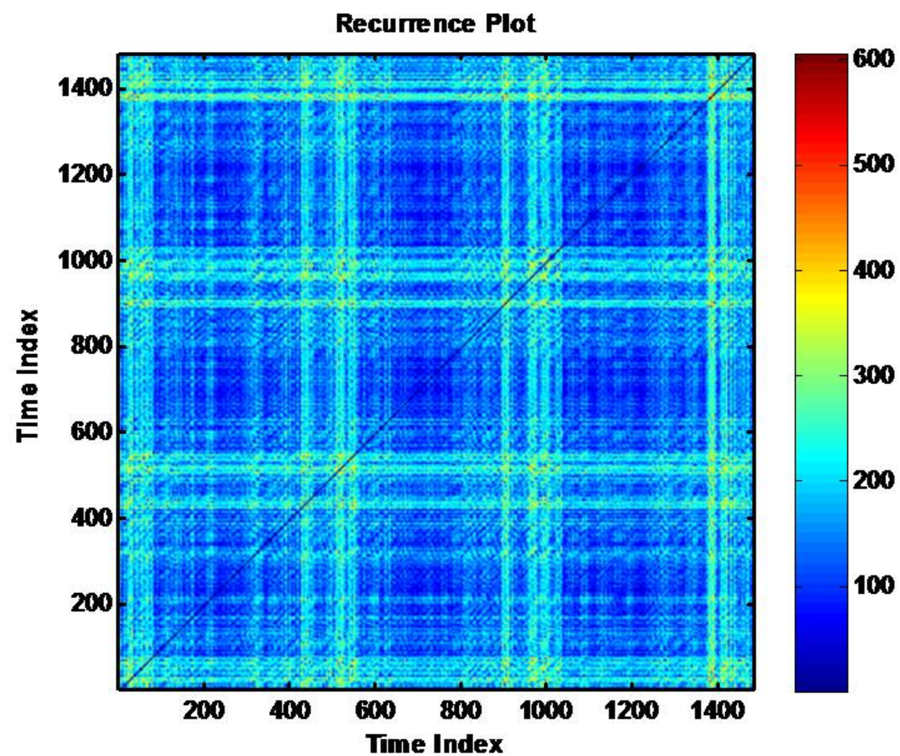

Figure 72: Recurrence plot obtained after the start of polishing: speed of the platen 300 rpm, load 10 lb, and slurry ratio 1:3

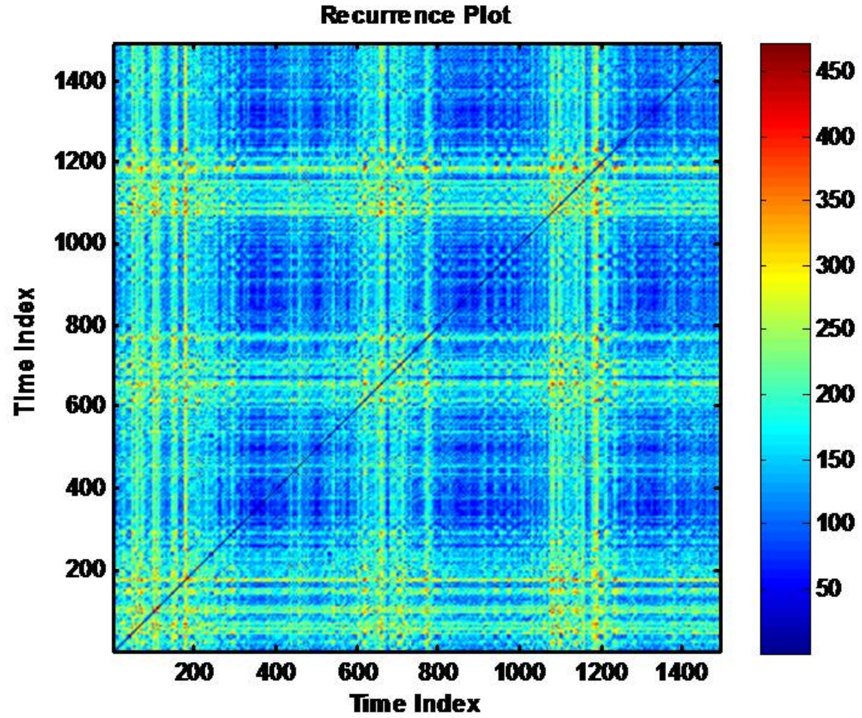

Figure 73: Recurrence plot: End of polishing: speed of the platen 300 rpm, load 10 lb, and slurry ratio 1:3

For good fit, both should have a high value. In addition, $\mathrm{df_r}$ is the degree of freedom of the error, i.e.,

$$\mathrm{df_r} = \text{total no. of variables} - \text{no. of features in the model} - 1$$

For an effective modeling, the number of degree of freedom should be at least 25. However, for our modeling, the minimum number of degree of freedom was 18. The models were effective in predicting the performance up to 92% accuracy.

Table 9: Machine parameters and slurry temp (°C)

Run	Load, lb	Rpm	Time, sec	Slurry ratio	Slurry temp rise	ΔpH
R1	10	500	30	1:3	3.85	0.85
R1	10	500	60	1:3	6	0.9
R1	10	500	90	1:3	6.3	1
R1	10	500	120	1:3	5.4	0.9

Table 10: Statistical features and MRR (mg/sec)

Run	Mean	Var.	Max.	mode	skew.	Kurt.	MRR
R1	2354.45	5911.76	2842.5	2350	-0.2	6.985	0.14
R1	2330.71	6354.7	2823	2338.5	0.198	5.598	0.124
R1	2296.10	6612.76	2840.5	2299.17	0.095	6.116	0.119
R1	2406.93	3687.17	2697.75	2406.75	-0.11	4.536	0.105

Table 11: Energy features, Temperature features (°C), peak to peak and Roughness, nm

Run	Energy, α	Energy, γ	Net temp rise	Temp. rise rate	PTP	Avg. Ra
R1	193.210	190.001	11.6	0.387	104.40	24
R1	193.338	188.282	20.7	0.345	108.55	13
R1	195.251	190.439	23.5	0.261	126.20	8
R1	191.996	187.448	32.73	0.273	120.64	7

Table 12: RQA (Nonlinear) features

Run	Time delay	Dim.	Recrate	Det.	Lmax	ENT	Lam	TT
R1	3.67	6.67	21.69	66.67	243.67	4.75	78.06	15.51
R1	3	5.84	14.78	50.10	129.5	3.43	61.8	7.34
R1	3.56	6.45	14.72	44.53	138.67	3.83	60.71	8.5
R1	2.92	6.25	9.174	28.6	94.17	3.84	45.50	6.13

Chapter 8: Sensor Fusion Regression Modeling

8.1 Technical approach:

Figure 74 gives the sensor fusion methodology applied in this investigation. All experiments were conducted using a vibration sensor and a temperature sensor. The input variables (machine parameters) are the load, rpm, and slurry ratio. The flow rate of the slurry was kept constant in all experiments. After the experiments, signal features were extracted using various statistical and nonlinear techniques.

The vibration signal features were divided into three parts i.e. statistical, time-frequency, and nonlinear features. Two temperature features, namely, temperature rise rate and net temperature rise were used for this study. In addition to this, slurry temperature was used as a feature. The models were developed first using the vibration features followed by temperature features using the response surface methodology (RSM). The RSM based regression modeling is developed as follows: statistical features only; statistical and frequency features; statistical, frequency, and nonlinear features; statistical, frequency, nonlinear features, and temperature features to improve roughness (Ra) and MRR models. This study leads to sensor fusion modeling for monitoring the CMP process involving mechanical and thermal effects. This model tracks roughness and MRR involving linear characteristics, time-frequency characteristics, and nonlinear characteristics. The statistical significant value (P-value) is chosen as 0.08.

Figure 75 shows that the plot between the residual and the fitted value showing no relation i.e. there is no pattern in the residual vs. fitted value.

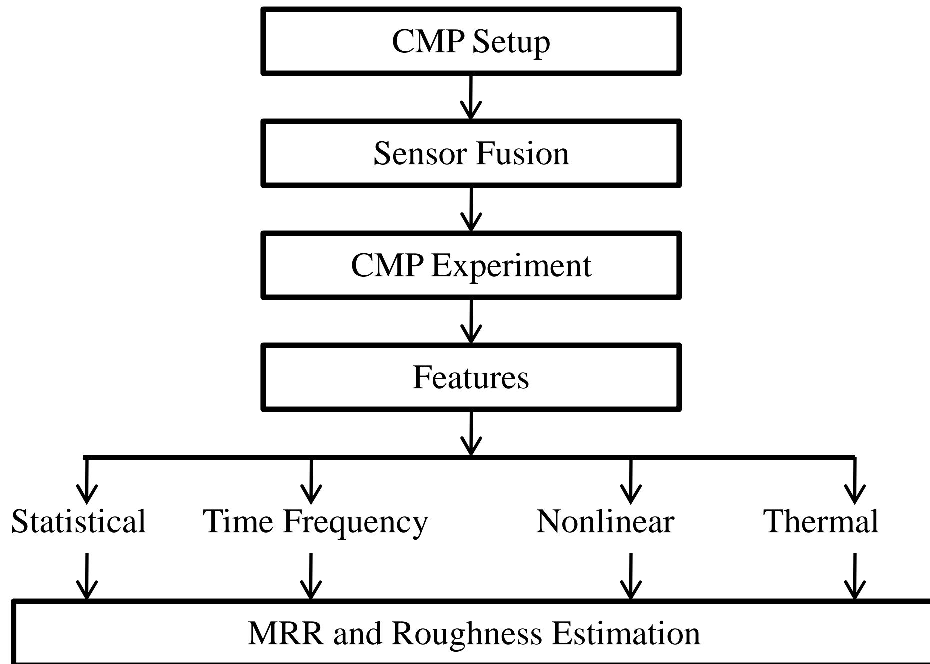

Figure 74: Sensor fusion methodology

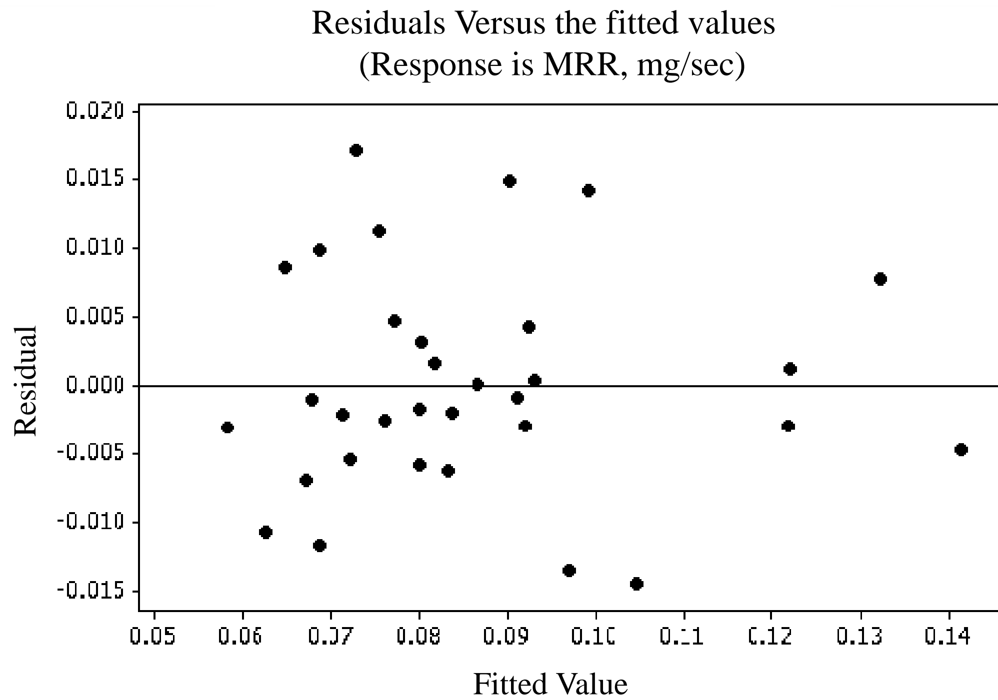

Figure 75: Plot of the residual versus the fitted values

8.2 Regression modeling of surface roughness:

In this, roughness of the copper sample is fitted against sensors features using response surface analysis incorporating two way interactions of the features which are found to be statistical significant in the model. The vibration and temperature sensor are found to capture the dynamics using a regression fit.

Various roughness models were presented in the following sections:

Modeling of surface roughness with process parameters in section 8.2.1, modeling of surface roughness with statistical features in section 8.2.2, modeling of surface roughness with statistical and Energy features in section 8.2.3, modeling of surface roughness with statistical, Energy, and RQA features in section 8.2.4, and modeling of surface roughness with statistical, Energy, RQA, and thermal features in section 8.2.5.

8.2.1 Regression model of surface roughness (nm) with process features:

The roughness of the copper sample is fitted against process features which are statistically significant. The two way interactions are found to be statistically insignificant as there p-value are more than 0.08. Equation [1] gives the regression model or best fit for surface roughness using process parameters. Table 13 shows significant values for each of the predictor variables. Since R^2 value is low (23.16 %), it is clear that process parameters are not sufficient for regression fitting of the roughness.

R^2= 23.16 %, R^2 (adj.) = 17.86 %, df_r=29

$$Ra = 48.86 - 14.73\ \text{load} + 12.08\ \text{slurry ratio} \quad [1]$$

Table 13: Regression model of Ra using process parameters

(R^2= 23.16 %, R^2 (adj.) = 17.86 %, df_r=29)

Predictor	P-value
constant	0.000
load	0.030
slurry ratio	0.071

8.2.2 Regression model of surface roughness (nm) with statistical features:

The surface roughness of the copper sample is fitted to the statistical features including their statistically significant two way interactions. The process parameters are not sufficient for modeling performance. Therefore, statistical features are used for modeling roughness. Equation [2] gives the regression model for surface parameters using statistical features.

Table 14 shows the significant value for each of the process parameters and its interaction. Since, p-value of the statistical features PTP amplitude, maximum, skewness, and kurtosis with their interactions are below 0.08, they are significant. The sensor based statistical features alone are able to estimate 66% of the roughness model.

R^2 = 66.6%, R^2 (adj.) = 58.6%, df_r=25

$$Ra = 156 - 105.69\ PTP - 160.99\ max - 83.80\ skew + 230.92\ krt - 194.27\ PTP*skew - 90.19\ max*krt. \quad [2]$$

Table 14: Regression model of Ra using statistical features

(R^2= 66.6%, R^2 (adj.) = 58.6%, df_r=25)

Predictor	P-value
constant	0.000
PTP	0.001
maximum	0.004
skewness	0.005
kurtosis	0.000
PTP* skewness	0.004
maximum*kurtosis	0.070

8.2.3 Regression model of surface roughness (nm) with statistical and Energy features:

Equation [3] gives the regression fit for the surface roughness using statistical and energy features. Table 15 shows the significant value for each of the statistical, energy, and their interactions. The model performance was not satisfactory using the statistical techniques. Also, the vibration signal includes time varying wave components. Therefore, energies features from the spectrogram are used for modeling. Since, p-value of energy γ, energy α and their interaction with the statistical features are below 0.08, they are significant. Use of energy features and their interactions with statistical features leads to an increase of approximately 15% in R^2.

$R^2 = 78.40\%$, R^2 (adj.) = 68.12%, $df_r=21$

$$Ra = -84814 - 0.758\,mean - 483083\,CoV + 742\,skew + 464\,energy\,\alpha - 0.00463\,energy\,\gamma + 36.7max + 2570\,CoV^{*}\,energy\,\alpha + 0.132skew^{*}energy\,\gamma - 2.01max^{*}skew - 0.196\,max^{*}\,energy\,\alpha. \quad [3]$$

($R^2 = 78.40\%$, R^2 (adj.) = 68.12%, $df_r=21$)

Predictor	P-value
constant	0.002
mean	0
coefficient of var.	0.801
skewness	0.368
energy α,db	0.132
energy γ,db	0.025
maximum	0.008
coefficient of var.*energy α,db	0.013
skewness*energy γ,db	0.041
skewness*maximum	0
maximum * energy α, db	0.001

* Coefficient of variance (COV), skewness, and energy α, db are taken because they are present in the interaction terms

8.2.4 Regression model of surface roughness (nm) with statistical, energy, and RQA features:

In this, the roughness of the copper sample is fitted against features, such as namely, statistical, energy, and RQA features including their statistically significant two way interactions. Equation [4] gives the regression fit for surface roughness. Table 16 shows the significant values for each of the statistical, energy, nonlinear features, and their interactions. It can be seen from section 7.3,

vibration signals are nonlinear; therefore, their nonlinear features are required to capture nonlinearity in the signals. In the model, the nonlinear features namely, RQA are LAM, LMAX and their interactions. Since p-value of the interactions are below 0.08, they are significant. There is an increase in R^2 by $\sim$ 8%. The degrees of freedom of the error for this model are 20.

$$R^2 = 84.08\%,\ R^2\ (\text{adj.}) = 75.33\%,\ df_r=20$$

$$Ra = 4955 - 4.26\ max + 5252\ skew - 4.5\ lam + 6.36\ Lmax + 0.0474\ energy\ \gamma + 0.000647\ max * max - 1.93\ max * skew + 0.0337\ max * lam - 0.0112\ max * Lmax - 0.00231\ energy\ \gamma * lam + 0.000659 \quad [4]$$

Table 16: Regression model of Ra with statistical, energy, and RQA features

(R^2= 84.08%, R^2 (adj.) = 75.33%, df_r=20)

Predictor	P-value
constant	0.465
maximum	0.192
skewness	0.413
lam	0.065
Lmax	0.336
energy γ,db	0.04
maximum*maximum	0.042
maximum*skewness	0
maximum*lam	0.009
maximum*Lmax	0
lam*energy γ,db	0.038
Lmax*energy γ,db	0.013

* maximum, skewness, Lam, Lmax, energy γ are included because they are present in the interaction terms

8.2.5 Regression model of surface roughness with thermal features only:

In this, roughness of the copper sample is fitted against temperature only. The temperature features like net temperature rise, temperature rise rate, slurry temperature rise and their interactions are found to be statistically significant. Equation [5] gives the regression model for

surface roughness using temperature features only. Table 17 shows the significant values for each of the thermal features and their interactions.

R-Sq = 73.94 %, R-Sq (adj.) = 67.69 %, df_r=25

Avg. Ra, nm = 61.525 – 60.81 slurry temp. rise – 2.882 net temp. rise + 45.751 temp. rise rate – 53.974 (temp. rise rate).^2 – 54.426 (slurry temp. rise * temp. rise rate) + 94.283 (net temp. rise * temp. rise rate). [5]

Table 17: Regression model of Ra with thermal features only

R-Sq = 73.94 %, R-Sq (adj.) = 67.69 %, df_r=25

Predictor	P-value
constant	0.000
slurry temp. rise	0.000
net temp. rise	0.868
temp. rise rate	0.015
(temp. rise rate).^2	0.014
slurry temp. rise * temp. rise rate	0.019
net temp. rise * temp. rise rate	0.030

* net temp. rise is included because it is present in the interaction terms

8.2.6 Regression model of surface roughness with statistical, Energy, RQA, and Temperature features:

In this, roughness of the copper sample is fitted against vibration and temperature sensors features including their statistically significant two way interactions. Equation [6] gives the regression model for surface roughness using vibration and temperatures features. Table 18 shows the significant value for each of the statistical, energy, RQA, temperature, and their interactions. The two- way interactions between vibration and temperature features are found to be statistical significant in the model. Thermal features taken are the net temperature rise and temperature rise rate. Use of thermal features leads to increase in R^2 of 10%. Good regression fit is obtained using both the sensors features with degree of the freedom of the error 18.

$$R^2 = 92.72\%,\ R^2\,(adj.) = 87.47\%,\ df_r=18$$

$$\text{Ra} = -\,3890 + 0.607\ \text{max} + 445\ \text{krt} + 13.7\ \text{energy}\ \alpha - 0.0128\ \text{energy}\ \gamma + 2.82\ \text{lam} + 1.42\ \text{Lmax} - 6.67\ \text{net temp. rise} + 7787\ \text{temp. rise rate} - 0.115\ \text{lam.}^2 - 0.141\ \text{krt} * \text{max} - 0.402\ \text{krt} * \text{Lmax} + 0.0313\ \text{Lmax} * \text{lam} - 40.3\ \text{energy}\ \alpha * \text{temp. rise rate.} \quad [6]$$

Table 19 shows the summary of all the results obtained from the models using response surface methodology. The model performance increased using vibration and thermal features. This table includes the estimation of prediction using above technique.

Table 18: Regression model of Ra with statistical, energy, RQA, and temperature features

(R^2= 92.72%, R^2 (adj.) = 87.47%, df_r=18)

Predictor	P-value
constant	0.000
maximum	0.000
kurtosis	0.126
energy α, db	0.131
energy γ, db	0.006
lam	0.037
Lmax	0.090
net temperature rise	0.000
temp. rise rate	0.001
lam*lam	0.000
maximum * kurtosis	0.000
kurtosis * Lmax	0.001
energy α, db * temp. rise rate	0.002
lam * Lmax	0.030

*Kurtosis and energy α are included because they are present in the interaction terms

Table 19: Sensor fusion based roughness estimation

Sensor	Features	R^2	R^2(adj.)	R^2(Pred.)	df_r
No sensor	Process parameters	23.16 %	17.86 %	6.44 %	29
Vibration sensor	Statistical features(Stats.)	66.60 %	58.60 %	54.42 %	25
Vibration sensor	Stats + Energy(Spectrogram)	78.40 %	68.12 %	36.36 %	21
Vibration sensor	Stats + Energy + RQA	84.08 %	75.33 %	53.17 %	20
Temperature sensor	Temperature	73.94 %	67.69 %	49.09 %	25
Vibration and Temperature sensor	Stats + Energy +RQA+ Temperature	92.72 %	87.47 %	65.44 %	18

8.3 Regression modeling of MRR:

In this, MRR of the copper sample is fitted against sensors features using response surface methodology incorporating two-way interactions of the features. The two-way interactions in the regression models are found to be statistical significant.

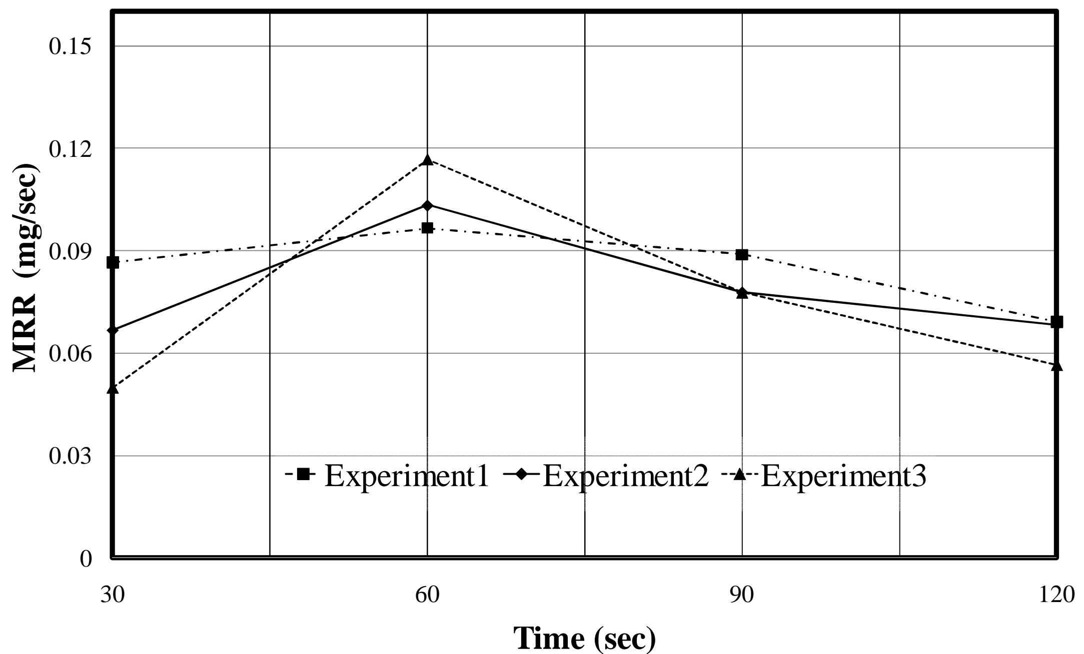

Figure 76: MRR repetition for Run R2 (see Table 7)

Vibration and temperature sensors are found to capture the process dynamics through good regression fit of the model. Various MRR regression fitting models were discussed in the following sections:

Modeling of MRR with process parameters in section 8.3.1; modeling of MRR with statistical features in section 8.3.2; modeling of MRR with statistical and energy features in section 8.3.3; modeling of MRR with statistical, energy, and RQA features in section 8.3.4; and modeling of MRR with statistical, RQA features, and temperature signal in section 8.3.5

The development of the regression model using vibration and temperature features are given the following:

8.3.1 Regression model of MRR (mg/sec) with process parameters:

In this, MRR of the copper sample is fitted against process features including their statistically significant two-way interactions. Figure 76 shows the material removal rate under run R2 conditions (see Table 7) with a constant carrier rpm of 60. The MRR increases at 60sec followed by a decreasing trend. Equation [7] gives the regression fit for the surface roughness. The Process parameters, namely, load, rpm, and slurry ratio are used for regression modeling of MRR. Table 20 shows the significant values for each of the process parameters. R^2 are found to be 49.53% with df_r =28. For effective modeling of MRR, process parameters are insufficient. The regression fit for MRR with process parameters is as follows

$$R^2 = 49.53\%,\ R^2\ (adj.) = 44.12\%,\ df_r = 28$$

$$MRR = 0.0451 + 3.24\times10^3\ load + 1.14\times10^4\ rpm - 5.76\times10^3\ slurry\ ratio. \quad [7]$$

Table 20: Regression model of MRR model using machine parameters alone

(R^2=49.53%, R^2 (adj.) =44.12%, df_r =28)

Predictor	P-value
constant	0
load	0.009
rpm	0
slurry ratio	0.055

8.3.2 Regression model of MRR (mg/sec) with statistical features:

In this, MRR of the copper sample is fitted against statistical features including their statistically significant two way interactions. Since modeling using process parameters are not sufficient to investigate the process; sensor features are extracted for modeling MRR effectively. Equation [8] gives the regression model for MRR. Table 21 shows the significant value for each of the statistical features and their interaction. The coefficient of determination is 74.55% with df_r = 25. Statistical features alone are able to explain one-third of the model. However, it is not sufficient for good modeling. The MRR model using statistical features are given in the following

$$R^2 = 74.55\ \%,\ R^2\ (adj.) = 68.44\%,\ df_r = 25$$

$$MRR = -5.64 - 2.14\times10^{4}\ mean - 2.2\times10^{5}\ var. + 4.61\times10^{3}\ max. - 0.0196\ krt. - 1\times10^{6}\ max*max + 5\times10^{5}\ var.*krt. \quad [8]$$

Table 21: Regression model of MRR using statistical features

(R^2= 74.55 %, R^2 (adj.) = 68.44%, df_r = 25)

Predictor	P-value
constant	0
mean	0.047
variance	0.017
maximum	0.627
kurtosis	0.298
maximum*maximum	0.006
variance*kurtosis	0.036

*maximum and Kurtosis were included because they were present in the interaction terms

8.3.3 Regression model of MRR (mg/sec) with statistical features and energy features:

Equation [9] gives the regression fit incorporating energy features from the spectrogram.

Table 22 shows the significant value for each of the statistical, energy and their interaction. The model performances using the statistical features alone are not sufficient for good estimation of the MRR; therefore, energy features were incorporated in it. The energy features from the spectrogram were calculated at 120-130 Hz. For this model, two energies are extracted using Matlab. After adding energy features, there was approximately a 15% increased in the coefficient of determination. The degree of freedom of the error is 25.

R^2 = 82.2 %, R^2 (adj.) = 77.9%, df_r = 25

$$MRR = -0.432+0.170\ skew + 1.43\times10^{4}\ var + 1.28\times10^{4}\ energy\ \alpha + 7\times10^{6}\ energy\ \gamma - 4.5\times10^{5}\ var * skew - 1\times10^{6}\ var * energy\ \gamma. \quad [9]$$

Table 22: Regression model of MRR using statistical and energy features

(R^2= 82.2 %, R^2 (adj.) = 77.9%, df_r = 25)

Predictor	P-value
constant	0.047
skewness	0.002
variance	0.021
energy α, db	0.064
energy γ, db	0.228
variance * skewness	0.001
variance *energy γ, db	0.032

8.3.4 Regression model of MRR (mg/sec) with statistical, energy and RQA features:

As shown in section 7.3, vibration signals are found to be nonlinear; therefore nonlinear features to capture nonlinearity were added in the model. Equation [10] gives the regression model for MRR. Table 23 shows significant value for each of the statistical, energy, and RQA features and their interactions. This leads to an increase in predictability of about approximately 7% with a degree of freedom 23. Since the p-value for nonlinear features namely determinism and dimension are below 0.08, they are statistically significant. Good regression fit is observed in this model.

R^2 = 87.2 %, R^2 (adj.) = 82.7 %, df_r = 23

$$MRR = -0.299 + 1.34\times10^{4}\ var + 0.203\ skew + 1.53\times10^{3}\ energy\ \alpha + 4\times10^{6}\ energy\ \gamma - 5.4\times10^{5}\ var*\ skew - 1\times10^{6}\ var*\ energy\ \gamma - 0.0169\ dim + 2.6\times10^{4}\ det. \quad [10]$$

Table 23: Regression modeling of MRR using statistical, energy, and RQA features

(R^2= 87.2 %, R^2 (adj.) = 82.7 %, df_r = 23)

Predictor	P-value
constant	0.135
variance	0.019
skewness	0.000
energy α, db	0.017
energy γ, db	0.415
variance * skewness	0.000
variance*energy γ, (db)	0.029
dimension	0.020
determinism	0.060

8.3.5 Regression model of MRR (mg/sec) with thermal features only:

Equation [11] gives the regression model for MRR using thermal features only. Table 24 shows significant value for each of the thermal features and their interactions. The thermal features are net temperature rise, temperature rise rate, and slurry temperature rise. Since the p-value of the features with their interactions is below 0.08, they are statistically significant. The coefficient of determination of this model is 81.10 % with degree of freedom of error 26.

R-Sq = 81.10 %, R-Sq (adj.) = 77.47 %, df_r=26

MRR = 0.08479 – 0.03208 slurry temp. rise – 0.02569 net temp. rise + 0.04538 temp. rise rate – 0.02331 (net temp. rise).^2 – 0.01883 (slurry temp. rise * temp. rise rate). [11]

Table 24: Regression modeling of MRR using thermal features only

(R-Sq = 81.10 %, R-Sq (adj.) = 77.47 %, df_r=26)

Predictor	P-value
constant	0.000
slurry temp. rise	0.000
net temp. rise	0.001
temp. rise rate	0.000
(net temp. rise).^2	0.005
slurry temp. rise * temp. rise rate	0.016

8.3.6 Regression model of MRR (mg/sec) with statistical, energy, RQA, and thermal features:

Equation [12] gives the regression model for MRR. Table 25 shows the significant value of each of the statistical, energy, RQA, thermal features and their interaction. After adding thermal features, R^2 of the model increase to 90.23%. Since the p-value of the interactions is below 0.08, they are statistically significant. The degree of freedom of error is 20.

R^2 = 90.23%, R^2 (adj.) = 84.86%, df_r=20

$$\text{MRR, mg/sec} = 0.11 + 3.89\times10^{3}\text{ temp rise rate} + 6.8\times10^{2}\text{ var.} - 1.2\times10^{2}\text{ skew.} - 3.4\times10^{3}\text{ time delay} - 6.9\times10^{4}\text{ energy }\alpha - 1.5\times10^{2}\text{ energy }\gamma - 2.3\times10^{2}\text{ temp. rise rate* energy }\alpha - 2.3\times10^{2}\text{ temp. rise rate * energy }\gamma - 0.0563\text{ var*skew} + 2.1\times10^{2}\text{ var.*energy }\alpha - 2.1\times10^{2}\text{ time delay* energy }\gamma. \quad [12]$$

Table 25: Regression modeling of MRR using statistical, energy, RQA, and Temperature features (R^2= 90.23%, R^2 (adj.) = 84.86%, df_r=20)

Predictor	P-value
constant	0.000
temp. rise rate	0.641
variance	0.000
skewness	0.043
time delay	0.449
energy α, db	0.320
energy γ, db	0.035
temp. rise rate* energy α, db	0.043
temp. rise rate* energy γ, db	0.012
variance* skewness	0.005
variance*energy α, db	0.014
time delay* energy γ, db	0.049

*Temp. rise rate, time delay and energy α are included because they are present in the interaction terms

Table 26 shows the summary of all the results obtained incorporating R-sq (Pred.). The R-sq (Pred.) decreases after including the temperature feature in the model. The overall coefficient of determination of the model is 90.23% with a degree of freedom of error 20.

Table 26: Sensor fusion based MRR estimation

	Features	R^2	R^2(adj.)	R^2(Pred.)	df_r
No sensor	Process parameters	49.53 %	44.12 %	34.08 %	28
Vibration sensor	Statistical features(Stats.)	74.55 %	68.44 %	42.33 %	25
	Stats + Energy(Spectrogram)	82.20 %	77.90 %	71.89 %	25
	Stats + Energy + RQA	87.20 %	82.70 %	76.27 %	23
Temperature sensor	Temperature	81.10 %	77.47 %	68.07 %	26
Vibration and Temperature sensor	Stats +Energy+ RQA+ Temperature	90.23 %	84.86 %	72.06 %	20

8.4 Regression modeling of Preston constant (K_p):

Preston [56] formulated an MRR for glass polishing. The Preston equation does not include chemical or thermal effect for CMP process. From the literature, it is known that the Preston constant can include chemical and mechanical effects. The work mentioned below focuses on including thermal and mechanical effect in the Preston constant. It is known from the literature that tribological and thermal effects play a main role in the CMP process. The temperature plays an important role in the chemical parts of the CMP process. The increase in temperature leads to an increase in chemical reaction of the process leading to increase in the MRR. The Preston constant (K_p) for the model can be calculated as:

$$K_p = \frac{MRR}{PV}$$

The MRR is the material removal rate, P is the load applied on the copper sample, and V is the relative velocity. Based on the experimental conditions, the K_p can be calculated. In our work, we have modeled Preston constant statistically using sensor fusion modeling techniques. The head rpm was constant in the model. In our model, the V was the platen rpm. This model is able to estimate K_p using a vibration signal and temperature signal. In the above model, the MRR was calculated using sensor features i.e.

$$MRR = KPV = f(sensor\ features)$$

$$K_p = \frac{MRR}{PV} = f(sensor\ featurea)$$

In this, Preston constant is fitted against sensors features using response surface analysis incorporating two way interactions of the features. The two way interaction in the regression models are found to be statistical significant in the model. Various K_p models were discussed in the following sections:

Modeling K_p with statistical features in section 8.4.1; modeling K_p with statistical and Energy features in section 8.4.2; modeling K_p with statistical, Energy, and RQA features in section 8.4.3; modeling K_p with statistical, RQA features, and temperature signal in section 8.4.4 and modeling $K_p$with statistical, RQA features, temperature signal, and process parameter in section 8.4.5.

Development of the regression models using vibration and temperature features are given the following

8.4.1 Regression model of K_p with statistical features:

In this, Preston constant is fitted against vibration sensors based statistical features including their statistically significant two way interactions. Equation [13] gives the regression model for Preston model using statistical features. Table 27 shows the significant value for each of the statistical features namely mean peak to peak amplitude, mean, variance, mode and their interaction. Using statistical features alone results in a higher estimation of the coefficient of determination with a degree of freedom of error 19. The coefficient of determination of the modal using statistical features is 74.88%. The p-value of the statistical features and their interactions is below 0.08 and they are statistically significant.

$R^2 = 74.88\%$, R^2 (adj.) = 59.02%, df_r=19

$$K_p = 4.2\times10^{-5} + 8.3\times10^{-5}\,PTP - 1.72\times10^{-4}\,mean - 2.21\times10^{-4}\,variance + 1.39\times10^{-4}\,mode + 8\times10^{-6}\,skew + 5.7\times10^{-5}\,krt. + 2.24\times10^{-4}\,CoV - 2.86\times10^{-5}\,PTP{*}mean + 3.8\times10^{-5}\,PTP{*}var + 2.91\times10^{-4}\,PTP{*}mode - 1.52\times10^{-4}\,PTP{*}skew + 6.2\times10^{-5}\,mode{*}skew. \quad [13]$$

Table 27: Regression model of K_p using statistical features

(R^2= 74.88%, R^2 (adj.) = 59.02%, df_r=19)

Predictor	P-value
constant	0.002
PTP	0.001
mean	0.002
variance	0.008
mode	0.001
skewness	0.390
kurtosis	0.000
coefficient of var.	0.010
PTP*mean	0.009
PTP*variance	0.023
PTP*mode	0.008
PTP*skewness	0.000
mode* skewness	0.013

*skewness is included because it is present in the interaction terms

8.4.2 Regression model of K_p with statistical and energy features:

In this, Preston constant is fitted against statistical and energy features which includes their statistically significant two way interactions. To increase the performance of the K_p model, energy features are incorporated in the model.

Table 28: Regression model of K_p model using statistical and energy features

(R^2= 80.29%, R^2 (adj.) = 64.05%, df_r=17)

Predictor	P-value
constant	0.429
PTP	0.019
mean	0.025
variance	0.026
mode	0.288
skewness	0.000
kurtosis	0.000
energy γ,db	0.028
coefficient of var.	0.007
PTP*skewness	0.000
variance*mode	0.009
variance*coefficient of variance	0.027
mode*kurtosis	0.053
mode* energy γ, db	0.008
skewness*energy γ, db	0.004

*mode is included because it is present in the interaction terms

The energy features from the spectrogram are extracted using Matlab. Equation [14] gives the regression model for Preston model.

Table 28 shows the significant value of each of the statistical features, energy features and their interactions. After including energy features, the estimation of the coefficient of determination increased approximately by 9% with a degree of freedom of error 17.

$$R^2 = 80.29\%,\ R^2\,(adj.) = 64.05\%,\ df_r = 17$$

$$K_p = 1.6\times10^{-5} + 3.1\times10^{-5}\ PTP - 8.4\times10^{-5}\ mean - 3.66\times10^{-4}\ var + 4.8\times10^{-5}\ mode + 4.3\times10^{-5}\ skew + 8.4\times10^{-5}\ krt + 3.82\times10^{-4}\ CoV - 3.5\times10^{-5}\ energy\ \gamma - 1.074\times10^{-4}\ PTP * skew + 3.8\times10^{-5} var * mode + 7.2\times10^{-5}\ var * CoV - 7.7\times10^{-5}\ mode * krt - 2.9\times10^{-5}\ mode * energy\ \gamma + 7.0\times10^{-}\ skew * energy\ \gamma. \quad [14]$$

8.4.3 Regression modeling K_p with statistical, energy, and RQA features:

Nonlinear features are extracted from the signal using recurrence quantification analysis for analyzing the dynamic nature of the CMP process. The RQA features were able to detect the deterministic nature of the vibration signals in the CMP process. Equation [15] gives the regression model for Preston constant. Table 29 shows the significant value for each of the statistical, energy, RQA features and their interactions. Since the p-value of the interactions of statistical and RQA features are below 0.08, they are significant. The coefficient of determination after adding RQA features increased from 80.29 % to 85.59 % with a degree of freedom of error 20.

$$R^2 = 85.59\%,\ R^2\,(adj.) = 77.66\%,\ df_r = 20$$

$$K_p = -1\times10^{-6} - 1.6\times10^{-5}\ skew - 1.03\times10^{-4}\ var - 2.1\times10^{-5}\ Lmax + 1.36\times10^{-4}\ lam + 9\times10^{-6}\ time\ delay + 3.1\times10^{-5}\ det - 9\times10^{-6}\ energy\ \gamma - 1.12\times10^{-4}\ (lam)^2 - 8.1\times10^{-5}\ skew * var - 1.49\times10^{-4}\ var * Lmax + 2.7\times10^{-4}\ var * lam. \quad [15]$$

Table 29: Regression model of K_p using statistical, energy, and RQA features

(R^2= 85.59%, R^2 (adj.) = 77.66%, df_r=20)

Predictor	P-value
constant	0.960
skewness	0.003
variance	0.000
Lmax	0.159
lam	0.000
time delay	0.052
determinism	0.001
energy γ, db	0.001
lam*lam	0.000
skewness* variance	0.000
variance*Lmax	0.000
variance* lam	0.000

*Lmax is included because it is present in the interaction terms

8.4.4 Regression modeling of K_p with thermal features only:

Equation [16] gives the regression model for Preston constant. Table 30 shows the significant value for each of the thermal features and their interactions. Since the p-value of the features and their interactions are below 0.08, they are significant. The coefficient of determination of this model is 68.75 % with degree of freedom of error 25.

R-Sq = 68.75 % , R-Sq (adj.) = 61.25 %, df_r=25

$$K_p = 3.1\times 10^5 - 2.5\times 10^5 \text{ slurry temp. rise} + 1\times 10^5 \text{ net temp. rise} + 1.3\times 10^5 \text{ temp. rise rate} + 2.3\times 10^5 (\text{slurry temp. rise})\text{.^2} - 2.5\times 10^5 (\text{slurry temp. rise} * \text{net temp. rise}) + 3.2\times 10^5 (\text{temp. rise rate} * \text{net temp. rise}) \quad [16]$$

Table 30: Regression model of K_p using thermal features only

(R-Sq = 68.75 %, R-Sq (adj.) = 61.25 %, df_r=25)

Predictor	P-value
constant	0.000
slurry temp. rise	0.000
net temp. rise	0.126
temp. rise rate	0.05
(slurry temp. rise).^2	0.002
slurry temp. rise * net temp. rise	0.009
temp. rise rate * net temp. rise	0.011

8.4.5 Regression modeling of K_p with statistical, energy, RQA, and thermal features:

Equation [17] gives the regression model for Preston constant.

Table 31 shows the significant value for each of the statistical, energy, RQA, thermal features and their interaction. Since the p-value for the thermal feature i.e. slurry temperature incorporated in the model is below 0.08, it is statistically significant. After incorporating this feature, the coefficient of determination increases by approximately 1%.

R^2 = 86.00%, R^2 (adj.) = 75.9%, df_r=19

$$K_p = 9.9\times10^{-5} + 4.23\times10^{-4}\,\text{var} - 4.7\times10^{-4}\,\text{CoV} + 9\times10^{-6}\,\text{energy}\,\alpha + 2\times10^{-4}\,\text{energy}\,\gamma - 4.6\times10^{-5}\,\text{mode} - 1\times10^{-6}\,\text{time delay} - 9\times10^{-6}\,\text{slurry temp rise} - 2.8\times10^{-4}(\text{var})^2 + 2.08\times10^{-4}\,\text{var}*\text{CoV} + 3.57\times10^{-4}\,\text{var}*\text{energy}\,\gamma - 3.92\times10^{-4}\,\text{CoV}*\text{energy}\,\gamma - 2\times10^{-5}\,\text{CoV}*\text{time delay} - 2.7\times10^{-5}\,\text{energy}\,\alpha*\text{mode}. \quad [17]$$

Table 31: Regression model of K_p using statistical, energy, RQA, and temperature features (R^2= 86.00% R^2 (adj.) = 75.9%, df_r=19)

Predictor	P-value
constant	0.000
coefficient of var.	0.000
variance	0.000
energy α, db	0.001
energy γ, db	0.000
mode	0.002
time delay	0.001
variance * variance	0.011
coefficient of var.* variance	0.043
coefficient of var.* energy γ, db	0.000
coefficient of var.* time delay	0.002
energy α, db* mode	0.001
variance * energy γ, db	0.000
slurry temp. rise	0.003

8.4.6 Regression modeling of K_p with statistical, RQA, thermal features, and process parameters:

In this, Preston constant of the wafer is fitted against process features, statistical features, RQA features, and thermal features. Also, includes their statistically significant two way interactions. Equation [18] gives the regression model for Preston constant. Table 32 shows the various sensor features and their interactions. There is an increase in estimation of K_p by 91% with a

degree of freedom of error 21. Since the p-value of the energy features is below 0.08, they are insignificant, therefore are not incorporated in the model.

$R^2 = 91.98$ %, R^2 (adj.) = 88.16%, $df_{r=}21$.

$$K_p = 2.1\times10^{-5} - 1.0\times10^{-5}\ \text{load} - 4\times10^{-6}\ \text{rpm} - 3\times10^{-6}\ \text{slurry temp rise} + 1.5\times10^{-5}\ \text{temp rise rate} + 1\times10^{-6}\ \text{skew} - 4\times10^{-6}\ \text{det} + 1.4\times10^{-5}\ \text{lam} + 1.5\times10^{-5}\ (\text{slurry temp rise})^2 + 1.2\times10^{-5}\ (\text{det})^2 - 1.6\times10^{-5}\ \text{temp rise rate}*\text{skew}. \quad [18]$$

Table 32: Regression model of K_p with sensors features and process parameter

(R^2= 91.98 %, R^2 (adj.) = 88.16%, dfr=21)

Predictor	P-value
constant	0.000
load	0.000
rpm	0.001
slurry temp. rise	0.152
temp. rise rate	0.006
skewness	0.948
determinism	0.221
lam	0.013
slurry temp. rise* slurry temp. rise	0.000
determinism* determinism	0.015
temperature rise rate* Skewness	0.046

*Slurry temperature rise, skewness, and determinism are included because they are present in the interaction terms

Table 33 shows the summary of all results from the model estimation by a response surface methodology. This R^2 prediction for the combined model is 79.96 % with a degree of freedom of error 21. The overall coefficient of determination of the model is 91.98%.

Table 33: Summary of the Kp model

Sensor	Features	R^2	R^2(adj.)	R^2(Pred.)	df_r
Vibration sensor	Statistical	74.88 %	59.02 %	50.01 %	19
	Statistical + Energy	80.29 %	64.05 %	19.58 %	17
	Statistical + Energy + RQA	85.59 %	64.39 %	64.39 %	20
Temperature sensor	Temperature	68.75 %	61.25 %	50.48 %	25
Vibration and Temperature sensor	Statistical + Energy + RQA + Temp	86.00 %	75.90 %	44.45 %	19
Process parameter, Vibration, and Temperature sensor	Process parameter+ Statistical + Energy + RQA + Temp	91.98 %	88.16 %	79.76 %	21

Chapter 9: Conclusions and Future Work

From a monitoring point of view, the performance parameters interactions with the input features should be known. This is perhaps the first time, a roughness model is attempted using experimental results from the sensor fusion approach. The sensor fusion based modeling is attempted to track roughness and MRR during the process. The empirical model includes mechanical and thermal parameters. The experimental investigation is conducted on a bench top machine using full factorial design of experiments to build the models. Various features such as statistical, time-frequency features, and nonlinear features are incorporated in the regression models to track the process parameters in the model. It was found from the literature that temperature plays an important role in the performance of the process. The inclusions of thermal features lead to an increase in the performance of the roughness regression model by approximately 10 %. Temperature features such as slurry temperature and the temperature of the copper sample are found to be statistically significant in the model. Also, the MRR and Preston constant are modeled using sensor fusion based features. Details of the roughness regression model for various parameters are given in Table 34.

From roughness model, it is concluded that the process parameters such as loading and rpm conditions are not sufficient for modeling. Using statistical features alone led to an estimate of the roughness of 66.6 %. After incorporating energy and RQA features, the regression model was able to estimate 84.08 % of the roughness of the copper wafer. The regression model is able to estimate approximately 92.72 % of the roughness after incorporating thermal features with a degree of freedom of error 18. Details of the MRR regression model for various parameters are given in Table 34.

Table 34: Regression models of surface roughness and MRR

Features	**Roughness model**				**MRR model**			
	R^2	R^2(adj.)	R^2(Pred.)	df_r	R^2	R^2(adj.)	R^2(Pred.)	df_r
Process parameters	23.16 %	17.86 %	6.44 %	29	49.53 %	44.12 %	34.08 %	28
Statistical features(Stats.)	66.60 %	58.6 %	54.42 %	25	74.55 %	68.44 %	42.33 %	25
Stats + Energy(Spectrogram)	78.40 %	68.12 %	36.36 %	21	82.20 %	77.90 %	71.89 %	25
Stats + Energy + RQA	84.08 %	75.33 %	53.17 %	20	87.20 %	82.70 %	76.27 %	23
Temperature	73.94 %	67.69 %	49.09 %	25	81.10 %	77.47 %	68.07 %	26
Stats + Energy +RQA+ Temperature	92.72 %	87.47 %	65.44 %	18	90.23 %	84.86 %	72.06 %	20

In the MRR regression model, the process parameters are able to estimate up to 50 % of the MRR of the copper sample. However, this estimation is not enough for effective modeling. Therefore, sensor based features were added in the model. Using statistical features alone, the estimation of the MRR is approximately 75 %. Then on incorporating energy and RQA features, the estimation of the MRR is approximately 91 %. The thermal features further increase the estimation to approximately 91 %.

In addition to the above, a model is proposed for modeling the Preston constant. The proposed model includes process parameters, vibration features, and thermal features. Details of the Preston Constant model for various parameters are given in Table 35.

Sensor based features are able to effectively estimate the process output variables. For further work, wavelet based features after denoising can be incorporated which can help in increasing the estimation of the process. Thus multiscale regression models can be helpful in monitoring purposes. The vibration sensor was sampled at 500 Hz. Higher sampling rate of the sensor can be helpful for predictive model performance by extracting features from the high frequency component of the Fast Fourier Transform.

Table 35: Regression models of Preston Constant

Features	R^2	R^2(adj.)	R^2(Pred.)	df_r
Statistical	74.88 %	59.02 %	50.01 %	19
Statistical + Energy	80.29 %	64.05 %	19.58 %	17
Statistical + Energy + RQA	85.59 %	64.39 %	64.39 %	20
Temperature	68.75 %	61.25 %	50.48 %	25
Statistical + Energy + RQA + Temp	86.00 %	75.90 %	44.45 %	19
Process parameter+ Statistical + Energy + RQA + Temp	91.98 %	88.16 %	79.76 %	21

In addition, acoustic or sound sensor features can be incorporated in the model. Temperature of the pad and various parameters of the pad, such as roughness, hardness of the pad can be incorporated in the model for increasing its performance. The features extracted from the signal can be used to build models for predicting the states of the system. These features can further be used for detecting various defects. Neural network and fuzzy logic based models can be developed for optimizing the model, thereby better understands the CMP process.

References

[1] P. B. Zantye, A. Kumar, and A. K. Sikder, "Chemical mechanical planarization for microelectronics applications," *Materials Science and Engineering: R: Reports,* vol. 45, no. 3-6, pp. 89-220, 2004.

[2] J. Yi, "Friction modeling in linear chemical-mechanical planarization," *IEEE Control Systems Magazine,* vol. 28, no. 5, pp. 59-78, 2008.

[3] J.-Y. lai, and N. Saka, "Mechanics, mechanisms and modeling of the CMP process," MIT, Ph.D thesis, 2001.

[4] J. M. Steigerwald, S. P. Murarka, and R. J. Gutmann, *Chemical mechanical planarization of microelectronic materials*: Wiley-Interscience, 1997.

[5] J. M. Steigerwald, S. P. Murarka, R. J. Gutmann, and D. J. Duquette, "Chemical processes in the chemical mechanical polishing of copper," *Materials Chemistry and Physics,* vol. 41, no. 3, pp. 217-217, 1995.

[6] S. Aksu, L. Wang, and F. M. Doyle, "Effect of hydrogen peroxide on oxidation of copper in CMP slurries containing glycine," *Journal of the Electrochemical Society,* vol. 150, no. 11, pp. G718-G723, 2003.

[7] G. J. Pietsch, G. S. Higashi, and Y. J. Chabal, "Chemomechanical polishing of silicon: Surface termination and mechanism of removal," *Applied Physics Letters,* vol. 64, no. 23, pp. 3115-3117, 1994.

[8] R. Carpio, J. Farkas, and R. Jairath, "Initial study on copper CMP slurry chemistries," *Thin Solid Films,* vol. 266, no. 2, pp. 238-244, 1995.

[9] Y. Hayashi, M. Sakurai, T. Nakajima, K. Hayashi, S. Sasaki, S.-i. Chikaki, and T. Kunio, "Ammonium-salt-added silica slurry for the chemical mechanical polishing of the interlayer dielectric film planarization in ULSI's," *Japanese Journal of Applied Physics,* vol. 34, no. Part 1, No. 2B, pp. 1037.

[10] Q.Luo, D.R.Campbell, and S.V.Babu, "Chemical-mechanical polishing of copper in alkaline media," *Thin Solid Films,* vol. 311, pp. 177-182, 1997, 1997.

[11] S. aksu, and F. M.Doyle, "Electrochemistry of copper in chemical mechanical planarization slurries containing glycine," *VMIC proceedings*, pp. 1-5, 2001, 2001.

[12] S. Aksu, and F. M. Doyle, "The role of glycine in the chemical mechanical planarization of copper," *Journal of the Electrochemical Society,* vol. 149, no. 6, pp. G352-G361, 2002.

[13] F. M. Doyle, and L. Wang, "Chemical and electrochemical characterization of peroxide induced passivation of copper in aqueous glycine solutions " *Proceedings VMIC* pp. 267-276, 2003.

[14] S. H. Bae, S.-M. Yang, and D. H. Kim, "Effects of chemical reaction on the polishing rate and surface planarity in the copper CMP" *Korea-Australia Rheology Journal,* vol. 14, 2, 2002.

[15] S. Haba, K. Fukuda, Y. Ohta, Y. Koubuchi, and T. Katouda, "Fumed silica slurry stabilizing methods for chemical mechanical polishing," *Japanese Journal of Applied Physics,* vol. 42, no. 2 A, pp. 418-423, 2003.

[16] S. Seal, S. C. Kuiry, and B. Heinmen, “Effect of glycine and hydrogen peroxide on chemical-mechanical planarization of copper,” *Thin Solid Films,* vol. 423, no. 2, pp. 243-251, 2003.

[17] T. Du, Y. Luo, and V. Desai, “The combinatorial effect of complexing agent and inhibitor on chemical-mechanical planarization of copper,” *Microelectronic Engineering,* vol. 71, no. 1, pp. 90-97, 2004.

[18] J.-C. Chen, S.-R. Lin, and W.-T. Tsai, “Effects of oxidizing agent and hydrodynamic condition on copper dissolution in chemical mechanical polishing electrolytes,” *Applied Surface Science,* vol. 233, no. 1-4, pp. 80-90, 2004.

[19] V. R. K. Gorantla., K. A. Assiongbon., S. V. Babu., and D. Roy., “Citric acid as a complexing agent in CMP of copper,” *Journal of the Electrochemical Society,* vol. 152, no. 5, pp. G404-G410, 2005.

[20] J.-C. Chen, and W.-T. Tsai, “Effects of hydrogen peroxide and alumina on surface characteristics of copper chemical-mechanical polishing in citric acid slurries,” *Materials Chemistry and Physics,* vol. 87, no. 2-3, pp. 387-393, 2004.

[21] Y. Ein-Eli, E. Abelev, and D. Starosvetsky, “Electrochemical aspects of copper chemical mechanical planarization (CMP) in peroxide based slurries containing BTA and glycine,” *Electrochimica Acta,* vol. 49, no. 9-10, pp. 1499-1503, 2004.

[22] S. Deshpande, S. C. Kuiry, M. Klimov, Y. Obeng, and S. Seal, “Chemical mechanical planarization of copper: role of oxidants and inhibitors,” *Journal of the Electrochemical Society,* vol. 151, no. 11, pp. G788-G794, 2004.

[23] V. R. K. Gorantla, E. Matijevic, and S. V. Babu, “Amino acids as complexing agents in chemical mechanical planarization of copper,” *Chemistry of Materials,* vol. 17, no. 8, pp. 2076-2080, 2005.

[24] T.-H. Tsai, Y.-F. Wu, and S.-C. Yen, “Glycolic acid in hydrogen peroxide-based slurry for enhancing copper chemical mechanical polishing,” *Microelectron. Eng.,* vol. 77, no. 3-4, pp. 193-203, 2005.

[25] Y. N. Prasad, and S. Ramanathan, “Chemical mechanical planarization of copper in alkaline slurry with uric acid as inhibitor,” *Electrochimica Acta,* vol. 52, no. 22, pp. 6353-6358, 2007.

[26] M. C. Kang, H.-S. Nam, H. Y. Won, S. Jeong, H. Jeong, and J. J. Kim, “Effects of OH radicals on formation of Cu oxide and polishing performance in Cu chemical mechanical polishing,” *Electrochemical and Solid-State Letters,* vol. 11, no. 2, pp. H32-H35, 2008.

[27] S.-C. Lin, H.-C. Huang, and H. Hocheng, “Effects of slurry components on the surface characteristics when chemical mechanical polishing NiP/Al substrate,” *Thin Solid Films,* vol. 483, no. 1-2, pp. 400-406, 2005.

[28] T. Gopal, and J. B. Talbot, “Effects of CMP slurry chemistry on the zeta potential of alumina abrasives,” *Journal of the Electrochemical Society,* vol. 153, no. 7, pp. G622-G625, 2006.

[29] R. Ihnfeldt, and J. B. Talbot, “The Effects of Copper CMP Slurry Chemistry on the Colloidal Behavior of Alumina Abrasives,” *Journal of the Electrochemical Society,* vol. 153, no. 11, pp. G948-G955, 2006.

[30] J. Wang, and A. G. Haerle, “Chemical mechanical planarization of copper using transition alumina nanoparticles,” *Thin Solid Films,* vol. 516, no. 21, pp. 7648-7652, 2008.

[31] J. McGrath, and C. Davis, “Polishing pad surface characterisation in chemical mechanical planarisation,” *Journal of Materials Processing Technology,* vol. 153-154, pp. 666-673, 2004.

[32] H. Lu, B. Fookes, Y. Obeng, S. Machinski, and K. A. Richardson, “Quantitative analysis of physical and chemical changes in CMP polyurethane pad surfaces,” *Materials Characterization,* vol. 49, no. 1, pp. 35-44, 2002.

[33] Z. Stavreva, D. Zeidler, M. Ploetner, and K. Drescher, “Characteristics in chemical-mechanical polishing of copper: Comparison of polishing pads,” *Applied Surface Science,* vol. 108, no. 1, pp. 39-44, 1997.

[34] H. Liang, F. Kaufman, R. Sevilla, and S. Anjur, “Wear phenomena in chemical mechanical polishing,” *Wear,* vol. 211, no. 2, pp. 271-279, 1997.

[35] W. Li, D. W. Shin, M. Tomozawa, and S. P. Murarka, “Effect of the polishing pad treatments on the chemical-mechanical polishing of SiO2 films,” *Thin Solid Films,* vol. 270, no. 1-2, pp. 601-606, 1995.

[36] G. Byrne, B. Mullany, and P. Young, “Effect of pad wear on the chemical mechanical polishing of silicon wafers,” *CIRP Annals - Manufacturing Technology,* vol. 48, no. 1, pp. 143-146, 1999.

[37] A. Tregub, G. Ng, J. Sorooshian, and M. Moinpour, “Thermoanalytical characterization of thermoset polymers for chemical mechanical polishing,” *Thermochimica Acta,* vol. 439, no. 1-2, pp. 44-51, 2005.

[38] B. J. Hooper, G. Byrne, and S. Galligan, "Pad conditioning in chemical mechanical polishing," *Journal of Materials Processing Technology,* vol. 123, no. 1, pp. 107-113, 2002.

[39] P. B. Zantye, S. Mudhivarthi, A. Kumar, and Y. Obeng, "Metrology and characterization of application specific chemical mechanical polishing pads," *Journal of Vacuum Science and Technology A: Vacuum, Surfaces and Films,* vol. 23, no. 5, pp. 1392-1399, 2005.

[40] L. Charns, M. Sugiyama, and A. Philipossian, "Mechanical properties of chemical mechanical polishing pads containing water-soluble particles," *Thin Solid Films,* vol. 485, no. 1-2, pp. 188-193, 2005.

[41] M. Yoshida, H. Ono, M. Nishiyama, T. Ashizawa, and T. Doi, " Effect of pad surface roughness on SiO2 removal rate in chemical mechanical polishing with ceria slurry " *Jpn. J. Appl. Phys.,* vol. 45,2A, pp. 733-735, 2006.

[42] V. H. Nguyen, A. J. Hof, H. van Kranenburg, P. H. Woerlee, and F. Weimar, "Copper chemical mechanical polishing using a slurry-free technique," *Microelectronic Engineering,* vol. 55, no. 1-4, pp. 305-312, 2001.

[43] V. H. Nguyen, R. Daamen, and R. Hoofman, "Impact of different slurry and polishing pad choices on the planarization efficiency of a copper CMP process," *Microelectronic Engineering,* vol. 76, no. 1-4, pp. 95-99, 2004.

[44] H. Kim, B. Park, S. Lee, H. Jeong, and D. A. Dornfeld, "Self-conditioning fixed abrasive pad in CMP," *Journal of the Electrochemical Society,* vol. 151, no. 12, pp. G858-G862, 2004.

[45] "Advances in Chemical-Mechanical Polishing," *Materials Research Society Symposium Proceedings, Materials Research Society, MRS,* vol. 816, 2004.

[46] K. Park, J. Oh, and H. Jeong, "Pad characterization and experimental analysis of pad wear effect on material removal uniformity in chemical mechanical polishing," *Japanese Journal of Applied Physics,* vol. 47, no. 10 PART 1, pp. 7812-7817, 2008.

[47] S. L. Wang, Y. J. Yuan, Y. L. Liu, and X. H. Niu, "Study on chemical mechanical polishing technology of copper," *Key Engineering Materials,* vol. 373-374, pp. 820-823, 2008.

[48] D. Kwon, K. Hyoungjae, and H. JEONG, "Heat and its effects to chemical mechanical polishing," *Journal of Materials Processing Technology,* vol. 178, no. 2006, pp. 82-87, 2006.

[49] V. R. Kakireddy, S. Mudhivarthi, and A. Kumar, "Effect of temperature on copper damascene chemical mechanical polishing process," *Journal of Vacuum Science and Technology B: Microelectronics and Nanometer Structures,* vol. 26, no. 1, pp. 141-150, 2008.

[50] H. J. Kim, H. Y. Kim, H. D. Jeong, E. S. Lee, and Y. J. Shin, "Friction and thermal phenomena in chemical mechanical polishing," *Journal of Materials Processing Technology,* vol. 130-131, pp. 334-338, 2002.

[51] Y. A. Sampurno, L. Borucki, Y. Zhuang, D. Boning, and A. Philipossian, "A Method for Direct Measurement of Substrate Temperature during Copper CMP," *Journal of the Electrochemical Society,* vol. 152, no. 7, pp. G537-G541, 2005.

[52] F. Sugimoto, Y. Arimoto, and T. Ito, “Simultaneous temperature measurement of wafers in chemical mechanical polishing of silicon dioxide layer,” *Japanese Journal of Applied Physics, Part 1: Regular Papers & Short Notes & Review Papers,* vol. 34, no. 12 A, pp. 6314-6320, 1995.

[53] S. Mudhivarthi, P. B. Zantye, A. Kumar, A. Kumar, M. Beerbom, and R. Schlaf, “Effect of temperature on tribological, electrochemical, and surface properties during copper CMP,” *Electrochemical and Solid-State Letters,* vol. 8, no. 9, pp. G241-G245, 2005.

[54] S. Mudhivarthi, P.zantye, A.kumar, and a. J.Y.shim, “Effect of tempearture on defect generation during copper chemical mechanical planarization,” *Material research society symposia proceedings,* vol. 867, pp. W 1.5.1 - 1.5.6, 2005.

[55] H. Jeong, Kim, H., Lee, Sunghoon, & Dornfeld, David. , *Multi- sensor monitoring system in Chemical Mechanical Planarization (CMP) for correlations with process issues*, CIRP Annals, vol. 55, 1, pp. 1-4, 2006.

[56] F. Preston, “The theory and design of plate glass polishing machine,” *Journal of the Society of Glass Technology,* vol. 11, 247, 1927.

[57] Q. Luo, S. Ramarajan, and S. V. Babu, “Modification of the Preston equation for the chemical-mechanical polishing of copper,” *Thin Solid Films,* vol. 335, no. 1-2, pp. 160-167, 1998.

[58] A. Maury, D. Ouma, D. Boning, and A. J. Chung, “A modification to Preston's equation and impact on pattern density effect modeling,” *Advanced Metalization Conference, San Diego, CA*, pp. 1-7, 1997.

[59] W.T. Tseng, and Y.L. Wang, "Re-examination of Pressure and Speed Dependences of Removal Rate during Chemical-Mechanical Polishing Processes," *Journal of the Electrochemical Society,* vol. 144, no. 2, pp. L15-L17, 1997.

[60] P. H. Chen, H.-C. Shih, B. W. Huang, and J. W. Hsu, "An engineering approach to predict the polishing rate in CMP with rotational equipment," *Journal of the Electrochemical Society,* vol. 151, no. 10, pp. G649-G651, 2004.

[61] J. Sorooshian, D. DeNardis, L. Charns, Z. Li, F. Shadman, D. Boning, D. Hetherington, and A. Philipossian, "Arrhenius Characterization of ILD and Copper CMP Processes," *Journal of the Electrochemical Society,* vol. 151, no. 2, pp. G85-G88, 2004.

[62] H. Hocheng, and Y.-L. Huang, *In situ endpoint detection by pad temperature in chemical-mechanical polishing of copper overlay*: Institute of Electrical and Electronics Engineers, 2004.

[63] L. Jianfeng, and D. A. Dornfeld, "Material removal mechanism in chemical mechanical polishing: theory and modeling," *Semiconductor Manufacturing, IEEE Transactions on,* vol. 14, no. 2, pp. 112-133, 2001.

[64] Z. Li, L. Borucki, I. Koshiyama, and A. Philipossian, "Effect of Slurry Flow Rate on Tribological, Thermal, and Removal Rate Attributes of Copper CMP," *Journal of the Electrochemical Society,* vol. 151, no. 7, pp. G482-G487, 2004.

[65] D. White, J. Melvin, and D. Boning, "Characterization and Modeling of Dynamic Thermal Behavior in CMP," *Journal of the Electrochemical Society,* vol. 150, no. 4, pp. G271-G278, 2003.

[66] L. Borucki, L. Charns, and A. Philipossian, “Analysis of frictional heating of grooved and flat CMP polishing pads,” *Journal of the Electrochemical Society,* vol. 151, no. 12, pp. G809-G813, 2004.

[67] Y. Y. Lin, and S. P. Lo, “A study of a finite element model for the chemical mechanical polishing process,” *International Journal of Advanced Manufacturing Technology,* vol. 23, no. 9-10, pp. 644-650, 2004.

[68] Y. Homma, K. Fukushima, S. Kondo, and N. Sakuma, “Effects of mechanical parameters on CMP characteristics analyzed by two-dimensional frictional-force measurement,” *Journal of the Electrochemical Society,* vol. 150, no. 12, pp. G751-G757, 2003.

[69] A. C. G Fu, S Guha, G Subhash, “A plasticity based model of material removal in chemical mechanical polishing” *IEEE Transactions on Semiconductor Manufacturing,* vol. 14, pp. 406-417, 2001.

[70] C.-W. Liu, B.-T. Dai, W.-T. Tseng, and C.-F. Yeh, “Modeling of the wear mechanism during chemical-mechanical polishing,” *Journal of the Electrochemical Society,* vol. 143, no. 2, pp. 716-721, 1996.

[71] D. L. Hetherington, D. J. Stein, J. P. Lauffer, E. E. Wyckoff, and D. M. Shingledecker, “Analysis of in-situ vibration monitoring for end-point detection of CMP planarization processes,” *Proc. SPIE,* vol. 3743, pp. 89-101, 1999.

[72] T. Kojima, M. Miyajima, F. Akaboshi, T. Yogo, S. Ishimoto, and A. Okuda, “Application of CMP process monitor to Cu polishing,” *Semiconductor Manufacturing, IEEE Transactions on,* vol. 13, no. 3, pp. 293-299, 2000.

[73] A. Fukuroda, K. Nakamura, and Y. Arimoto, "*In-situ* CMP monitoring technique for multi-layer interconnection," Int. *Electron Devices Meeting,* pp. 469-472, 1995.

[74] T. Kojima, M. Miyajima, F. Akaboshi, T. Yogo, and S. Ishimoto, "Practical use of CMP process monitor in Cu polishing," *Semiconductor Manufacturing Conference Proceedings, IEEE International Symposium* pp. 187-190, 1999.

[75] S. Bukkapatnam, P. Rao, and R. Komanduri, "Experimental dynamics characterization and monitoring of MRR in oxide chemical mechanical planarization (CMP) process," *International Journal of Machine Tools and Manufacture,* vol. 48, no. 12-13, pp. 1375-1386, 2008.

[76] U. Phatak, S. Bukkapatnam, Z. Kong, and R. Komanduri, "Sensor-based modeling of slurry chemistry effects on the material removal rate (MRR) in copper-CMP process," *International Journal of Machine Tools and Manufacture,* vol. 49, no. 2, pp. 171-181, 2009.

[77] A. Maury, A. K. Nanda, and O. Rodriguez, *Device and method for polishing a semiconductor substrate*, US Patent No. 6051500, Lucent Tech., 18 April, 2000.

[78] J. Kramer, T. Gyulai, and A. Reichel, *Method and system for controlling the chemical mechanical polishing by using a seismic signal of a seismic sensor*, US Patent No. 7198542, Advanced Micro Devices, 3 April, 2007.

[79] Pattengale Jr., and P. Hardy, *CMP process endpoint detection method by monitoring and analyzing vibration data*, Int. Patent No. 20060063383, 23 March, 2006.

[80] K. P. Lim, and K. E. Lee, *Real time monitoring of CMP pad conditioning process*, US Patent No. 7163435, Tech Semiconductor Singapore Pte. Ltd. , 16 Jan., 2007.

[81] G. S. Sandhu, and T. T. Doan, *Method for controlling a semiconductor (CMP) process by measuring a surface temperature and developing a thermal image of the wafer*, US Patent No. 5196353, Micron Technology, Inc. (Boise, ID), 23 March, 1993.

[82] H.-c. Chen, Hsu, Shun-liang, *Chemical/mechanical planarization (CMP) endpoint method using measurement of polishing pad temperature*, US Patent No. 5643050 Taiwan Semiconductor Manufacturing Company Ltd. (Hsin-Chu, TW), 28 Jan., 1997.

[83] H. Hocheng, Huang, Yun-liang *Method for detecting the endpoint of a chemical mechanical polishing (CMP) process*, US Patent No. 6872662, 29 March, 2005.

[84] J.-e. Koo, J.-w. Lee, S.-b. Lee, D.-h. Hong, S.-r. Hah, and H.-s. Son, *Chemical mechanical polishing apparatus*, US Patent No. 6976902, Samsung Electronics Co., Ltd., 20 Dec., 2005.

[85] H. S. Lee, B. Y. Park, S. M. Park, H. J. Kim, and a. H. D. Jeong, "The characteristics of frictional behavior in CMP using an integrated monitoring system," *Key Eng. Mater.,* vol. 339, pp. pp. 152–157., 2007.

[86] Y. P. Chang, M. Hashimura, and D. A. Dornfeld, "An investigation of the AE signals in the lapping process," *CIRP Annals - Manufacturing Technology,* vol. 45, no. 1, pp. 331-334, 1996.

[87] I. Inasaki, "Sensor Fusion for Monitoring and Controlling Grinding Processes," *The International Journal of Advanced Manufacturing Technology,* vol. 15, no. 10, pp. 730-736, 1999.

[88] J. Choi, D. Lee , and D. and Dornfeld, "Acoustic emission characteristics of oxidation and dissolution in copper CMP," *207th Meeting of The Electrochemical Society, Quebec, Canada*, 2005 (abstract only).

[89] J. Tang, D. Dornfeld, S. Pangrle, and A. Dangca, "In-process detection of microscratching during CMP using acoustic emission sensing technology," *Journal of Electronic Materials,* vol. 27, no. 10, pp. 1099-1103, 1998.

[90] H. Hocheng, and Y.-L. Huang, "*In-situ* endpoint detection by acoustic emissions in chemical-mechanical polishing of metal overlay," *IEEE Transactions on Semiconductor Manufacturing,* vol. 20, no. 3, pp. 306-312, 2007.

[91] R. Ganesan, T. K. Das, A. K. Sikder, and A. Kumar, "Wavelet-based identification of delamination defect in CMP (Cu-low k) using nonstationary acoustic emission signal," *IEEE Transactions on Semiconductor Manufacturing,* vol. 16, no. 4, pp. 677-685, 2003.

[92] P. W. Carter, Chamberlain, Jeffrey P. , *CMP process involving frequency analysis-based monitoring*, US Patent No. 6431953, Cabot Microelectronics Corporation (Aurora, IL), 13 August, 2002.

[93] A. Fukuroda, Y. Arimoto, and K. Nakamura, *Polishing apparatus and polishing method*, US Patent No. 5904609, Fujitsu Limited (Kawasaki, JP), 18 May, 1999.

[94] K. Ono, S. Oguri, K. Sasabe, M. Kurita, Y. Kojima, T. Egawa, and K. Shigeta, *Polishing apparatus*, US Patent No. 6634924 Ebara Corporation ,Kabushiki Kaisha Toshiba, 21 Oct., 2003.

[95] T. Kaushal, C. Dam, and Y. Hu, *Chemical mechanical polishing endpoint detection*, USA US 6709314B2, Applied materials Inc,CA, 23 March, 2004.

[96] T. K. Oba, *Chemical mechanical polishing machine and chemical mechanical polishing method*, United States, Semiconductor Leading Edge Technologies, Inc. (Kanagawa, JP), 30 April, 2002.

[97] H.-p. Wang, and Q. Liu, *Method and apparatus for detecting micro-scratches in semiconductor wafers during polishing process*, US Patent No. 6488569, Florida State University (Tallahassee, FL), 3 Dec., 2002.

[98] R. Sampson, *Use of acoustic spectral analysis for monitoring/control of CMP processes.*, US Patent No. 6424137, STMicroelectronics,Inc,USA, 23 July, 2002.

[99] R. Ganesan, T. K. Das, A. K. Sikder. A. Kumar, *System and method for the identification of chemical mechanical planarization defects*, US 7377170
University of South Florida (Tampa, FL, US), 27 may, 2008.

[100] D. A. Dornfeld, and J. Tang, *Semiconductor wafer chemical-mechanical planarization process monitoring and end-point detection method and apparatus*, US Patent No. 6910942, The regents of the university of california,CA., 28 June, 2005.

[101] C. C. Yu, and G. S. Sandhu, *Chemical mechanical planarization (CMP) of a semiconductor wafer using acoustical waves for in-situ end point detection*, US Patent No. 5240552, Micron Technology, Inc. (Boise, ID), 31 August, 1993.

[102] N. Gitis, and M. Vinogradov, *Method and apparatus for controlled polishing*, US Patent No. 2002/0037681 A1, 17 Dec., 2002.

[103] T. S. Kaushal, Dam, Chuong Quang, Hu, Yongqi, *Chemical mechanical polishing endpoinat detection*, US Patent No. 6709314, Applied Materials Inc. (Santa Clara, CA), 23 March, 2004.

[104] I. Salugsugan, *Audio end point detector for chemical-mechanical polishing and method therefor*, US Patent No. 5245794, Advanced Micro Devices, Inc. (Sunnyvale, CA), 21 Sep., 1993.

[105] C. C. Yu, *Acoustical method and system for detecting and controlling chemical-mechanical polishing (CMP) depths into layers of conductors, semiconductors, and dielectric materials*, United States US 5222329, Micron Technology, Inc. (Boise, ID), 29 June, 1993.

[106] J. Sinclair, and L. L. Lee, *Wafer carrier for chemical mechanical planarization polishing*, US Patent No. 6113479, Applied Materials, 17 Dec., 2000.

[107] L.-j. Chen, *Chemical/mechanical polish (CMP) thickness monitor*, United States, Industrial Technology Research Institute (Hsinchu, TW), 1 July, 1997.

[108] K. Noh, "Modeling of dielectric erosion and copper dishing in copper CMP," Mechanical Engineering, MIT, Ph.D thesis, 2005.

[109] Y. Y. Chen, and J.-C. Lin, "Intelligent dual-speed design for face-up chemical mechanical polishing," *Advanced Intelligent Mechatronics. Proceedings, 2005 ,IEEE/ASME*, pp. 1133 - 1138, 2005.

[110] Moteiv, "Tmote sky data sheet, San Francisco, CA, 2006. Available online," http://www.moteiv.com/products/docs/tmote-sky-datasheet.pdf.

[111] R. Ganesan, “Real-time monitoring of complex sensor data using wavelet-based multiresolution analysis,” *The International Journal of Advanced Manufacturing Technology,* vol. 39, no. 5, pp. 543-558, 2008.

[112] R. Ganesan, A. N. V. Rao, and T. K. Das, *A multiscale bayesian SPRT approach for online process monitoring*, New York, NY, ETATS-UNIS: Institute of Electrical and Electronics Engineers, 2008.

[113] G. Litak, A. K. Sen, and A. Syta, “Intermittent and chaotic vibrations in a regenerative cutting process,” *Chaos, Solitons & Fractals,* vol. 41, no. 4, pp. 2115-2122, 2009.

[114] A. Facchini, and H. Kantz, “Curved structures in recurrence plots: The role of the sampling time,” *Physical Review E,* vol. 75, no. 3, pp. 036215 (1-8), 2007.

[115] A. Vazquez, R. Manasseh, R. M. Sánchez, and G. Metcalfe, “Experimental comparison between acoustic and pressure signals from a bubbling flow,” *Chemical Engineering Science,* vol. 63, no. 24, pp. 5860-5869, 2008.

[116] A. M. Fraser, and H. L. Swinney, “Independent coordinates for strange attractors from mutual information,” *Physical Review A,* vol. 33, no. 2, pp. 1134-1140, 1986.

[117] C. Rhodes, and M. Morari, “Determining the model order of nonlinear input/output systems,” *AIChE Journal,* vol. 44, no. 1, pp. 151-163, 1998.

[118] H.kantz, and T.Schreiber, *Nonlinear time series analysis*: Cambridge university Press, Cambridge U.K, 1997.

[119] J. P. Eckmann, S. O. kamphorst, and D.Ruelle, “Recurrence plots of dynamical systems,” *EPL (Europhysics Letters),* vol. 4, no. 9, pp. 973-977, 1987.

[120] A. Antoniou, and C. E. Vorlow, “Recurrence quantification analysis of wavelet pre-filtered index returns,” *Physica A: Statistical Mechanics and its Applications,* vol. 344, no. 1-2, pp. 257-262, 2004.

[121] N. Marwan, M. Carmen Romano, M. Thiel, and J. Kurths, “Recurrence plots for the analysis of complex systems,” *Physics Reports,* vol. 438, no. 5-6, pp. 237-329, 2007.

[122] C. L. Webber, and Z. J. P., "Recurrence quantification analysis of nonlinear dynamical systems," *Tutorials 2: Contemporary nonlinear methods for the behavioral sciences,* Riley MA, 2005, pp. 26-94

[123] S. Schinkel, O. Dimigen, and N. Marwan, “Selection of recurrence threshold for signal detection,” *The European Physical Journal - Special Topics,* vol. 164, no. 1, pp. 45-53, 2008.

[124] J. M. Nichols, S. T. Trickey, and M. Seaver, “Damage detection using multivariate recurrence quantification analysis,” *Mechanical Systems and Signal Processing,* vol. 20, no. 2, pp. 421-437, 2006.

[125] S.R.Schmidt, and R.G.launsby, *Understanding industrial designed experiments*, 4th edition ed.: Air academy Associates. , 1997.

Appendix

Here the plots of the time series of the vibration signal at Z-axis as well as power spectra of the time series acquired at different runs are presented. For every run, (a) time series of 2000 data points, (b) wave form of 500 data points long, and (c) power spectrum of 2048 dyadic points are plotted. These plots are one at the start and the other at the end (i.e. 2 min. after the start) of polishing. The details of the experimental runs are provided in Table 7.

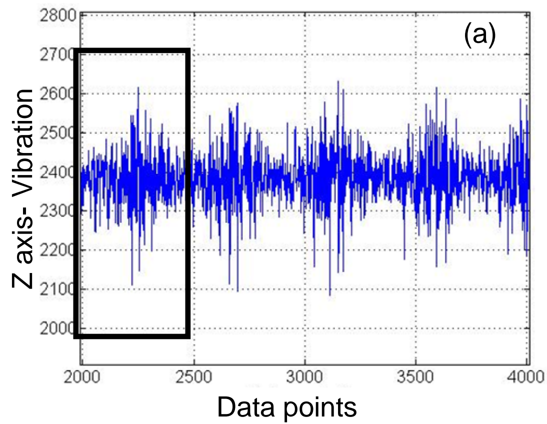

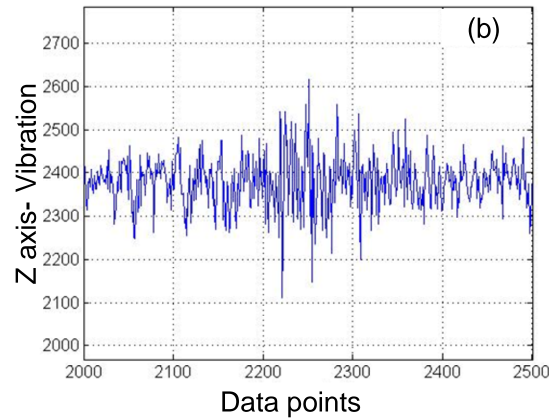

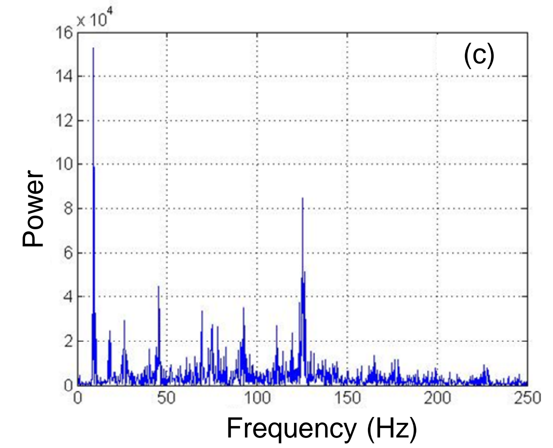

Run R1: Start of polishing: (a) Time series of signals (b) Wave form of the time series (c) Power spectrum

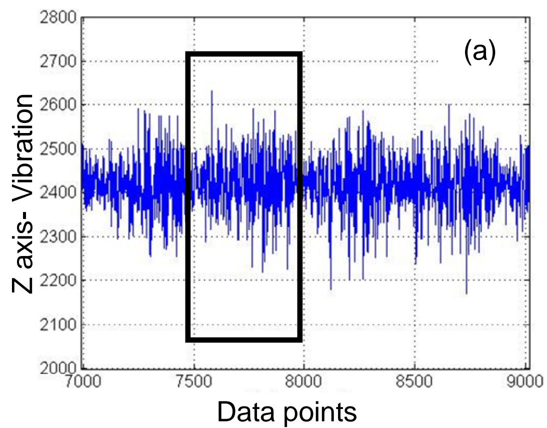

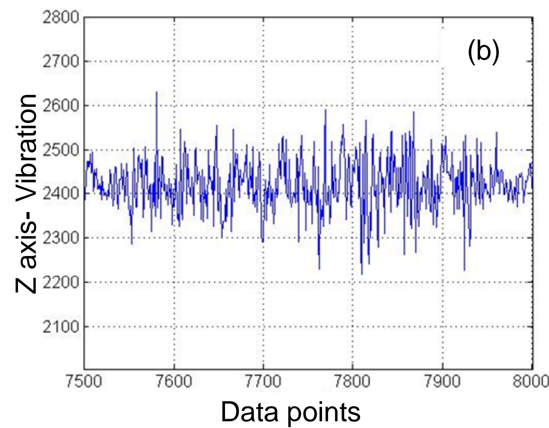

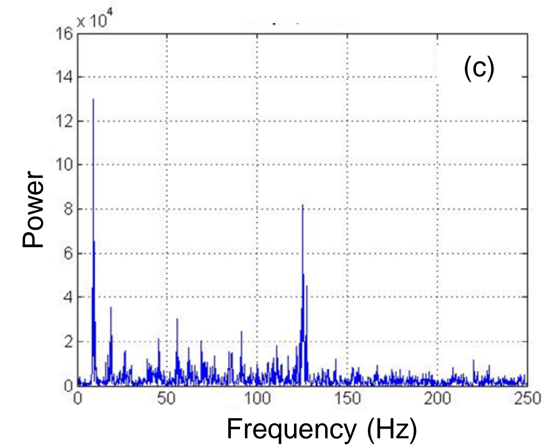

Run R1: End of polishing: (a) Time series of signals (b) Wave form of the time series (c) Power spectrum

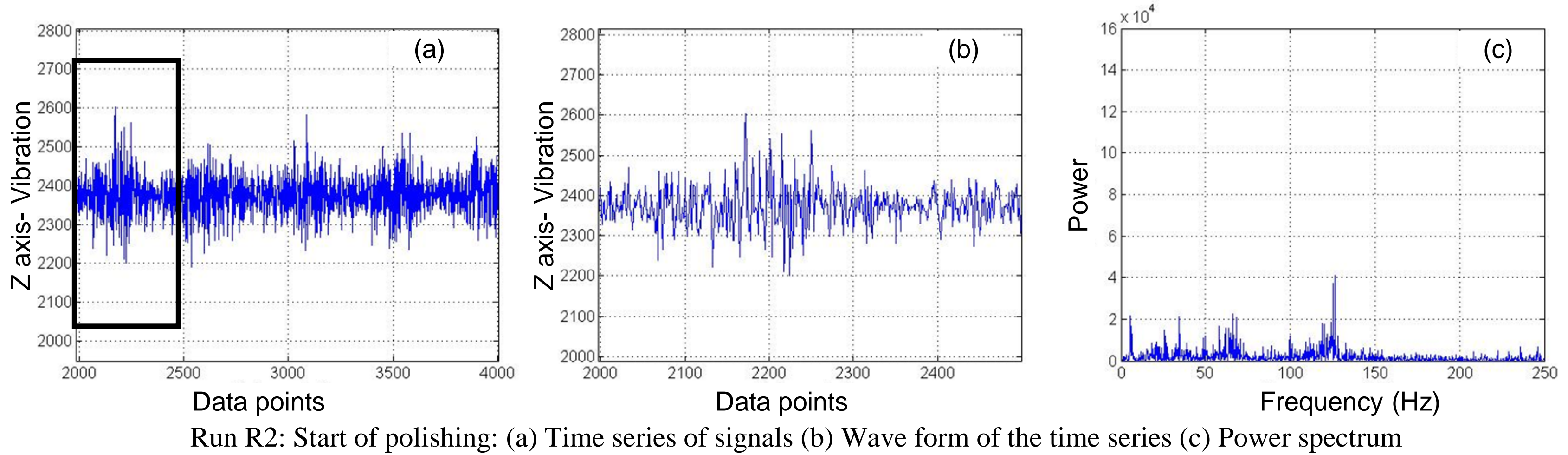

Run R2: Start of polishing: (a) Time series of signals (b) Wave form of the time series (c) Power spectrum

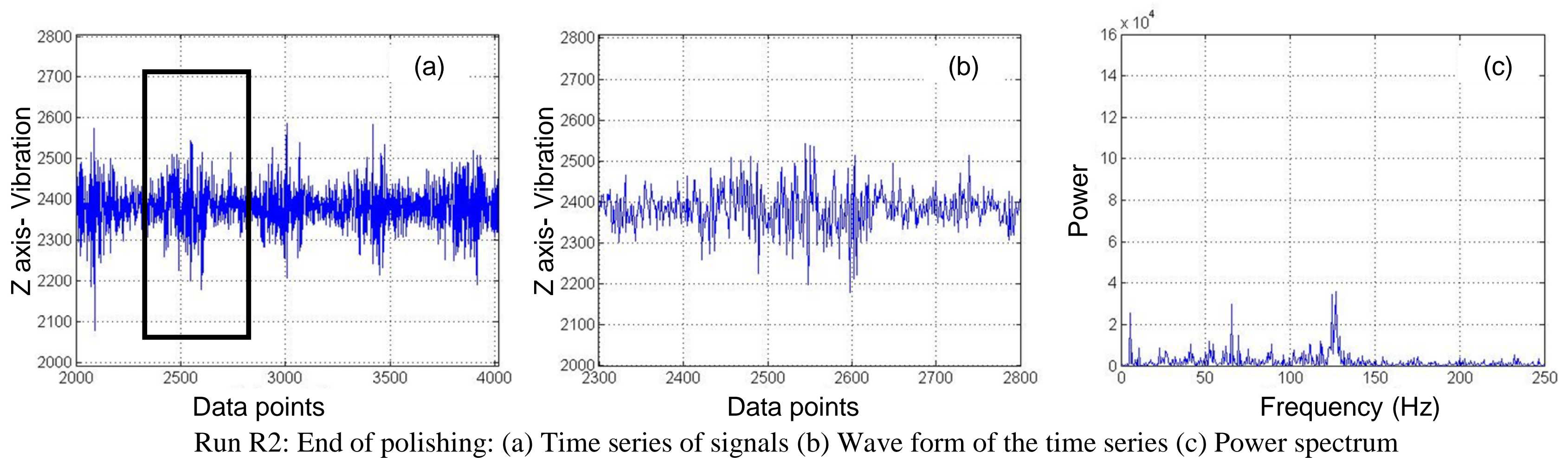

Run R2: End of polishing: (a) Time series of signals (b) Wave form of the time series (c) Power spectrum

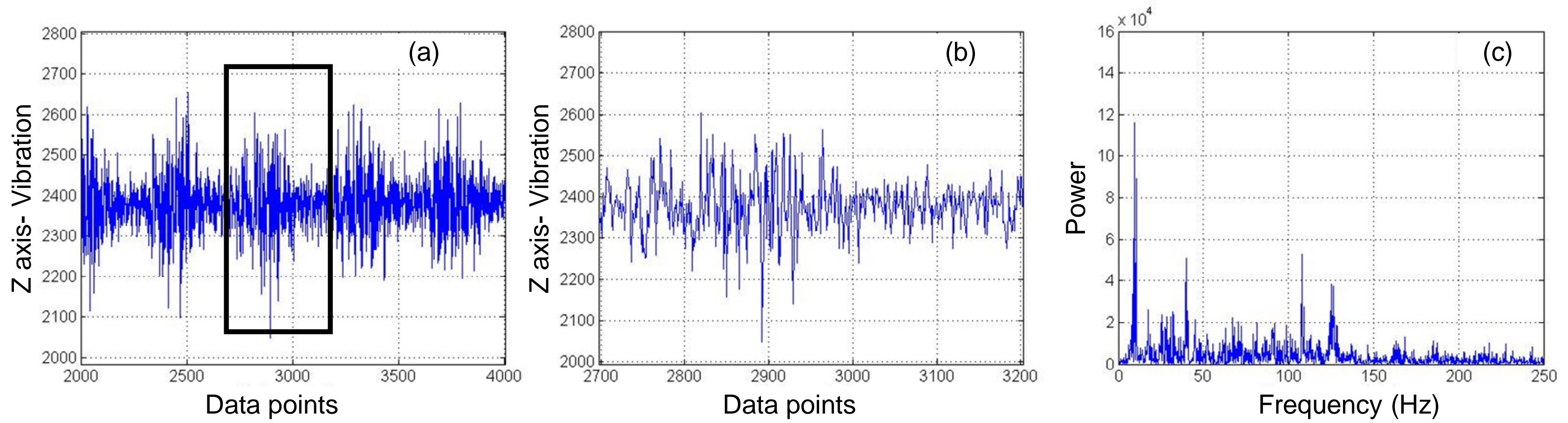

Run R3: Start of Polishing: (a) Time series of signals (b) Wave form of the time series (c) Power spectrum

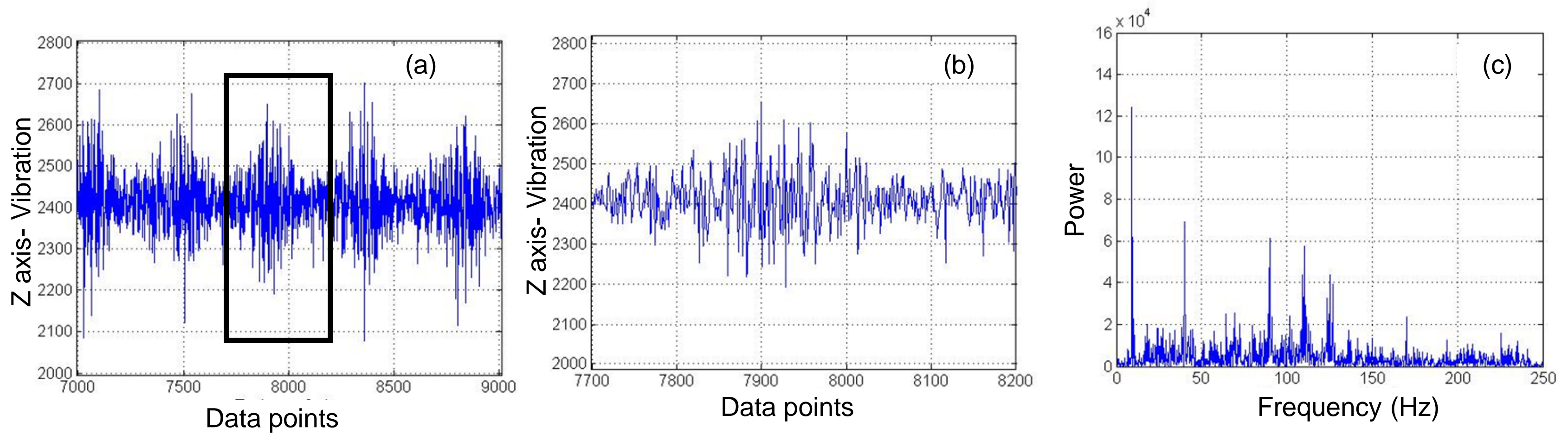

Run R3: End of polishing: (a) Time series of signals (b) Wave form of the time series (c) Power spectrum

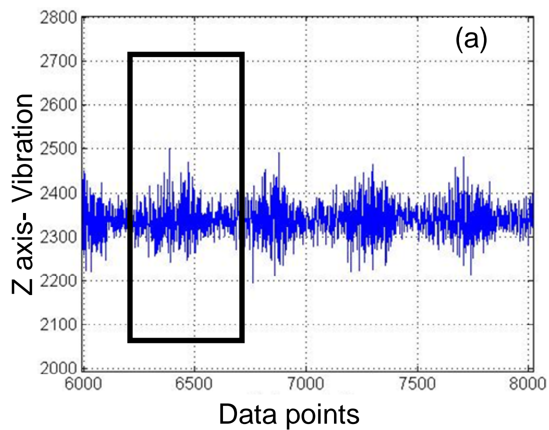

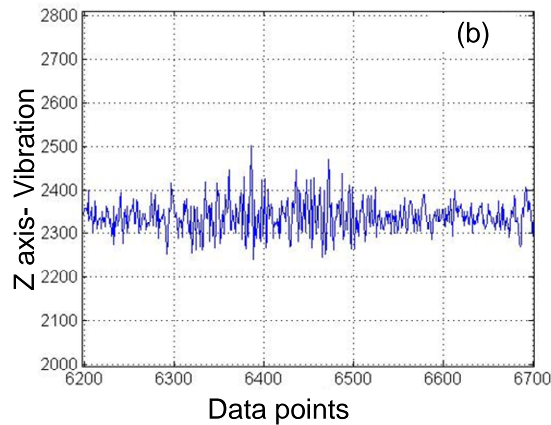

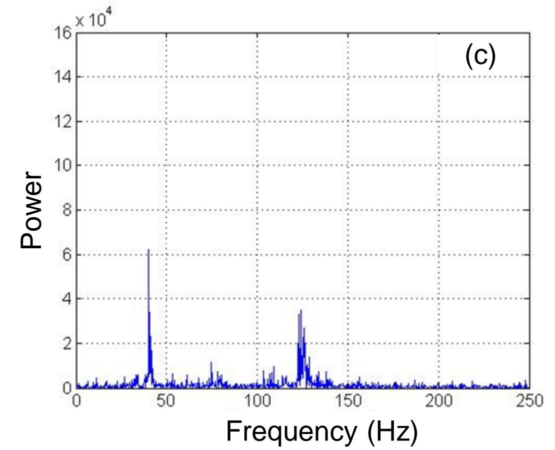

Run R4: Start of polishing: (a) Time series of signals (b) Wave form of the time series (c) Power spectrum

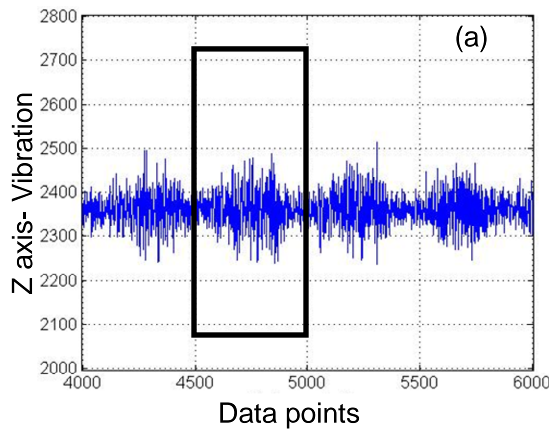

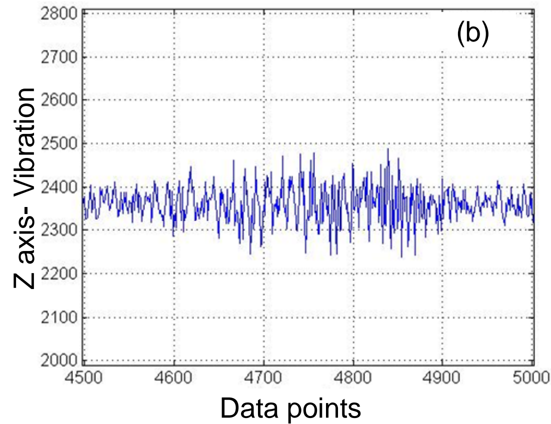

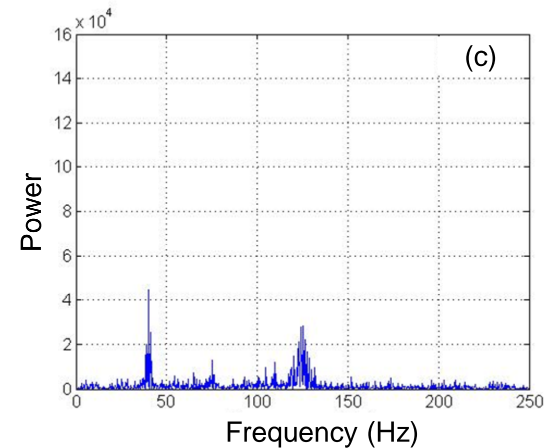

Run R4: End of polishing: (a) Time series of signals (b) Wave form of the time series (c) Power spectrum

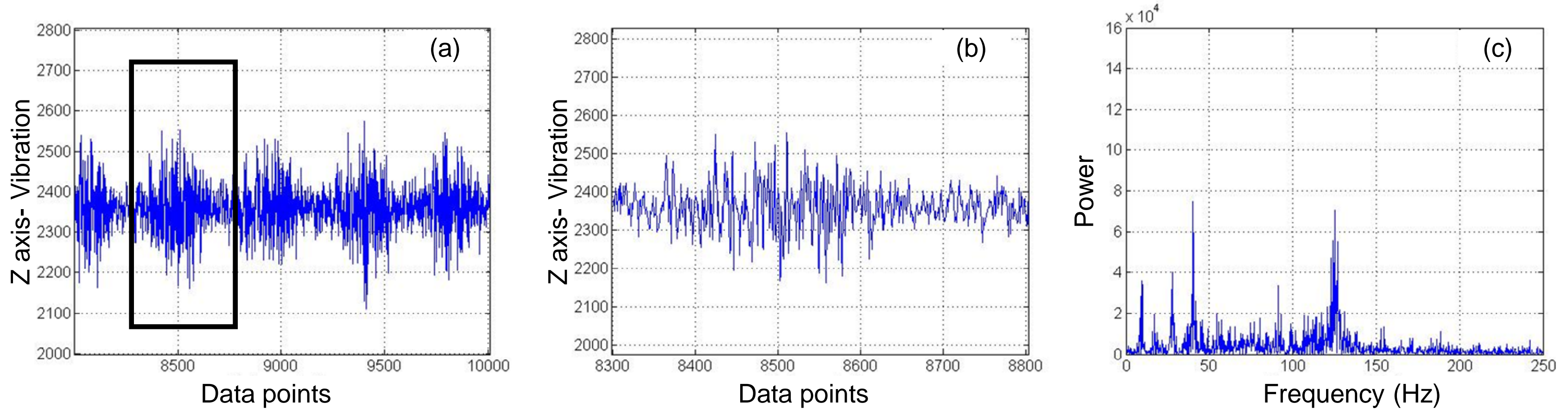

Run R5: Start of polishing: (a) Time series of signals (b) Wave form of the time series (c) Power spectrum

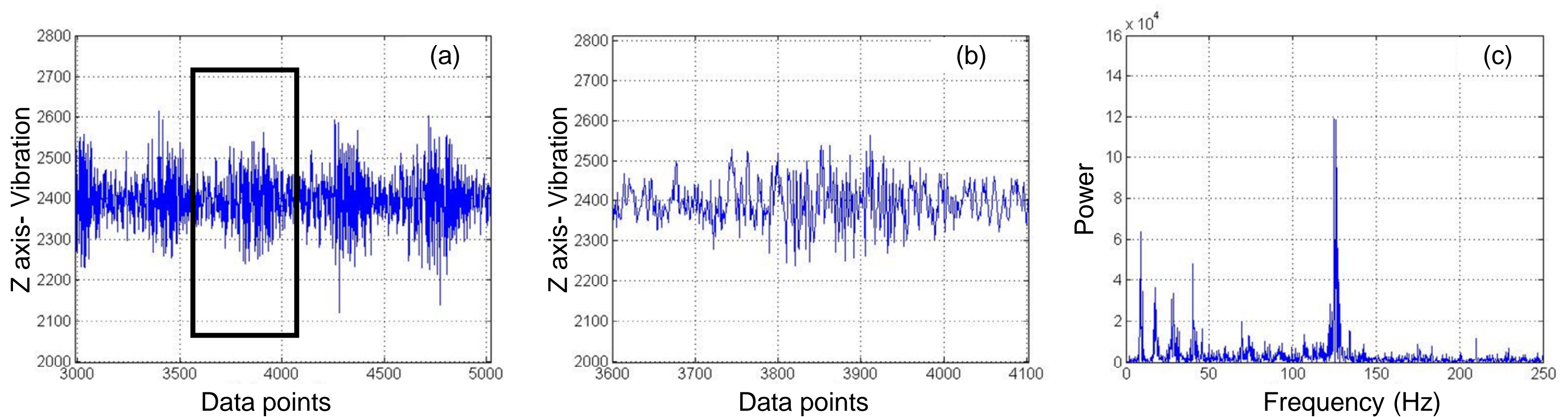

Run R5: End of polishing: (a) Time series of signals (b) Wave form of the time series (c) Power spectrum

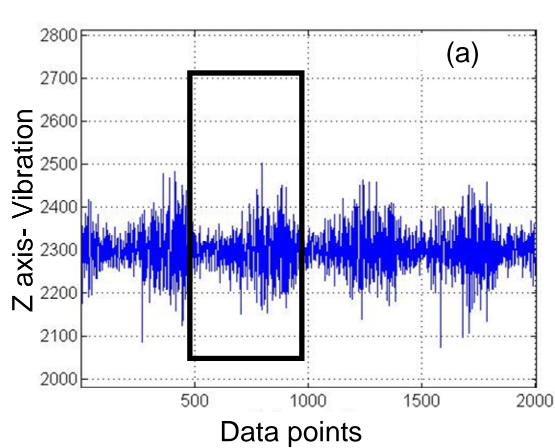

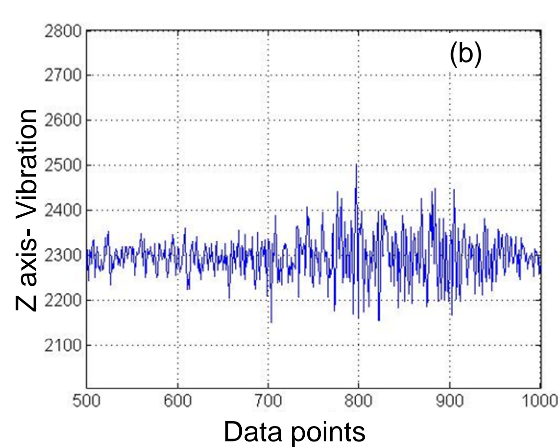

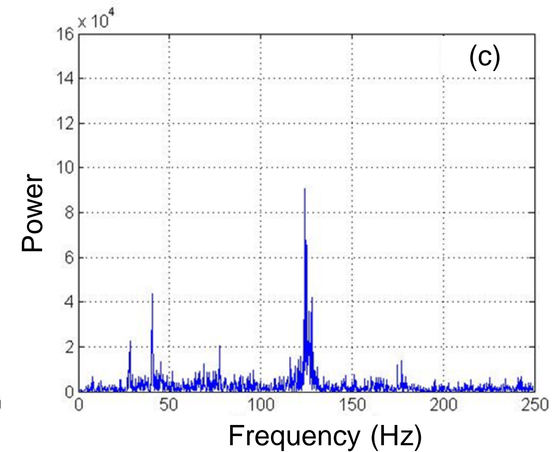

Run R6: Start of polishing: (a) Time series of signals (b) Wave form of the time series (c) Power spectrum

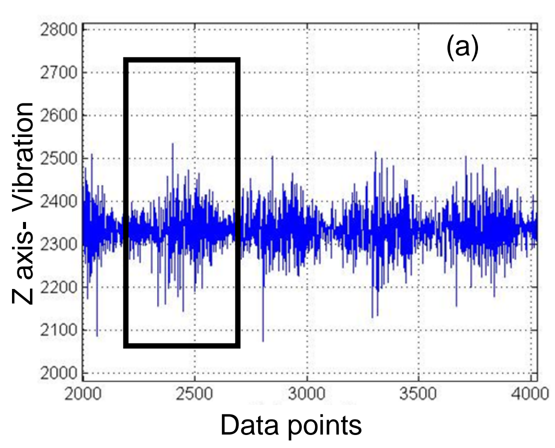

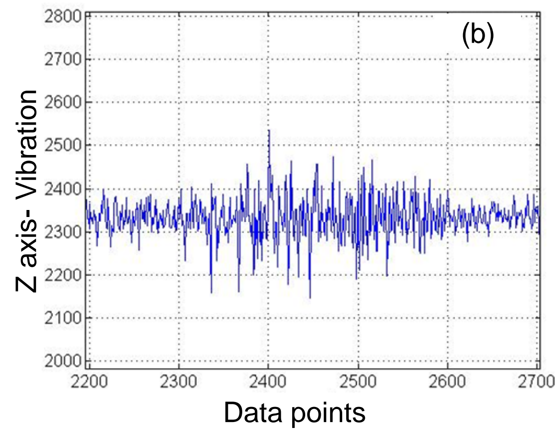

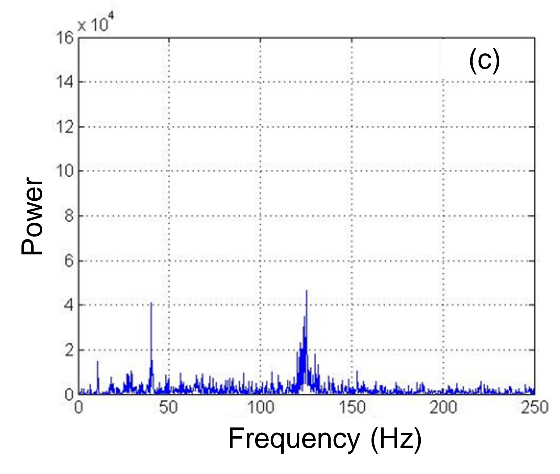

Run R6: End of polishing: (a) Time series of signals (b) Wave form of the time series (c) Power spectrum

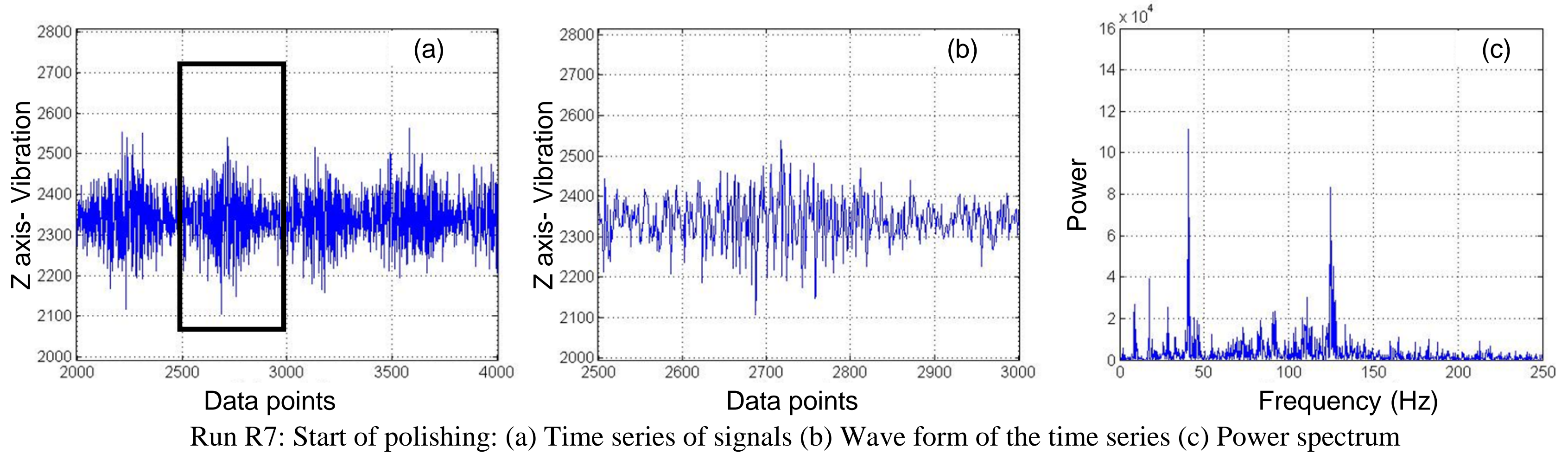

Run R7: Start of polishing: (a) Time series of signals (b) Wave form of the time series (c) Power spectrum

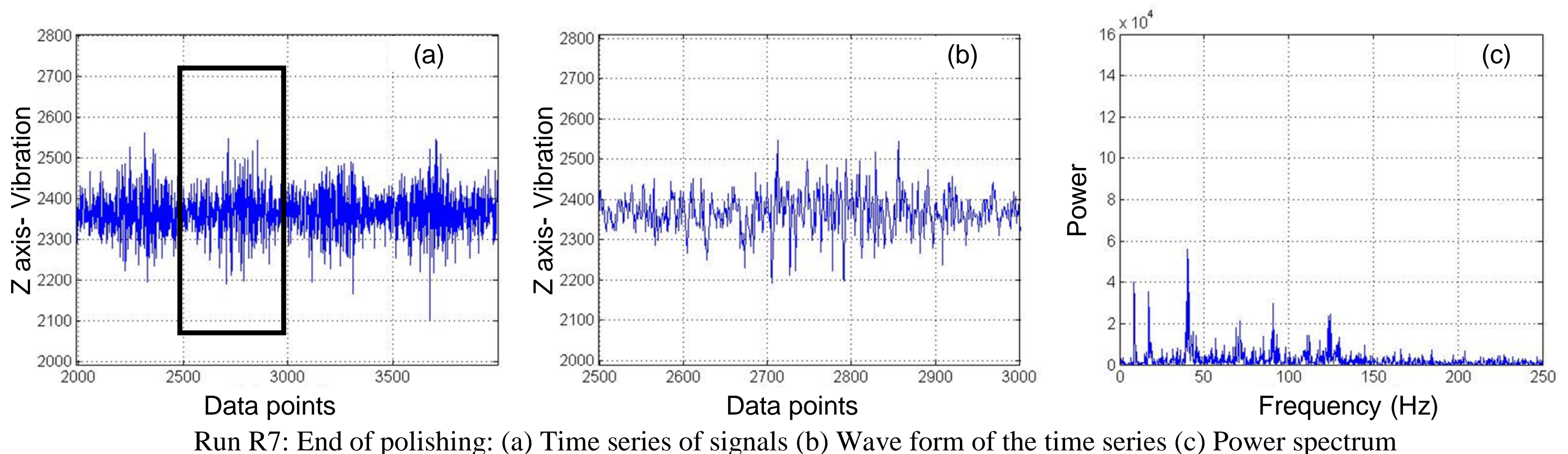

Run R7: End of polishing: (a) Time series of signals (b) Wave form of the time series (c) Power spectrum

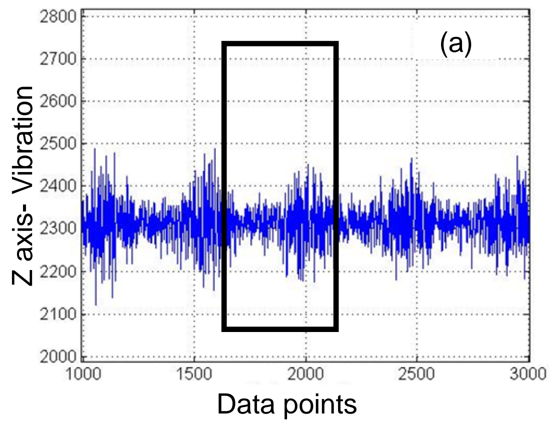

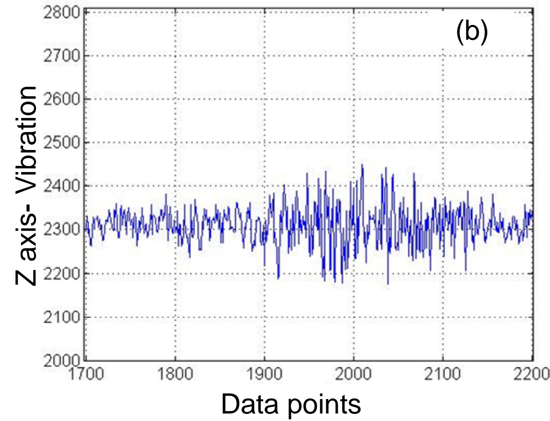

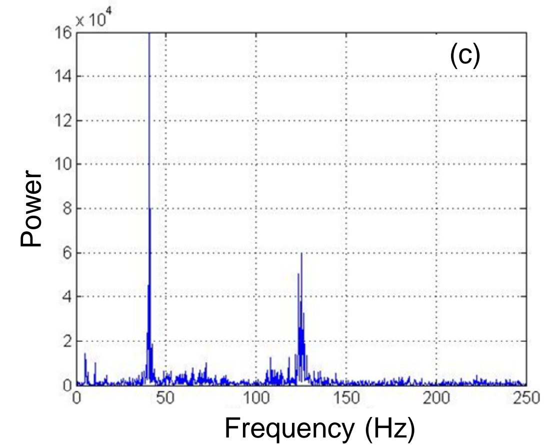

Run R8: Start of polishing: (a) Time series of signals (b) Wave form of the time series (c) Power spectrum

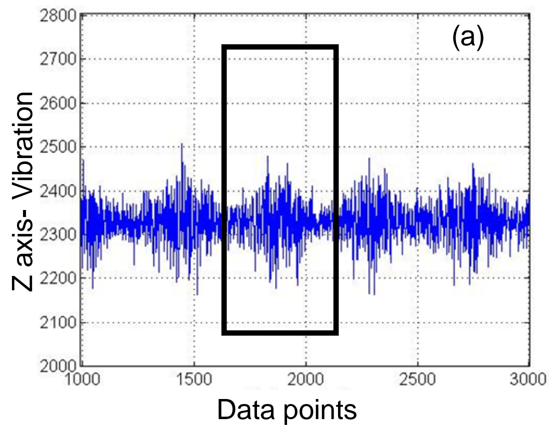

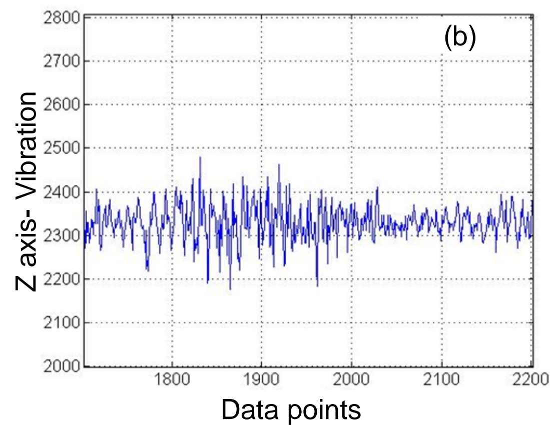

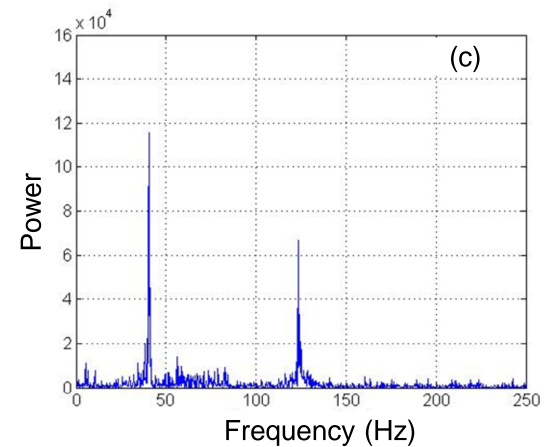

Run R8: End of polishing: (a) Time series of signals (b) Wave form of the time series (c) Power spectrum

VITA

AMIT OHRI

Candidate for the Degree of

Master of Science

Thesis: Wireless Sensor Fusion for Monitoring Chemical Mechanical Planarization (CMP) Process

Major Field: Mechanical Engineering

Biographical:

Personal Data:

Son of Mr.Rajinder Ohri and Mrs.Sarita Ohri born on 8 August, 1983 in Punjab, India. Resident of Punjab

Education:

Completed the requirements for the Master of Science in Mechanical Engineering at Oklahoma State University, Stillwater, Oklahoma in December, 2010.

Completed the requirements for the Bachelor of Technology in Mechanical Engineering at Punjab Technical University in First Class, Jalandhar, India in 2006

Experience:

Jan 2008-May 2010, Graduate Research Assistant, Chemical Mechanical Polishing lab, Sensor Networks and Complex Manufacturing Research, Advanced Research Technology Research Center (ATRC), Oklahoma State University.

Professional Memberships:
American Society of Mechanical Engineers (ASME)
Indian Society of Mechanical Engineers

Name: AMIT OHRI Date of Degree: December, 2010

Institution: Oklahoma State University Location: Stillwater, Oklahoma

Title of Study: Wireless Sensor Fusion approach for Monitoring Chemical Mechanical Planarization (CMP) Process

Pages in Study: 153 Candidate for the Degree of Master of Science

Major Field: Mechanical Engineering

Scope and Method of Study: Wireless sensor fusion modeling is developed using response surface methodology. Factorial design of experiments is executed for capturing the process dynamics through sensors signals. The wireless sensors are mounted in the rear of the copper sample for capturing the process dynamics in the form of heat and vibration. Various vibration and temperature features, such as statistical, time-frequency, and nonlinear features are extracted. Then to model and to correlate the process through sensor features for real time monitoring of the CMP process. Roughness and MRR are modeled empirically using vibration features followed by thermal features. In addition, the same strategy has used to develop the Preston constant model.

Findings and Conclusions: The study is based on regression modeling of the surface roughness and MRR using sensors fusion features extracted from vibration and thermal signals. A good estimation of the models is obtained using sensor fusion modeling. In the roughness model, the process parameters are not able to estimate significantly the roughness of the sample. Therefore, sensor feature are incorporated in the model. The energy features from the spectrogram are able to increase model performance by 15 %. The RQA based features are able to increase prediction performance by 47 %. The thermal features are able to improve the coefficient of determination approximately by 10 % and prediction performance by approximately 23 %. In case of the MRR model, energy features are able to improve the coefficient of determination by approximately 9 %. This feature is able to improve prediction performance by 58 % without any increase in the degree of freedom of error. Also temperature feature increased the performance of the MRR model by 1 %. The performance of the Preston constant model is estimated by 91.98 % using all the sensor features.

ADVISOR'S APPROVAL: Dr. Ranga Komanduri
Advisor